A COMPUTATIONAL FLUID DYNAMICS (CFD) ANALYSIS OF DEVELOPING TURBULENT FLOW IN STRAIGHT DUCTS

A Thesis

by

SULAIMAN MOHAMMED S ALSALEEM

Submitted to the Office of Graduate and Professional Studies of
Texas A&M University
in partial fulfillment of the requirements for the degree of

MASTER OF SCIENCE

Chair of Committee,	Michael Pate
Committee Members,	Bryan P. Rasmussen
	Jorge L. Alvarado
Head of Department,	Andreas A.Polycarpou

May 2017

Major Subject: Mechanical Engineering

ABSTRACT

A computational fluid dynamics (CFD) analysis was performed on developing turbulent flow of air in straight ducts. A uniform inlet velocity was assumed for two different scenarios, namely at the straight duct inlet and at the inlet of a right-angle elbow located immediately upstream of the straight duct. Using STAR CCM+ commercial software, velocity gradient profiles and pressure gradient profiles were obtained for different flow rats and duct sizes representing a range used in engineering practice including round and rectangular duct geometries with the latter having aspect ratios of 1, 1.5, and 2.

The results show that the velocity and pressure developing lengths in round ducts were shorter than those in corresponding square ducts by around 13% and 19%, respectively. Also, the velocity and pressure developing lengths in round ducts were shorter than the corresponded rectangular ducts with a 1.5 aspect ratio by around 25% and 30% respectively. Similarly, the developing length in the round ducts were shorter than the corresponding rectangular ducts with an aspect ratio of 2 by around 36% based on the velocity profiles and 40% based on the pressure profiles. All of the above results indicate that the developing length of the flow is geometry dependent in addition to being Reynolds number dependent.

Comparing the CFD results for the square and rectangular ducts shows that the velocity developing length of the square duct was 15 % and 27 % less than the developing length for the 1.5 and 2 aspect ratio ducts, respectively. Similarly, the pressure drop developing length in the square duct was 16% and 27 % less than those for the 1.5 and 2 aspect ratio ducts, respectively.

Last but not least, comparing the CFD entrance length of a round duct with a well-known experimental entrance length correlation, the results of the CFD approach used in this study were within 10% of the experimental results.

ACKNOWLEDGEMENTS

I would like to express my special gratitude towards my committee chair, Dr. Michael Pate for his generous support and for imparting his knowledge and expertise in this study. I would like to thank my committee members, Dr. Bryan Rasmussen and Dr. Jorge Alvarado, for their guidance and support throughout the course of this research. I also would like to thank Dr. Gerald Morrison for sharing his CFD simulation expertise and helping me with some of issues I had with the simulation software. Finally, I would like to thank my parents for their unconditional support throughout the course of this research.

CONTRIBUTORS AND FUNDING SOURCES

Contributors

This work was supported by a thesis committee consisting of Dr. Michael Pate [advisor] and Dr. Bryan Rasmussen [member] of the Department of Mechanical Engineering and Dr. Jorge Alvarado [member] of the Department of Engineering Technology and Industrial Distribution. The software package used in this study was provided by CD-adapco Siemens through their representative Mr. Christopher Penny.

Funding Sources

Graduate study was supported by Saudi Arabian Cultural Mission (SACM).

NOMENCLATURE

δ	Boundary layer thickness (mm)
σ_k	Constant
σ_d	Constant
C_D	Constant
C_u	Constant
C_ε	Constant
β	Constant
γ	Constant
σ_w	Constant
ρ	Density $(\frac{\text{kg}}{\text{m}^3})$
$(L/D)_{FDX}\big/(L/D)_{FDy}$	Developing length ratio
$(L/D)_{FD}$	Dimensionless developing length
$(L/D)_{Round}$	Dimensionless developing length of round duct
$(L/D)_{Square}$	Dimensionless developing length of square duct
$(\frac{L}{D})_{Rect,Ar=1.5}$	Dimensionless developing length of rectangular duct with aspect ratio of 1.5
$(\frac{L}{D})_{Rect,Ar=2}$	Dimensionless developing length of rectangular duct with aspect ratio of 2
$(L/D)_{Elbow}$	Dimensionless developing length of duct with elbow
(H/D)	Dimensionless duct height
$(L/D)_{FD_{EXP}}$	Dimensionless experimental developing length
(L/D)	Dimensionless length of the horizontal duct
(y/D)	Dimensionless length of the vertical duct
$(L/D)_{FD_P}$	Dimensionless pressure-based developing length

$(L/D)_{FD_V}$	Dimensionless velocity-based developing length
u^+	Dimensionless x-direction velocity
y^+	Dimensionless y-direction wall coordinate
D	Duct Diameter (m)
μ	Dynamic viscosity (Pa. s)
κ	Experimental constant ≈ 0.4
f	Friction factor
u^*	Friction velocity (m/s)
τ_{lam}	Laminar shear stress (Pa)
l_m	Mixing Length (m)
ΔP	Pressure drop (Pa)
$\frac{dP}{dx}$	Pressure gradient (Pa/m)
$\frac{\epsilon}{D}$	Relative roughness
Re	Reynolds number
ω	Specific dissipation rate
T	Temperature (K)
$\overline{u'}$	Time-averaged x-direction fluctuating velocity (m/s)
τ_{tot}	Total shear stress (Pa)
ϑ_t	Turbulent diffusivity (m^2/s)
ϵ	Turbulent dissipation rate
P	Turbulent energy production term (j)
TI	Turbulent intensity
k	Turbulent kinetic energy (j)
l	Turbulence length scale (m)
τ_{tur}	Turbulent shear stress (Pa)
μ_t	Turbulent viscosity (Pa. s)
$\frac{dv}{dx}$	Velocity gradient (s^{-1})

u	x-direction (axial) instantaneous velocity $(\mathrm{m/s})$
$\overline{u}$	x-direction mean velocity component $(\mathrm{m/s})$
u'	x-direction fluctuation velocity component $(\mathrm{m/s})$
v	y-direction instantaneous velocity $(\mathrm{m/s})$
v'	y-direction fluctuation velocity component $(\mathrm{m/s})$
w	z- direction instantaneous velocity $(\mathrm{m/s})$
w'	z-direction fluctuation velocity component $(\mathrm{m/s})$

TABLE OF CONTENTS

Page

LIST OF FIGURES

LIST OF TABLES

Page

I. INTRODUCTION
AND LITERATURE REVIEW

1.1 Introduction

The analysis of duct flow is important in many engineering applications. Such applications range from heating, ventilation, and air conditioning (HVAC) systems in buildings to large pipelines that carry crude oil and natural gas across the country, and from water pumping networks in buildings to more complex bio-engineering systems such as the development of engineered veins that carry blood throughout the human body. Consequently, it has become quite necessary to carry out more research and more investigations to understand the nature of flow inside pipes and ducts, especially for the case of turbulent internal flows in the entrance region.

Although the theory of fluid flow is well understood, analytical solutions are not yet available for internal turbulent flow and only limited to simple cases such as laminar flow in circular ducts. As a result, experimental investigations and numerical modeling have to be used for more complicated problems. As for experimental approaches in fluid analysis, although it can provide trusted results especially with advanced test set ups, it is limited by instrument uncertainties, and usually require high initial costs to prepare for the experiments. As a result, numerical and CFD approaches have been extensively used to understand the internal turbulent flow behavior.

The research work performed and presented here focuses on understanding and locating the developing length of internal turbulent flows rather than the nature of turbulence structure itself. In engineering practice, knowledge of the developing length of the flow is an essential variable in designing ducts and installing instruments, as they both require assurance that the fully developed flow region is reached where the flow becomes stable with a constant velocity profile distribution.

1.2 Theoretical Background

Internal fluid flow applications are involved in many engineering practices, ranging from refrigerant flow in small air conditioners in our homes to complicated cooling systems in nuclear reactors, and therefore, it is necessary to further expand our knowledge and understanding of the physics of fluid flow, especially for the case of turbulent flow.

We encounter turbulent flow everywhere in life, for instance, atmospheric movements, ocean currents and many large waterfalls (Çengel,2014). In engineering practice, one can say that most fluid flow applications are considered to be turbulent such as oil and gas pipelines and high speed flow applications. As a result, for the past few decades, large amounts of research has been conducted to understand this complicated flow mechanism and tried to develop correlations or equations that can be used to describe and quantify turbulence parameter mainly by following experiments and numerical approaches.

1.2.1 Turbulence

Turbulence is a phenomenon of fluid flow, which occurs at high Reynolds number. In fluid mechanics, Reynolds number represents the ratio of inertia forces to viscous forces, which means that flow becomes turbulent flow when the intertie forces dominate the viscous effects. Turbulent flow is a highly irregular flow and characterized by random and rapid fluctuations of eddies throughout the flow compared to smooth pathlines in laminar flow (Çengel, 2014). Such fluctuations are observed to provide an extra transfer momentum and energy in fluid element, and therefore enhancing mass, momentum, and heat transfer associated with the turbulent flow. In addition, turbulent flow consists of a spectrum of different eddy sizes where the largest eddies are on the order of the flow geometry (Laufer,1953), while the smallest eddies are dissipated into internal energy due to flow viscous forces.

As shown in Figure 1 below, the instantaneous velocity is fluctuating continuously about some mean value, such that the flow velocity can be expressed as the sum of the average or mean value $\bar{u}$ and a fluctuating component u'

$$u = \bar{u} + u' \tag{1.1}$$

The same behavior is applied to other fluid properties such as temperature, pressure, and density (for the case of compressible fluid flow).

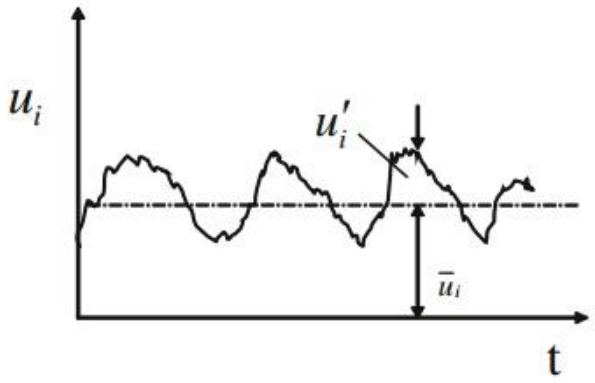

Figure 1. Mean and fluctuating velocity components in turbulent flow. Reprinted from (Han, 2011).

Since averaging the fluctuating velocity is carried out over a large time interval, it is safe to assume that the time average of the fluctuating component is zero.

$$\bar{u'} = lim\frac{1}{t}\int_0^t u'(t)dt = 0 \tag{1.2}$$

One important aspect in the turbulent flow analysis is to determine the shear stress in turbulent boundary layers since it helps us to quantify the Reynolds stress in the turbulent flow and to develop the velocity profile in the turbulent boundary layers by using the law of wall, as will be presented later in this section. Unfortunately, both the experimental and numerical studies show that shear stress calculations in turbulent flow are not as straightforward as with laminar flow. In fact, it consists of a laminar component of the shear stress and a turbulent component that accounts for the turbulent fluctuations.

Applying Newton's Second Law on a differential fluid element in the turbulent boundary layer, results in the following, (Çengel, 2014)

$$\delta F = (\rho v' dA)(-u') = -\rho u' v' dA \tag{1.3}$$

$$\frac{\delta F}{dA} = -\rho u' v' \tag{1.4}$$

$$\tau_{tur} = -\rho \overline{u'v'} = \mu_t \frac{\partial \bar{u}}{\partial y} \tag{1.5}$$

$$\tau_{tot} = (\mu + \mu_t)\frac{\partial \bar{u}}{\partial y} = \rho(\vartheta + \vartheta_t)\frac{\partial \bar{u}}{\partial y} \tag{1.6}$$

For laminar boundary layer flows, the velocity profile can be obtained by solving the conservation equations for mass and momentum. However, for turbulent boundary layer flows, there is not yet a complete analytical solution for the velocity profile due to the turbulent random motions of the flow. Hence the concept of a Prandtl mixing length was developed and applied to achieve the law of the wall for the velocity profile, namely a semi-empirical velocity profile, in a turbulent boundary layer.

A typical velocity profile in the fully developed laminar flow is parabolic while it is much fuller in the turbulent flow with a sharp drop near the pipe wall (Çengel,2014). Based on the perpendicular distance away from the wall, turbulent boundary layers are divided into three regions as shown in Figure 2 below; adjacent to the wall region is the

viscous (laminar) sublayer, where the flow behaves in a laminar manner. This layer is small in thickness compared to the other layers but its importance is the result of the large velocity gradient involved. Then, there is a buffer layer, where turbulent characteristics are introduced to the flow but it is still dominated by viscous (laminar) effects. The remaining part of the flow nearest to the center is the turbulent layer, where the turbulent effects dominate over the viscous effects, as shown in Figure 2 below.

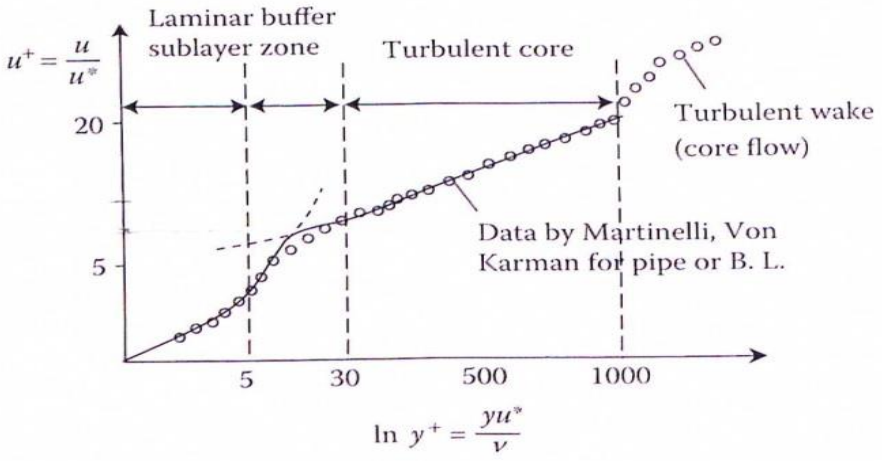

Figure 2. Semi-empirical law of wall velocity profile for turbulent boundary layer. Reprinted from (Han, 2011).

The friction velocity, dimensionless x-direction velocity and dimensionless y-direction terms are usually used in the law of wall derivations, and expressed as

$$u^* = \sqrt{\frac{\tau_w}{\rho}} \tag{1.7}$$

As was shown in Figure 2, the laminar sublayer region, $0< y^+ < 5$, where viscous effects dominate turbulent effects, the normalized law of wall equation satisfactorily correlates with experimental data for smooth ducts is as follows

$$u^+ = y^+ \tag{1.8}$$

For the turbulent region, $y^+ \geq 30$, Prandtl mixing length theory is applied assuming that the velocity fluctuation is proportional to the velocity gradient, and mixing length is in a linear relationship with distance from the wall, the resulting law of wall velocity profile is

$$u^+ = \frac{1}{\kappa} \ln y^+ + C \tag{1.9}$$

1.2.2 Friction Factor and Pressure Drop in Turbulent Flow

In addition to the fluid velocity profile in ducts, friction factor of the duct, pressure drops and pressure gradients along the duct or pipe length are all important variables that need to be considered in the internal flow analysis. The friction factor in the fully developed turbulent flow depends both on the Reynolds number of the flow and relative roughness of the duct or pipe. To date, there is no functional relationship describing this dependence based on analytic analysis. However, several curve fitting experimental correlations are available with one being developed by Colebrook (1939), which has been frequently used in the turbulent flow analysis, as shown in Equation (1.10) below

$$\frac{1}{f} = -2.0 \log\left(\frac{\frac{\epsilon}{D}}{3.7} + \frac{2.51}{Re\sqrt{f}}\right) \tag{1.10}$$

In addition to the friction facto, the pressure drop of a working fluid flowing inside a duct is also a function of fluid velocity squared, fluid properties and duct geometry

including duct length and diameter. The functional relationship for pressure drop used in either turbulent or laminar flow can be expressed as

$$\Delta P = \frac{\rho f \, L \, V^2}{2 \, D} \tag{1.11}$$

1.2.3 Mechanism of Internal Flow

When a fluid with uniform inlet velocity enters a round duct or any other duct geometry for that matter, the fluid particles in direct contact with the top and bottom duct walls are stationary due to the no slip condition and as one moves away from the walls towards the center of the duct, the velocity increases where it reaches its maximum value. The no-slip condition of fluid particles near the duct wall causes the flow to develop a region where viscous shearing forces exist, and the velocity changes significantly, creating what is known as the velocity boundary layer. This boundary layer grows in the direction of the flow, and the velocity in the middle region of the duct, where friction effects are negligible, remains flat with zero velocity gradient.

As noted, the velocity boundary layer grows and becomes thicker in the direction of the flow until the boundary layers from all sides finally merge into one point at the duct center somewhere along the duct length downstream from the inlet. The region from the duct entrance to this point is known as the entrance or developing region, and the length of this region is called the entrance length or the developing length. The region downstream of the point where the boundary layers merge is known as the fully developed region, and the flow becomes stable such that constant velocity profiles occur in the direction of the flow. Figure 3 illustrates the concept of the velocity boundary layer and shows the development of the velocity profile along the duct.

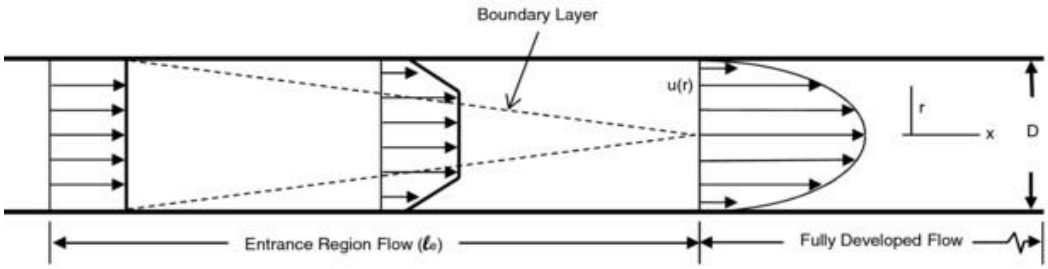

Figure 3. Mechanism of internal flow. Reprinted from (Çengel,2014).

Unfortunately, there is not yet a formal definition or documentary evidence of the fully developed condition that is widely accepted (Doherty, Ngan, Monty, & Chong, 2007). Moreover, there is no analytical equation available in the literature to calculate the developing length in turbulent flow, but there are a number of experimental and numerical correlations that have been developed to estimate this length. This task becomes even more complicated in the case of turbulent flow inside non-circular duct as presented in this research.

The main criteria used to identify the point where the fully developed flow is reached inside the pipe is by analyzing the velocity profile of the flow. For the case of steady, turbulent flow inside round ducts, the time-averaged velocity profile remains unchanged in the fully developed flow region, and can be expressed as

$$\frac{\partial u\,(r,x)}{\partial x} = 0 \tag{1.12}$$

$$u = u(r) \tag{1.13}$$

In addition to the velocity profile, the pressure drop or pressure gradients can be used to locate the location of reaching the fully developed condition. At the duct inlet where the velocity boundary layers are at the thinnest, the pressure gradients are at their largest

value. As boundary layers grow and become thicker in the direction of the flow, pressure gradients decrease until they reach a constant value somewhere downstream of the duct inlet, thus signifying that fully developed flow is achieved as shown in Figure 4.

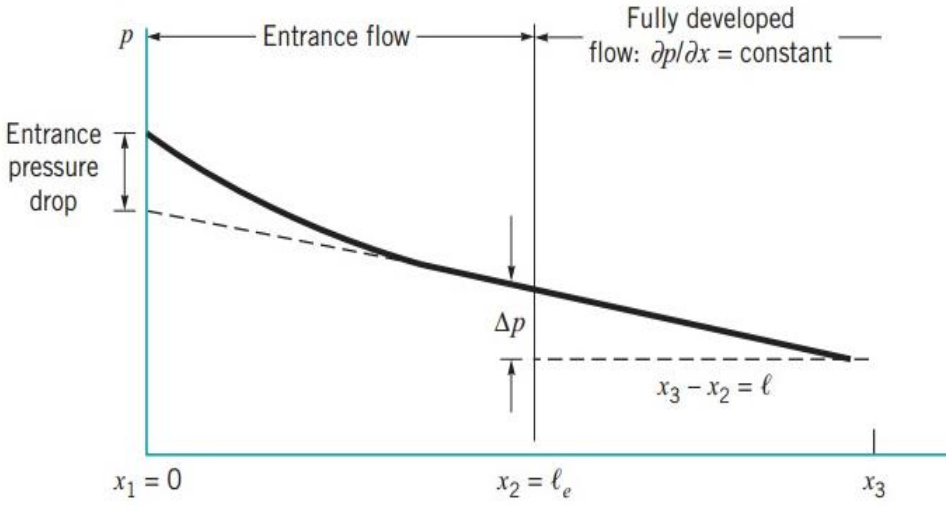

Figure 4. Variation of pressure profile in direction of the flow. Reprinted from (Munson, Okiishi, and Huebsch, 2009).

More complicated criteria for locating the fully developed flow location along the pipe have been introduced by some recent researchers based on analyzing the large scale structure in the turbulent flow. According to the Kolmogorov scaling theory, "Turbulent energy enters the flow at low wave number, large scale, and cascades through the inertial range to the dissipation scales where it dissipated". The analysis is performed by using Fourier transforms to identify the wave number of structures that have contributed most to the turbulent energy of the flow (Doherty, Ngan, Monty, & Chong 2007). However, an analysis based on this approach is beyond the scope of this research.

1.3 Review of Literature

Prior to perform the CFD simulations and analysis, it is important to evaluate and study relevant research. The literature review section below lists some of the main theories and physics of the turbulence phenomena in general. Also, it describes in some detail the fully developed flow criteria employed in many of the past experimental and numerical investigations so that a relevant criteria can be adopted for the study reported herein.

1.3.1 Turbulent Flow

A large number of research analysis have been carried out on turbulent pipe flow in the past few years. Laufer J (1953) investigated the structure of turbulence in fully developed pipe flow. By experimentally measuring different turbulence quantities in pipe flow, including mean velocities and Reynolds stress, Laufer observed that the production, dissipation, and diffusion of turbulent energies have sharp maximums near the edge of the laminar sublayer. It was concluded that the turbulence production, diffusion, and viscous actions at the near wall region, are all of about equal importance. However, at the center of the pipe, energy diffusion plays the predominant role. Also, it was observed that within turbulent boundary layers an existence of a strong transfer of kinetic energy from the laminar sub-layer while equally strong pressure energy transfers toward it.

Taylor (1984) developed a mathematical model for air flowing through sampling pipes with the energy conservation equation being applicable for the case of a steady, incompressible fluid flow through a smooth pipe. Taylor also used Darcy's equation to calculate frictional head loss in pipes, and noted that this equation is applicable to laminar flow as well as for turbulent flow. N.C. Markatos (1986) concluded that turbulence is the most complicated kind of fluid motion, and hence there is a real need for researchers and designers to quantitatively predict turbulence quantities and turbulent flow behavior. A number of mathematical models have been developed to describe

turbulent flow, which has been the basis for computational and numerical modelling software in simulating complicated turbulent flow. Marcatos presented in detail turbulence model equations including the zero-equation model, one-equation model, and two- equations model, and listed the major advantages and disadvantages of each turbulent model. Also, common turbulent flow applications of each turbulent model were addressed with each showing successfully agreement with experimental results.

Koh (1992) derived an equation to represent the mean velocity distribution across the inner layer of a turbulent boundary layer and derived a friction factor correlation for fully developed turbulent pipe flow by using a velocity profile distribution. In addition, a number of derivations and analytical results have been presented and discussed in various books. In Bejan, "Convection Heat Transfer".1984. The author derived and demonstrated an expression defining the velocity distribution in a pipe with turbulent flow. White, F.M, Fluid Mechanics, 3rd edition, 1994 has investigated turbulence theory and turbulent flow and presented a relationship that defines friction factor in turbulent pipe flow.

Hunt and Morrison (2000) studied in detail the eddy structure in turbulent boundary layers. They emphasized that understanding eddy structures will enable researchers and designers to improve the statistical modelling and sub-grid elements in numerical simulations of turbulent flow. Hunt and Morrison proposed a new analysis for the driving mechanism and the statistics for turbulent boundary layers at high Reynolds numbers, with their analysis being based on the results of linear rapid distortion theory and field experimental data. Using their model, they were able to derive, for the case of high Reynolds numbers, the main statistical quantities such as variances, spectra, and turbulent length scales by using surface similarity and inhomogeneous linear theory.

1.3.2 Criteria for Defining Developing Flow

Research has been carried out to locate where in-tube turbulent flow becomes fully developed exactly and to identify the criteria that should be used to determine whether

the flow is fully developed. Early research is this area took the mean velocity only into consideration in defining the development length. For example, Barbin and Jones (1963) experimentally investigated turbulent air flow in pipes by measuring mean velocities, turbulent intensities, and Reynolds stresses in the inlet region of smooth pipes. They observed a developing length of 43.5D for the case of a Reynold number of 388,000, based on the pipe diameter and mean velocity, but fully developed flow was not attained in that mean velocities, turbulence intensities, and Reynolds stress were still changing at this distance from the inlet.

Laufer (1953) claimed that fully developed mean flow was achieved in an experiment at 40D, while later work by Perry and Abell (1978), suggested that at higher Reynolds numbers up to 175000, a development length of 71.9D is required for the flow to be fully developed. Doherty, Ngan and Chong (2007) also investigated the development of turbulent pipe flow. They stated that the development length of duct flows has been approached in many ways over the years, and yet there is no accurate definition or criteria of where fully developed flow is achieved. Furthermore, they tried to examine different criteria to define fully developed flow phenomena. Based on a mean velocity analysis, Doherty, Ngan and Chong (2007) found that results reasonably agree with the findings of Abell and Perry (1978) who suggested that the mean velocity was invariant after 71.9D. However, they found that this length is further increased by the addition of the development of the large scale flow structures as a criteria for fully developed flow. They proposed that since these large scale structures require a longer development length, it is more a conservative approach to use this method as the main criteria in defining fully developed flow rather than the mean velocity profile approach.

Saho et al (2009) used a Computational Fluid Dynamics (CFD) package, namely FLUENT, to investigate the accuracy of numerical modelling of laminar flow for the purpose of determining the friction factor of a pipe. Flow governing differential equations including the continuity equation and the Naiver-stokes equations were iterated and numerically solved with CFD software. The numerical results gave a friction

factor of 0.0151 for an entrance length of 2.7068 m while experimental results gave a similar friction factor value of 0.0157.

Bhandari and Dr. Singh (2012) developed a CFD model by using ANSYS FLUENT for turbulent flow in a round pipe to visualize the fluid flow and the fully developed flow condition. They observed that for the case of air with an inlet velocity of 1 m/s, the numerically obtained centerline velocity for the fully developed region was around 1.19 m/s while the experimental centerline velocity was 1.22 m/s. Similarly, the experimental value of skin friction factor came out to be 0.01, while the value obtained computationally was 0.00795. They mentioned that the results revealed that the axial velocity increases along the length of the pipe and after a certain distance, it becomes constant signifying fully developed flow. The results also revealed that the skin friction factor decreases along the length of the pipe, and also becomes constant as the fully developed flow is achieved, which is in conformity to experimental results. Bhandari and Dr. Singh (2012) concluded that the developing length for air with the 1 m/s inlet velocity is around 27.5D, and that the CFD analysis successfully represents the hydrodynamics of the system.

Joshi, Bisht, and Gupta (2014) performed a similar analysis in that they investigated experimentally and numerically an axi-symmetric model of fully developed turbulent flow in pipe of 0.2 m diameter with Freon ($1330\ \mathrm{kg/m^3}$ density) as the working fluid. They observed that for an inlet velocity of Freon of 0.01 m/s, the numerical centerline velocity for fully developed region is around 0.012 m/s, while the experimental value was calculated to be 0.0127 m/s. Similarly, for fully developed turbulent flow of Freon, the numerical value of the skin friction factor was around 0.01, while the experimental value was calculated to be 0.01075. They also concluded that the developing length for Freon with 0.01m/s inlet velocity is around 75D.

Kai and Ping (2013) preformed a CFD numerical simulation analysis of small and medium caliber 90° circular bends. They used a $K-\varepsilon$ turbulence model with FLUENT package software to simulate velocity and pressure profiles along a vertical to horizontal

90° elbow system, and observed that the standard $K-\varepsilon$ model is in a good agreement with experimental results as it accurately reflects the elbow internal flow pattern and secondary flow effect. Similarly, Didwania, Singh, Malik, and Sisodiya (2014) analyze turbulent flow over a 90° bend for ducts used in centralized A.C plants by using experiments and numerical using CFD simulations. By comparing numerical results against experiment data, they observed that using a $K-\varepsilon$ turbulence model for simulating a duct-elbow flow system predicts physical characteristics of turbulent flow more accurately than other turbulence models.

1.4 Scope of Work

The aim of this study is to use Computational Fluid Dynamics (CFD) models solved with START CCM+ software to determine and analyze the turbulent flow behavior of air in circular and non-circular ducts, including both straight duct systems and ducts downstream of right-angle elbows, to understand the factors that affect the developing length of turbulent flow. Moreover, numerical mathematical correlations are developed for a range of round and rectangular duct geometries that can be then used to determine where the fully developed turbulent flow is achieved based on both velocity and pressure profiles. The numerical results will be compared against analytical solutions and some experimental correlations available in the literature, to assure the validity of the CFD simulations and to develop a correction factor between the experimental and numerical results.

II. GOVERNING EQUATIONS FOR TURBULENT FLOW

2.1 Introduction

Computational Fluid Dynamics (CFD) modelling is based on the fundamental governing equations of fluid dynamics; conservation of mass, conservation of momentum, and conservation of energy. Since the driving force of fluid flow is the pressure difference between the upstream and downstream of the flow along with the viscous boundary layer effects over the wall surface in internal flow, the conservation of mass and conservation of momentum equations have to be applied to each fluid element in the flow domain in order to solve for the velocity distribution in the duct flow. This section presents the general form of these governing equations for turbulent fluid flow along with the derivation of the Navier-Stokes equation of turbulent fluid flow, as presented by (White,1994).

2.2 Continuity Equation

The continuity equation, also known as the conservation of mass equation basically states that the fluid mass cannot change for each fluid element, or infinitesimal control volume in the fluid domain. Another view of the equation is the rate of increase of mass in the fluid element is equal to the net rate of flow of mass into or out of the fluid element. The following equations are presented by White assuming that both velocity and density are continuum functions, which means that no empty spaces exist between fluid particles.

$$\frac{\partial \rho}{\partial t} + \frac{\partial}{\partial x}(\rho u) + \frac{\partial}{\partial y}(\rho v) + \frac{\partial}{\partial z}(\rho w) = 0 \qquad (2.1)$$

For steady or unsteady, incompressible flow, the continuity equation is reduced to

$$\frac{\partial u}{\partial x} + \frac{\partial v}{\partial y} + \frac{\partial w}{\partial z} = 0 \tag{2.2}$$

For turbulent, time averaged flow, it becomes

$$\frac{\partial}{\partial x}(\overline{\rho u}) + \frac{\partial}{\partial y}(\overline{\rho v}) + \frac{\partial}{\partial z}(\overline{\rho w}) = 0 \tag{2.3}$$

and

$$\frac{\partial}{\partial x}(\overline{\rho' u'}) + \frac{\partial}{\partial y}(\overline{\rho' v'}) + \frac{\partial}{\partial z}(\overline{\rho' w'}) = 0 \tag{2.4}$$

2.3 Momentum Equation

The conservation of momentum equations are based on the Newton's second law of motion, which states that the net rate of momentum is equal to the net forces acting on a fluid element for a given direction.

x-direction

$$\rho g_x - \frac{\partial P}{\partial x} + \frac{\partial \sigma_{xx}}{\partial x} + \frac{\partial \tau_{yx}}{\partial y} + \frac{\partial \tau_{zx}}{\partial z} = \rho\left(\frac{\partial u}{\partial t} + u\frac{\partial u}{\partial x} + v\frac{\partial u}{\partial y} + w\frac{\partial u}{\partial z}\right) \tag{2.5}$$

y-direction

$$\rho g_y - \frac{\partial P}{\partial y} + \frac{\partial \tau_{xy}}{\partial x} + \frac{\partial \sigma_{yy}}{\partial y} + \frac{\partial \tau_{zy}}{\partial z} = \rho\left(\frac{\partial v}{\partial t} + u\frac{\partial v}{\partial x} + v\frac{\partial v}{\partial y} + w\frac{\partial v}{\partial z}\right) \quad (2.6)$$

2.4 Navier-Stokes Equation for Newtonian Fluid

For a Newtonian fluid, the viscous stresses are proportional to the element strain rates and the coefficient of viscosity. Navier-Stokes state that for incompressible flow, the following relationships are applied.

$$\sigma_{xx} = 2\mu \frac{\partial u}{\partial x} \quad (2.7)$$

$$\sigma_{yy} = 2\mu \frac{\partial v}{\partial y} \quad (2.8)$$

$$\sigma_{zz} = 2\mu \frac{\partial w}{\partial z} \quad (2.9)$$

$$\tau_{xy} = \tau_{xy} = \mu\left(\frac{\partial u}{\partial y} + \frac{\partial v}{\partial x}\right) \quad (2.10)$$

$$\tau_{xz} = \tau_{zx} = \mu\left(\frac{\partial w}{\partial x} + \frac{\partial u}{\partial z}\right) \quad (2.11)$$

For steady flow with constant fluid properties and no body forces, the Navier-Stokes equations can be written as

x-direction

$$\frac{\partial}{\partial x}\rho u^2 + \frac{\partial}{\partial y}\rho uv + \frac{\partial}{\partial z}\rho uw = \frac{-\partial P}{\partial x} + \mu\left(\frac{\partial^2 u}{\partial x^2} + \frac{\partial^2 u}{\partial y^2} + \frac{\partial^2 u}{\partial z^2}\right) \quad (2.12)$$

y-direction

$$\frac{\partial}{\partial x}\rho uv + \frac{\partial}{\partial y}\rho v^2 + \frac{\partial}{\partial z}\rho vw = \frac{-\partial P}{\partial y} + \mu(\frac{\partial^2 v}{\partial x^2} + \frac{\partial^2 v}{\partial y^2} + \frac{\partial^2 v}{\partial z^2}) \quad (2.13)$$

Furthermore, for turbulent, incompressible time-averaged flow, they can reduced to

x-direction

$$u\frac{\partial u}{\partial x} + v\frac{\partial u}{\partial y} + w\frac{\partial u}{\partial z} = \frac{-\partial P}{\rho \partial x} + \vartheta\left(\frac{\partial^2 u}{\partial x^2} + \frac{\partial^2 u}{\partial y^2} + \frac{\partial^2 u}{\partial z^2}\right) - (\frac{\partial \overline{u'^2}}{\partial x} + \frac{\partial \overline{v'u'}}{\partial y} + \frac{\partial \overline{w'u'}}{\partial z}) \quad (2.14)$$

y-direction

$$u\frac{\partial v}{\partial x} + v\frac{\partial v}{\partial y} + w\frac{\partial v}{\partial z} = \frac{-\partial P}{\rho \partial y} + \vartheta\left(\frac{\partial^2 v}{\partial x^2} + \frac{\partial^2 v}{\partial y^2} + \frac{\partial^2 v}{\partial z^2}\right) - (\frac{\partial \overline{u'v'}}{\partial x} + \frac{\partial \overline{v'^2}}{\partial y} + \frac{\partial \overline{w'v'}}{\partial z}) \quad (2.15)$$

The Reynolds-Averaged Navier-Stokes (RANS) equations are solved numerically by using a suitable turbulent model to quantify the turbulence parameters that appeared in the conservation equations above, as will be explained in detail in the following section.

III. CFD MODELLING OF TURBULENT FLOW

3.1 Introduction

This section presents the turbulent flow model based on a Computational Fluid Dynamics (CFD) approach that is used in this study. An overview of the CFD model will be introduced and then followed by a detailed description of each step in the simulation process for the case of turbulent air flow inside ducts. The analysis in this research is carried out with the aid of the "STAR CCM+" commercial software that simulates turbulent in tube flow based on the Finite Volume Method.

3.2 Overview of CFD

Computational Fluid Dynamics (CFD) use numerical methods and algorithms to solve and analyze fluid flow problems. In other words, CFD or numerical solutions are used to predict fluid flow, internal or external, heat transfer, mass transfer, combustion and chemical reactions by solving governing equations using a numerical process. These numerical models can it turn be easily used to predict complicated problems, which in turn saves the time and cost of setting up experiments, collecting data, and analyzing the results.

In the STAR CCM+ software, the CFD code is based on three main stages; pre-processor, solver, and post-processor. The pre-processor stage involves tasks such as geometry modelling, fixing the computational domain, mesh generation, selection of the physical or chemical models, choosing fluid properties, and specifying the appropriate initial and boundary conditions.

In the solver stage, the flow governing equations in the form of partial differential equations (PDE) are numerically discretized and converted to algebraic equations, which are then solved by computers. This numerical discretization process is usually performed by using numerical methods, such as the Finite Difference Method, Finite Element Method, or Finite Volume Method.

The Finite Difference Method (FDM) approximates the flow governing differential equations with difference equations over a given region, and then can be solved by using computer algorithms. On the other hand, the Finite Element Method (FEM) discretizes the region into small elements, and then solves the resulting algebraic equations element by element over the whole region. The Finite Volume Method (FVM) is the most common discretization technique used for solving fluid mechanics problems. FVM divides the computational domain into a fixed control volume, known as cells, such that the variable of interest e.g., velocity or pressure are at the centroid of each cell. Next, the partial differential equations or the flow governing equations are integrated over each control volume, and then the resulting discretized equations are solved by computer algorithms as with other numerical methods.

The post-processor stage is used to process and display the results obtained from the solver. The flow or heat transfer variables, such as velocity, pressure, or heat flux, can be presented in vector plots or contour plots for external or internal flow problems. The CFD solving steps and an overview of the three code-based stages are shown in Figures 5 and 6, respectively.

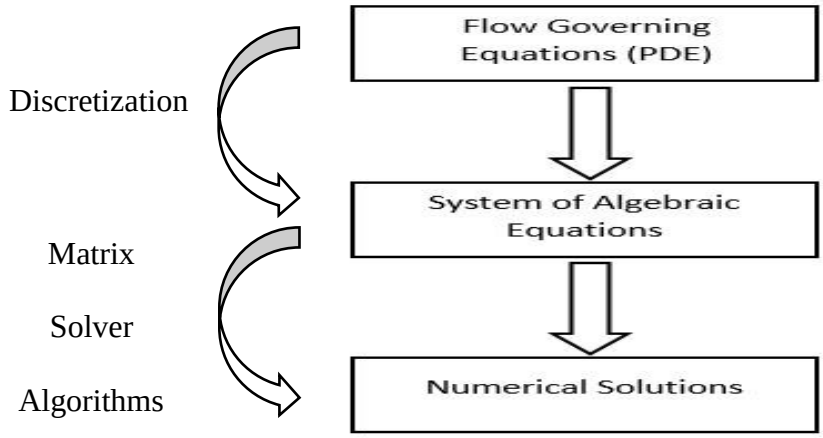

Figure 5. CFD solving steps.

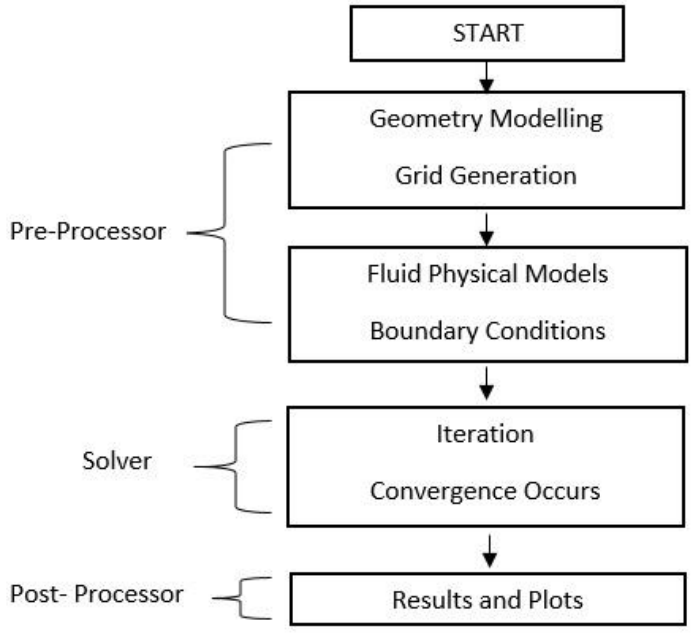

Figure 6. Overview of CFD.

3.3 Mesh Generation

After the geometry has been created in the pre-processor stage, by either using the same CFD software or a CAD software, the geometry or the physical domain is divided into small cells or elements where the flow variables are solved at the centers of these discrete cells. This process of dividing the physical part into smaller cells is known as a mesh generation in CFD process. The quality of the generated mesh has a direct impact on the computational speed, degree of convergence, and the accuracy of the numerical solution.

These generated cells or grids come in different shapes depend on the flow condition, laminar or turbulent, external or internal flow, and the geometry structure. The three-dimensional cell shapes include a tetrahedron, triangular prism, quadrilateral pyramid, and hexahedron.

STAR CCM+ contains different types of meshing models for generating the volume mesh of the geometry, with the selection depending on the flow problem in order to assure the quality of the generated mesh. By the aid of the STAR CCM+ manual available through Steve Portal | Siemens PLM Software, the major types of meshing models in STAR CCM+ are described in the following sections.

3.3.1 Tetrahedral Mesh

The tetrahedral Mesh model provides an efficient and simple solution for many complex mesh generation problems using the tetrahedral cell shape to build the mesh core that can produce the fastest mesh model for the computation process, and the one that uses the least amount of memory. However, only few applications are suggested for use of this mesh model.

3.3.2 Polyhedral Mesh

The polyhedral Mesh model is easy, efficient to build, and requires approximately five times fewer cells compared to the tetrahedral mesh model. Moreover, it is more numerically stable, less diffusive, and more accurate than an equivalent tetrahedral mesh. The model uses an arbitrary polyhedral cell shape to build the core mesh, and it requires almost the same amount of surface preparation as the tetrahedral Mesh model.

3.3.3 Trimmed Mesh

The trimmed mesh provides a simple and efficient method for producing a high quality mesh for both simple and complicated geometries, and it is recommended when the surface quality of the geometry is not good enough to use a polyhedral mesh. It uses a trimmed hexahedral cell shape to build the core mesh, and it is known to have the ability to refine cells in a wake region, which makes this model ideal for use in external aerodynamic applications.

3.3.4 Thin Mesher

A thin mesher model is typically used to generate a prismatic layered volume mesh for thin areas or regions within the geometry so that the high quality cells can capture the solid material thickness adequately.

3.3.5 Prism Layer Mesher

The prism layer mesher cells are created next to the wall boundaries in order to accurately capture the near wall velocity profile and temperature profile in turbulent flow applications and also to predict the flow variables such as pressure drop, laminar

and turbulent shear stresses, and turbulent viscosity. Although the prism layer mesher is an optional model, it is strongly recommended to be used in internal turbulent flow applications.

Two properties are usually required to quantify when the prism layer mesh model is used; the thickness of the prism layer and the number of the prism layers. The thickness of the prism layers determines the height of these layers and it can be either a relative thickness to the base mesh size or an absolute thickness with a length unit.

The number of the prism layers property, as the name suggests, sets the number of prism layers needed for a given volume mesh.

3.4 Fluid Physical Models

After the geometry has been created and meshed by using an appropriate mesh model, the fluid physical models have to be chosen prior to specify the boundary conditions and running the simulation. Table 1 below summarizes the main physical models available in STAR CCM+ software.

Table 1 List of all fluid physical models available in STAR CCM+

Category	Available Physical Models
Flow Characteristics	Inviscid, laminar, or turbulent
	Newtonian and Non-Newtonian viscosities
	Incompressible and compressible
	Multiphase mixtures
	Porous resistance
	Gravitational acceleration
	Passive scalars
Space	Axisymmetric
	Shell three dimensional
	Three dimensional
	Two dimensional
Time	Explicit unsteady
	Harmonic balance
	Implicit unsteady
	Steady
Material	Gas
	Liquid
	Solid
	Multi-component (gas, liquid, solid)
	Multi-phase
Flow	Coupled flow (gas, liquid)
	Segregated flow (gas, liquid)
	Viscous flow (liquid)
Equation of State	Constant density (gas, liquid)
	Polynomial density (gas, liquid)
	Ideal gas (gas)
	Real gas (gas)
	User defined (gas, liquid)
Turbulence Models	K-Epsilon turbulence
	K-Omega turbulence
	Reynolds stress turbulence
	Spalart-Allmaras turbulence
Other Optional Models	Segregated fluid temperature
	Segregated fluid enthalpy
	Mesh deformation
	Exact wall distance
	Cell quality remediation
	Turbulence suppression
	Two-layer all y+ wall treatment (k-epsilon model)
	All y+ wall treatment (k-omega model)

3.5 Turbulence Models

The turbulence modelling task is basically the selection of a certain turbulence model to predict the turbulence effects within the fluid flow, which is an inexact representation of the physical phenomena in the flow. In other words, turbulence models are used to model the additional turbulence terms that appeared in the Navier-Stokes equations rather than solving them directly. Over the past few decades, a large number of turbulence models have been introduced in order to solve the turbulent flow problems that exist in most engineering applications. As with most commercial CFD codes, the STAR CCM+ software uses Reynolds-Averaged Navier Stokes (RANS) based turbulence models for modelling turbulent flow problems.

The RANS model classifications are based on the number of partial differential equations being solved, namely zero equation models, one equation models, two-equation models, and seven-equations models as presented below.

3.5.1 Zero-Equation Model

As the name suggests, the zero-equation turbulence model uses only algebraic equation, and no partial differential equations to describe the transport of the turbulent stresses. These algebraic models are fast and easy to implement, but they are limited in use to simple turbulent flow problems. Furthermore, they use mixing length theory to express the kinematic turbulent viscosity, as following

$$\vartheta_t \propto v\, l$$

Assuming the velocity scale is proportional to the length scale and shear stress (e.g., velocity gradient), the result is

$$v \propto l\, \frac{\partial u}{\partial y}$$

Using Prandtl's mixing length theory (1925), the kinematic turbulent viscosity can be expressed as

$$\vartheta_t = {l_m}^2 \frac{\partial u}{\partial y} \tag{3.1}$$

where,

$$l_m = \kappa y \text{ , for } y < \delta \tag{3.2}$$

$$l_m = \delta, \text{ for } y \geq \delta \tag{3.3}$$

This model is frequently ignored in CFD commercial software due to its limited usage in engineering practice, as it cannot describe the turbulent flow when the turbulent length scale varies. Also, it only calculates the mean flow variable, regardless of the fluctuation in the flow, and it cannot describe the flow when circulation or separation occurs.

3.5.2 One-Equation Model

Unlike the zero-equation model described above, the one equation turbulence model solves a single transport partial differential equation for turbulent kinetic energy with the turbulent length scale obtained from an algebraic expression and the turbulent viscosity expressed in term of kinetic energy. There are several models that are one equation based, such as the Prandtl's one-equation model, the Baldwin-Barth model, and the Spalart-Allmaras model.

By assuming the velocity scale is proportional to the square root of kinetic energy, the kinematic turbulent viscosity can be express as

$$v \propto \sqrt{K}$$

$$\vartheta_t = l_m \sqrt{K} \tag{3.4}$$

A general form of the one-equation model with kinetic energy (diffusion, production, and dissipation terms) can be expressed as

$$u_i \frac{\partial K}{\partial x_i} = \frac{\partial}{\partial x_i}\left[\left(\vartheta + \frac{\vartheta_t}{\sigma_k}\right)\frac{\partial K}{\partial x_i}\right] + \vartheta_t\left(\frac{\partial U_j}{\partial x_i} + \frac{\partial U_i}{\partial x_j}\right)\frac{\partial u_j}{\partial x_i} - C_D\frac{K^{3/2}}{l_m} \tag{3.5}$$

Although the one-equation turbulence model is more accurate than the zero-equation model, especially in capturing the separation and recirculation phenomena, it is still considered weak for use with many complex internal flow applications and massively separated flows.

3.5.3 Two-Equation Models

Due to the lack of accuracy of the zero-equation and one-equation turbulence models in simulating internal flow, more advanced two-equations turbulence models have been introduced, and they have been successfully used in many turbulent flow applications. Most CFD software use transport equations based on two main models, namely the $k-\epsilon$ and $k-\omega$ models.

The $k-\epsilon$ model (Versteeg and Malalasekera, 2007) uses two partial differential equations to describe turbulence effects; one for the turbulent kinetic energy (k), and the

other for the turbulent dissipation rate (ϵ). The turbulent viscosity can be express as a function of k and ϵ as follow

$$\mu_t = C_u \frac{k^2}{\epsilon} \tag{3.6}$$

The resulting k equation model is

$$\frac{\partial k}{\partial t} + u_j \frac{\partial k}{\partial x_j} = \frac{\partial}{\partial x_j}\left(\frac{\vartheta_t}{\sigma_k}\frac{\partial k}{\partial x_j}\right) + \vartheta_t \frac{\partial u_j}{\partial x_i}\left(\frac{\partial u_j}{\partial x_i} + \frac{\partial u_i}{\partial x_j}\right) - \varepsilon \tag{3.7}$$

and the ϵ equation model is

$$\frac{\partial \varepsilon}{\partial t} + u_j \frac{\partial \varepsilon}{\partial x_j} = \frac{\partial}{\partial x_j}\left(\frac{\vartheta_t}{\sigma_\epsilon}\frac{\partial \epsilon}{\partial x_j}\right) + C_{\epsilon,1}\frac{\epsilon}{k}\left[\vartheta_t \frac{\partial u_j}{\partial x_i}\left(\frac{\partial u_j}{\partial x_i} + \frac{\partial u_i}{\partial x_j}\right)\right] + C_{\epsilon,2}\frac{\varepsilon^2}{k} \tag{3.8}$$

To avoid some issues associated with the $k-\epsilon$ model above, such as lack of accuracy in simulating the near the wall region , the $k-\omega$ model (Wilcox,2008) is usually used in many internal flow applications. This model accurately predicts the flow behavior in the viscous sublayer region as well as the fully turbulent layer away from the wall. Similar to the $k-\epsilon$ model, the $k-\omega$ model solves for turbulent kinetic energy of the flow (k) and the specific rate of dissipation of kinetic energy (ω).

The resulting k equation model is

$$\frac{\partial k}{\partial t} + \frac{\partial (u_j k)}{\partial x_j} = P - \beta^* \omega k + \frac{\partial}{\partial x_j}\left[\left(\vartheta + \sigma_k \frac{k}{\omega}\right)\frac{\partial k}{\partial x_j}\right] \tag{3.9}$$

while the ω equation model is

$$\frac{\partial \omega}{\partial t} + \frac{\partial (u_j \omega)}{\partial x_j} = \frac{\gamma \omega}{k} P - \beta \omega^2 + \frac{\partial}{\partial x_j}\left[\left(\vartheta + \sigma_w \frac{k}{\omega}\right)\frac{\partial \omega}{\partial x_j}\right] + \frac{\sigma_d}{\omega}\frac{\partial k}{\partial x_j}\frac{\partial \omega}{\partial x_j} \qquad (3.10)$$

3.6 Boundary Conditions

After selecting the appropriate fluid models and choosing an accurate turbulence model for the CFD problem of interest, the boundary conditions of the problem have to be specified in order to solve the partial differential equations. If the problem is solved by using the unsteady solver, initial conditions are required as well.

For internal turbulent flow problems solved by the STAR CCM+ software, three main types of boundary conditions are entered; inlet boundary conditions, outlet boundary conditions, and wall boundary conditions, as shown in Table 2.

Table 2 Summary of the inlet and outlet boundary conditions of the flow

Type of BC	**Inlet Boundary Conditions**		**Outlet Boundary Conditions**	
Flow Parameters	Velocity (V_{in})	Pressure (P_{in})	Velocity (V_{out})	Pressure (P_{out})
Turbulence Parameters	Turbulent viscosity ($\mu_{t_{in}}$)		Turbulent viscosity ($\mu_{t_{out}}$)	
	Turbulence Intensity (TI_{in})		Turbulence Intensity (TI_{out})	
	Turbulence length scale (l_{in})		Turbulence length scale (l_{out})	

As shown in Table 2, adiabatic turbulent internal fluid flow problems with an isothermal surface temperature require that a total of six boundary conditions be specified in order to solve the continuity and Navier-Stokes partial differential equations. The flow boundary required can be either 1.) an inlet velocity vector (or a magnitude value) with an outlet gauge pressure value or 2.) an inlet gauge pressure value with an outlet flow velocity. For the turbulence boundary conditions, a turbulence intensity is required at the inlet and outlet of the duct, in addition to either a turbulent viscosity or a turbulence length scale at the duct inlet and outlet. For the wall boundary conditions, the assumption of a no-slip condition is applied such that $u|_{r=R} = 0$

3.7 Turbulence Parameters

In STAR CCM+, turbulence effects in the fluid flow can be quantified by the turbulence intensity of the flow at a given Reynolds number and either a turbulence length scale for a given duct size or a turbulent viscosity based on the chosen turbulent model.

3.7.1 Turbulence Intensity

Turbulence Intensity (TI) is used to quantify the degree of the turbulence of the flow. It is defined as the ratio of the Root Mean Square (RMS) of the fluctuating velocity at a given location of the flow divided by the average flow velocity at the same location for a specified period of time.

$$TI = \frac{u'}{\bar{u}} \tag{3.11}$$

In internal flow problems, turbulence intensity varies along the duct length as the turbulence level is continuously changing and, therefore, in a CFD simulation, it is necessary to specify this turbulence quantity at the inlet and in the fully developed region where the quantity becomes constant. At the inlet, turbulent intensity is mainly dependent on the upstream history and condition of the flow prior entering the duct. For example, if the flow entering the duct comes from a turbine or a compressor or other complex rotating machinery, the inlet turbulence intensity can range from 5% to a maximum of 20%. For moderate applications, like flow comes from large pipes or air handling units in HVAC, the turbulence intensity can be assumed to be between 1% and 5%. For low turbulence applications, such as the external flow across cars or flow in small tubes, the turbulence intensity is assumed to be less than 1%. (Schlichting,2000)

For the fully developed region of the duct, the turbulence intensity is mainly a function of Reynolds number. By using the classical solutions for developed flow inside ducts, the fully developed turbulence intensity can be estimated by using the following empirical correlation (Schlichting,2000)

$$TI_{FD} = 0.16\, Re_D{}^{\left(-\frac{1}{8}\right)} \tag{3.12}$$

3.7.2 Turbulence Length Scale

The turbulence length scale (l) quantity is used to describe the size of the large eddies that contain the turbulent energy in turbulent flow and frequently used as a boundary condition in internal turbulent flow simulations.

Based on the turbulence model used, experimental correlations have been developed to quantify the turbulence length scale quantity for different turbulent flow applications. In the case of duct flow and by using two-equation turbulence models, it is reasonable to assume a turbulence length of 7% of the duct diameter for moderate turbulent flow applications. (Schlichting,2000)

3.7.3 Turbulent Viscosity

The turbulent viscosity or eddy viscosity (μ_t) quantifies the transfer of momentum caused by the turbulent eddies in the flow. As shown in a previous section, each turbulent model quantifies the turbulent viscosity differently, and then once determined, it can be used as a boundary condition value of the flow and/or in calculating the Reynolds stresses of the flow.

3.8 Convergence

After setting the boundary conditions for the CFD problem, initial values, or guesses, entered by the user for the mean inlet velocity or pressure, outlet velocity or pressure, and the turbulence parameters at the duct inlet and outlet. The CFD solver starts the solving process by varying and iterating the initial conditions of the flow and by using the entered inlet and outlet boundary conditions to find a numerical solution for the partial differential equations of the flow. As the software approaches a solution, the simulation is converged. On the other hand, when a poor mesh quality is used or a wrong physical model is implemented, the software deviates away from the solution, and the simulation in such cases is diverged.

The solution residuals are one of the most fundamental measures of convergence in CFD simulations as they directly evaluate the solution errors associated with the flow variables in each control volume. As a result, each control volume will have a residual value for each of the partial differential equations being solved. In STAR CCM+, these residual values can be observed by using the residual plot in the solution window as shown in Figure 7.

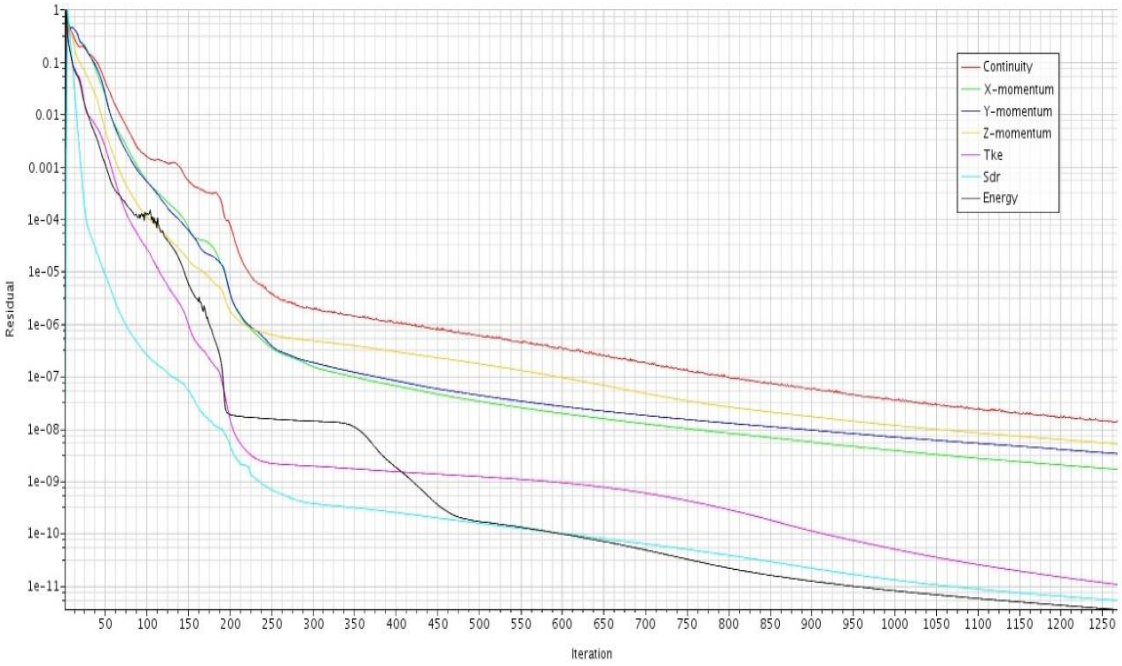

Figure 7. Residual plot window in STAR CCM+.

As shown in Figure 7 above, the residual values decrease with iterations until they finally reach smaller values of errors as the solution is converged. However, one should know that a converged solution does not necessarily mean that it is correct. The user has to use engineering knowledge along with comparing the solution to other analytical and experimental results in order to validate the numerical model.

3.9 Summary

This section has shown how numerical solutions are calculated by using the STAR CCM+ CFD software. Sections that follow will present solution steps for different duct geometries, and the resulting velocity and pressure profiles will be analyzed and developing length correlations will be formulated based on these profiles.

IV. ROUND DUCT CASE

4.1 Introduction

This section introduces the numerical modelling and CFD analysis by focusing on a round geometry of internal turbulent flow in ducts. Since a uniform inlet flow inside a round duct is considered the simplest internal flow cases, it makes sense to numerically investigate and analyze it first and then follow with other duct geometries such as square and rectangular ducts, which will be covered in later sections. In this section, CFD models of different round duct diameters with different uniform inlet velocities are simulated for the purpose of studying the flow behavior in the developing region of the duct. One can then identify the parameters affecting the fully developed flow condition while deriving numerical correlations to locate the position where fully developed flow is achieved inside the round ducts, based on both velocity and pressure profiles.

4.2 Problem Description

- The working fluid is air at room temperature and atmospheric pressure with thermophysical properties presented in Table 3.

Table 3 Thermophysical properties of air in round ducts

Thermophysical Property	Value
$\boldsymbol{T}(\mathbf{K})$	300
$\boldsymbol{\mu}\ (\frac{\mathbf{Kg}}{\mathbf{m.s}})$	1.84×10^{-5}
$\boldsymbol{\rho}\ (\frac{\mathbf{Kg}}{\mathbf{m^3}})$	1.18

- Three ducts dimeters were chosen to represent a range of practical applications; 0.2 m, 0.4 m, and 0.6 m.
- Air enters the channel at different uniform velocities representing a range used in actual engineering practice and design; 3 m/s, 6 m/s, and 9 m/s.
- Assumptions applied to this analysis are
    - Steady incompressible flow.
    - Smooth stainless steel round ducts.
    - Negligible gravity effects on fluid flow.
    - Round duct is completely filled with the fluid being transported.

4.3 Modelling and Simulation

The round duct geometry was created by using SOLIDWORKS software, and then imported to the STAR CCM+ CFD commercial software in order to simulate the fluid flow. As explained earlier, STAR CCM+ uses a control volume based finite volume method to solve the coupled, non-linear partial differential governing equations for the fluid as shown in Figure 8 below.

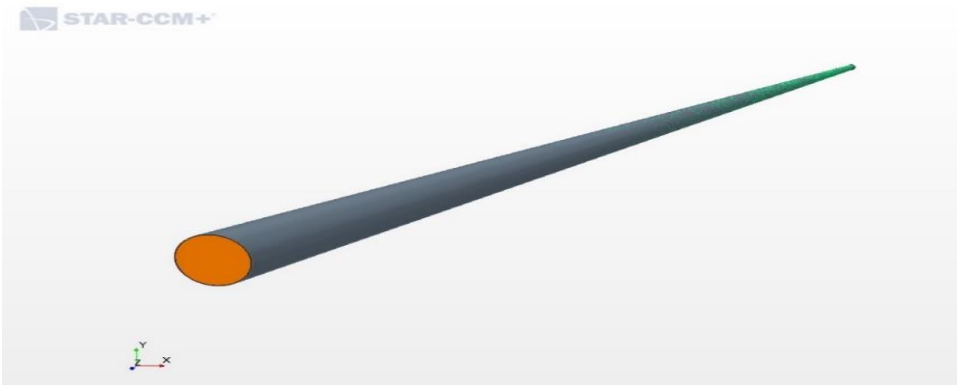

Figure 8: Computational domain of round duct flow.

4.3.1 Mesh Generation

The first step in the CFD simulation of the fluid flow is to generate a mesh, or grid, that represents the duct geometry. In order to do so, the below mesh models were chosen in STAR CCM+ to most accurately simulate the turbulent fluid flow inside the round duct.

- Surface Remesher.
- Polyhedral Mesher.
- Embedded Thin Mesher.
- Prism Layer Mesher.

By following the user guide in STAR CCM+ for pipe flow applications, the geometry mesh base size is selected as 5 cm with a surface growth rate of 1.7. Also, two layers of the thin mesh model and nine layers of prism mesh are applied for all pipe sizes. Table 4 below summarizes all of the selected mesh parameter values.

Table 4 Summary of mesh parameter values used in round duct models

Mesh Parameters	**Input Value**
Base Size	0.05 m
Number of Prism Layers	9
Surface Growth Rate	1.7
Thin Mesh Layers	2
Relative Maximum Size	40
Relative Minimum Size	60

For the prism layer mesh model, the prism layer absolute thickness and the near wall thickness values are selected for each pipe size in order to accurately capture the near wall velocity profiles and viscous sublayer of the turbulent flow. The absolute prism layer thickness values selected are 8.903 mm, 13.35 mm, and 17.80 mm for pipe sizes

of 0.2 m, 0.4 m, and 0.6 m respectively. Moreover, the near wall prism layer thickness values selected are 0.053 mm, 0.079 mm, and 0.106 mm for pipe sizes of 0.2 m, 0.4 m, and 0.6 m, respectively. Table 5 below lists the prism layer thickness values for all pipe sizes. Once the volume mesh was generated, the overall number of cells was found to be 1,781,788 cells for the 0.2 m diameter pipe, 2,147,000 cells for the 0.4 m diameter pipe, and 4,049,269 cells for the 0.6 m diameter pipe, as tabulated in Table 5 and plotted in Figures 9 through 11.

Table 5 Detailed prism layer mesh specifications and overall cells number for all of the round duct sizes

Pipe Diameter (m)	Prism Layer Absolute Thickness (mm)	Thickness of Near Wall Prism Layers (mm)	Overall Number of Cells
D=0.2	8.903	0.053	1,781,788
D=0.4	13.35	0.079	2,147,000
D=0.6	17.80	0.106	4,049,269

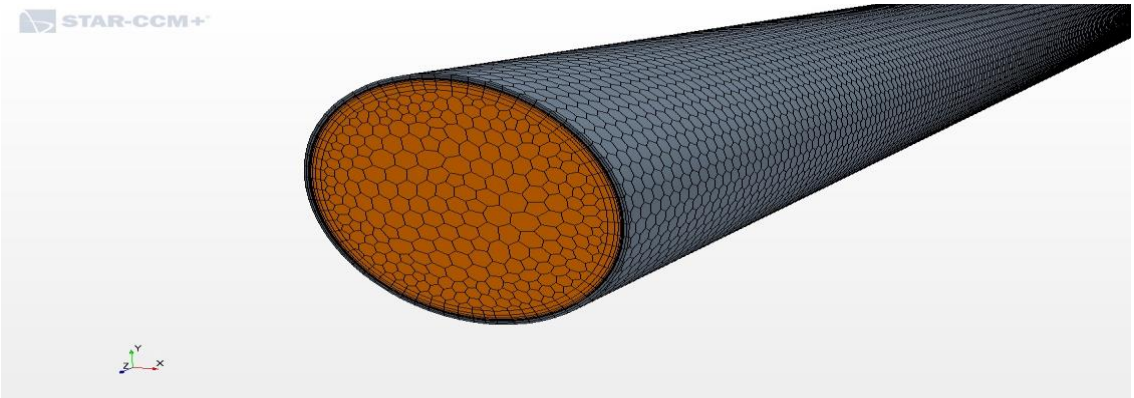

Figure 9. Generated volume mesh for a round pipe of $d = 0.2$ m.

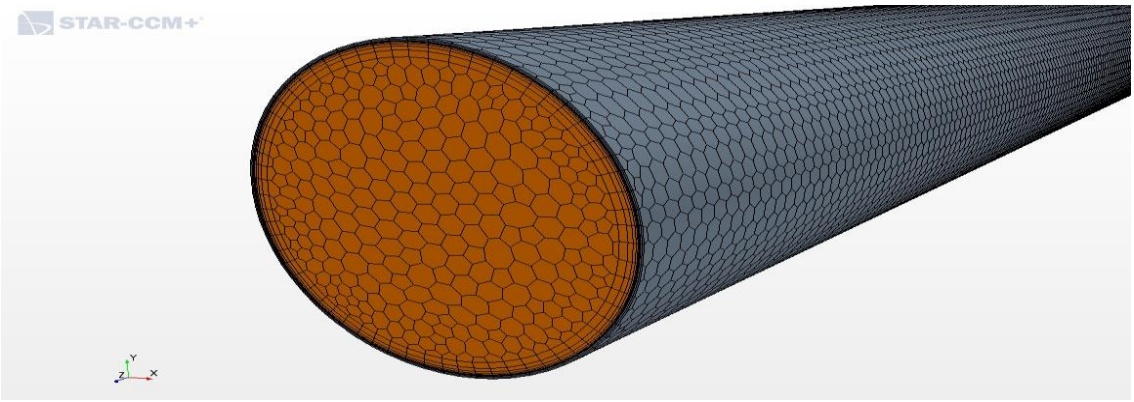

Figure 10. Generated volume mesh for a round pipe of $d = 0.4$ m.

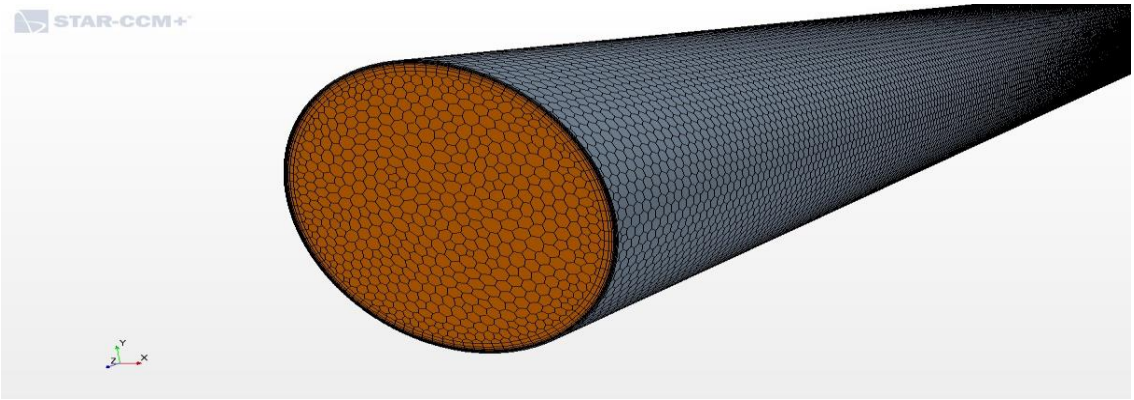

Figure 11. Generated volume mesh for a round pipe of $d = 0.6$ m.

4.3.2 Fluid Physical Properties

Once the mesh or grid was established for each pipe size, the next step was to choose the appropriate physical models to accurately simulate the fluid flow. By following the STAR CCM+ user guide, the fluid physical models recommended to use for the internal turbulent flow simulation are as follows:

- Constant density Air.
- Three dimensional steady flow.
- Turbulent Flow.
- K − ω Turbulence Model.
- All $y+$ wall treatment.
- Reynolds-Averaged Navier-Stokes.
- Segregated Flow Model.
- Turbulence Suppression Transition Model.
- Cell Quality Remediation.

4.3.3 Boundary Conditions

The next step was to identify and specify the appropriate boundary conditions of the flow at the duct inlet, $\frac{L}{D}$ of 0, and exit, $\frac{L}{D}$ of 100, with the exit being an arbitrary chosen value that assured achieving the fully developed flow in all cases. For all duct sizes, the flow was assumed to enter with uniform flow velocities of 3 m/s, 6 m/s, and 9 m/s. The duct is considered long enough to assume atmospheric pressure at the duct outlet, which corresponds to zero gage pressure.

In this analysis, the turbulence parameters are quantified by the turbulent intensity of the flow and the turbulence length scale. At the inlet, the turbulence intensity is mainly a function of the upstream history of the flow and the nature of the flow application. For moderate flow applications such as HVAC air flow, is it reasonable to assume 5% inlet turbulence intensity as mentioned earlier. However, at the exit in the fully developed region, the turbulent intensity is usually estimated by using Equation (3.12) below

$$TI_{FD} = 0.16\, Re_D^{\left(-\frac{1}{8}\right)} \tag{3.12}$$

For the turbulence length scale, which is a quantity related to the size of large eddies that contain the turbulent energy, the following relation may be used as an approximation in the fully developed region of the flow

$$l_{FDF} = 0.07 * D_h \tag{4.1}$$

In addition to the inlet and outlet boundary conditions, a stationary wall boundary condition, namely a no-slip assumption, is applied at the wall of the round duct, such that the velocity increases from zero at the wall to a maximum velocity in the middle of the duct. A symmetry boundary condition is applied on the other side of the round duct to accelerate the computation process. Moreover, for this model, a wall function method is used for the near wall treatment in order to accurately simulate the flow inside the round duct, as shown in Figure 12 and Tables 6 through 9 below.

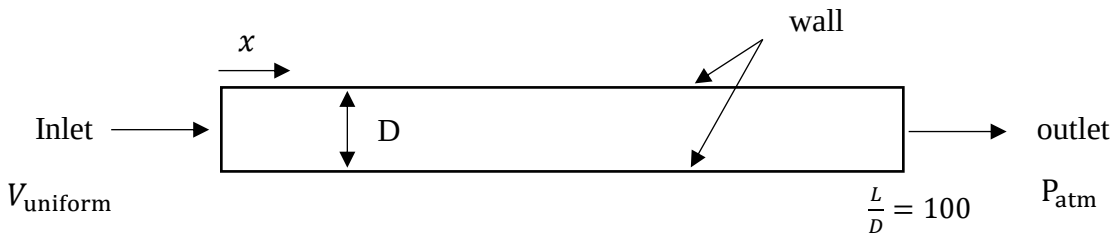

Figure 12. Types of boundary conditions used in round duct models.

Table 6 Summary of boundary conditions for all round duct sizes

Uniform Inlet Velocity (m/s)	3, 6 , 9
Outlet gauge Pressure (Pa)	Zero

Table 7 Summary of turbulence parameters boundary conditions for round duct of $d =$ 0.2 m

Turbulence Parameters	V= 3m/s	V= 6m/s	V= 9m/s
TI_{in} **(Intensity)**	5%		
l_{in} **(Length scale)**	0.02 m		
TI_{FD} **(Intensity)**	4.3%	3.9%	3.7%
l_{FD} **(Length scale)**	0.014 m		

Table 8 Summary of turbulence parameters boundary conditions for round duct of $d =$ 0.4 m

Turbulence Parameters	V= 3m/s	V= 6m/s	V= 9m/s
TI_{in} **(Intensity)**	5%		
l_{in} **(Length scale)**	0.031 m		
TI_{FD} **(Intensity)**	3.9%	3.6%	3.4%
l_{FD} **(Length scale)**	0.028 m		

Table 9 Summary of turbulence parameters boundary conditions for round duct of $d =$ 0.6 m

Turbulence Parameters	V= 3m/s	V= 6m/s	V= 9m/s
TI_{in} **(Intensity)**	5%		
l_{in} **(Length scale)**	0.05 m		
TI_{FD} **(Intensity)**	3.7%	3.4%	3.2%
l_{FD} **(Length scale)**	0.042 m		

4.4 Results and Discussion

After the simulations have been set up for all nine round duct models, consisting of three different duct sizes with three different uniform inlet velocities, STAR CCM+ was used to determine velocity and pressure profiles for each case. Then, by using these plots, velocity gradient profiles dv/dx and pressure gradient profiles dp/dx were developed

as function of dimensionless duct length $\left(\frac{L}{D}\right)$ for each Reynolds number case, which is a necessary step to locate where the fully developed flow occurs.

The criteria used to define where the fully developed flow is reached inside the ducts is to assume that the flow will be fully developed where the (dv/dx) value is around 99% of the fully developed region (dv/dx),which is $(dv/dx)_{FD}$ equals to 0. Similarly, by using the pressure gradient profiles, the flow is assumed to be fully developed where (dp/dx) reaches 99% of the (dp/dx) in the fully developed region, assuming that $(dp/dx)_{FD}$ is constant.

For the round duct size of 0.2 m, by using the above approach and criteria, the dimensionless developing length $(L/D)_{FD}$ found to be 27 with the lowest inlet velocity of 3 m/s, 31.3 with 6 m/s, and 34 with the highest velocity of 9 m/s. As for the round duct of 0.4 m diameter, the dimensionless developing length $(L/D)_{FD}$ was 31.3 with a velocity of 3 m/s, 36 with a velocity of 6 m/s, and 39 with a $9\ \mathrm{m/s}$ velocity. For the largest duct size of 0.6 m, the dimensionless developing lengths $(L/D)_{FD}$ are $34, 39,$ and 43.5 for flows with inlet velocities of $3\ \mathrm{m/s}, 6\ \mathrm{m/s}$, and $9\ \mathrm{m/s}$, respectively.

The above results show that the dimensionless developing lengths $\left(\frac{L}{D}\right)_{FD}$ increase with the increasing Reynolds number of the flow, while it remains almost constant with different flow velocities and duct sizes that share an identical Reynolds number. These results are presented in both tabular and graphical forms in Table 10 and Figures 13 through 18.

Table 10 Summary of dimensionless developing length $(L/D)_{FD}$ for all round duct cases based on velocity profiles with their corresponding Reynolds numbers

V-based Profile	v= 3m/s		v= 6m/s		v= 9m/s	
D (m)	Re	$(L/D)_{FD}$	Re	$(L/D)_{FD}$	Re	$(L/D)_{FD}$
0.2	38,480	27	76,960	31.3	115,430	34
0.4	76,960	31.3	153,910	36	230,870	39
0.6	115,430	34	230,870	39	346,300	43.5

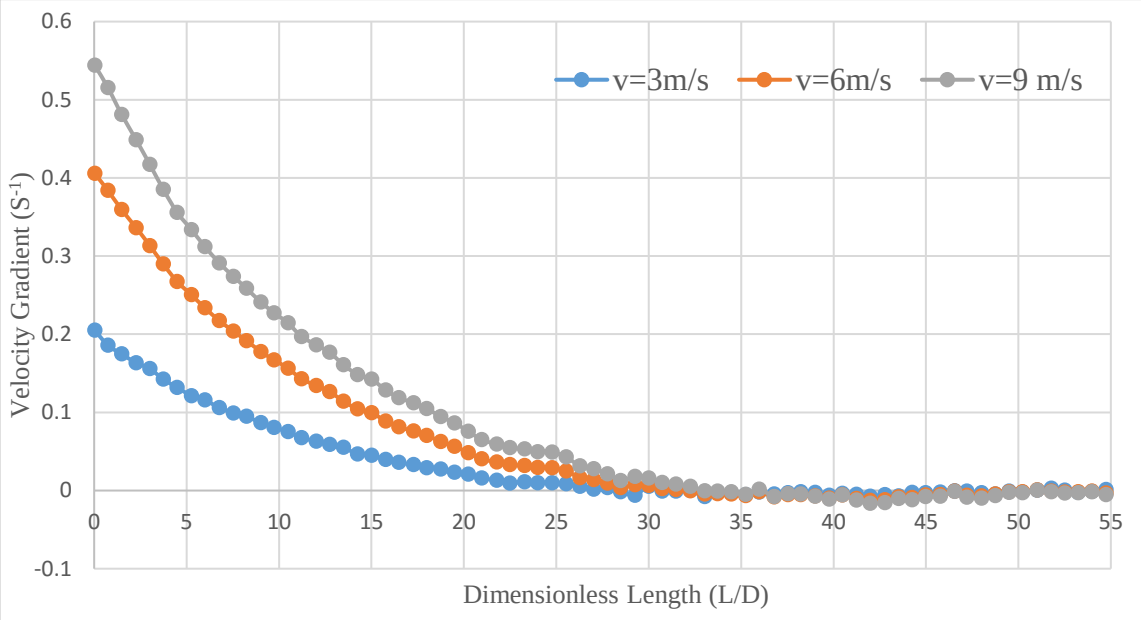

Figure 13. Velocity gradient profiles in a round duct with $d = 0.2$ m for different uniform inlet velocities.

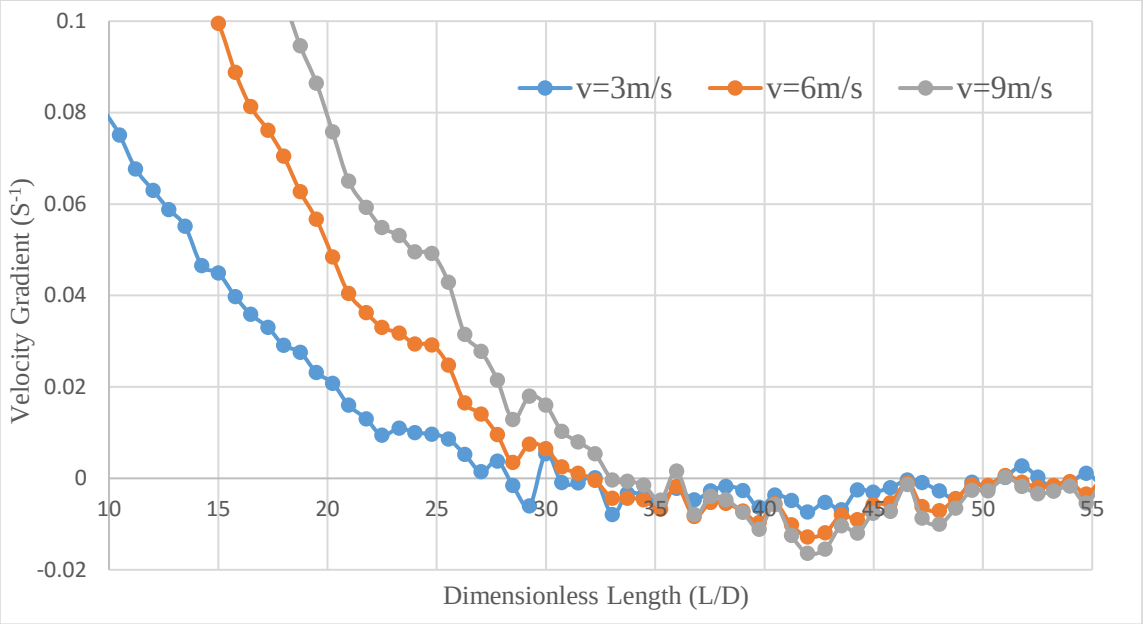

Figure 14. Enlarged velocity gradient profiles in a round duct with $d = 0.2$ m for different uniform inlet velocities.

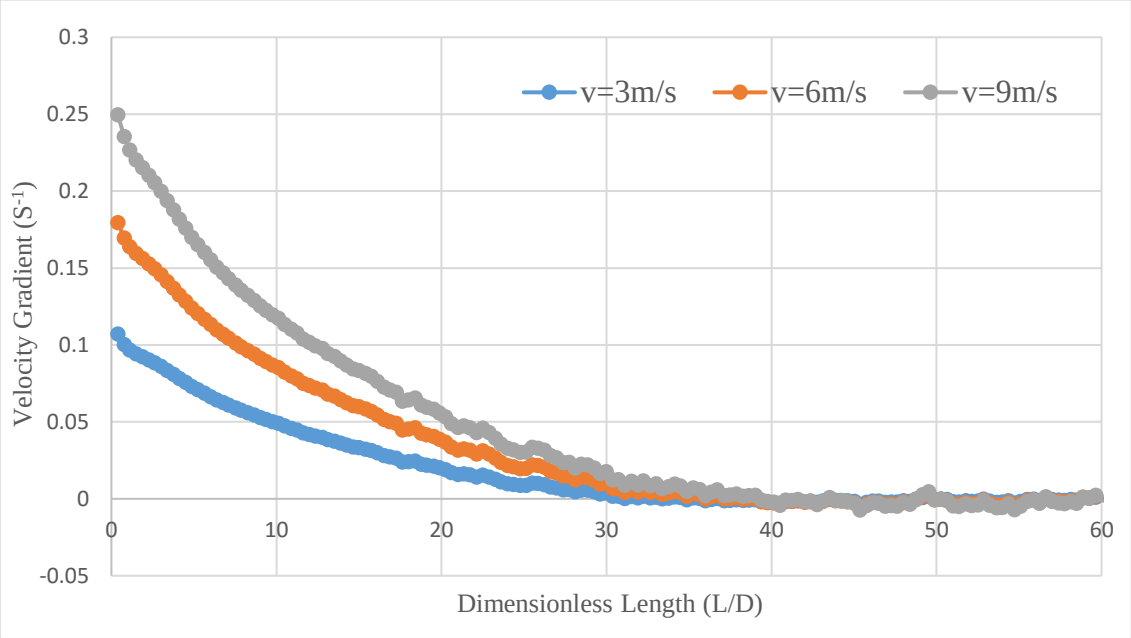

Figure 15. Velocity gradient profiles in a round duct with $d = 0.4$ m for different uniform inlet velocities.

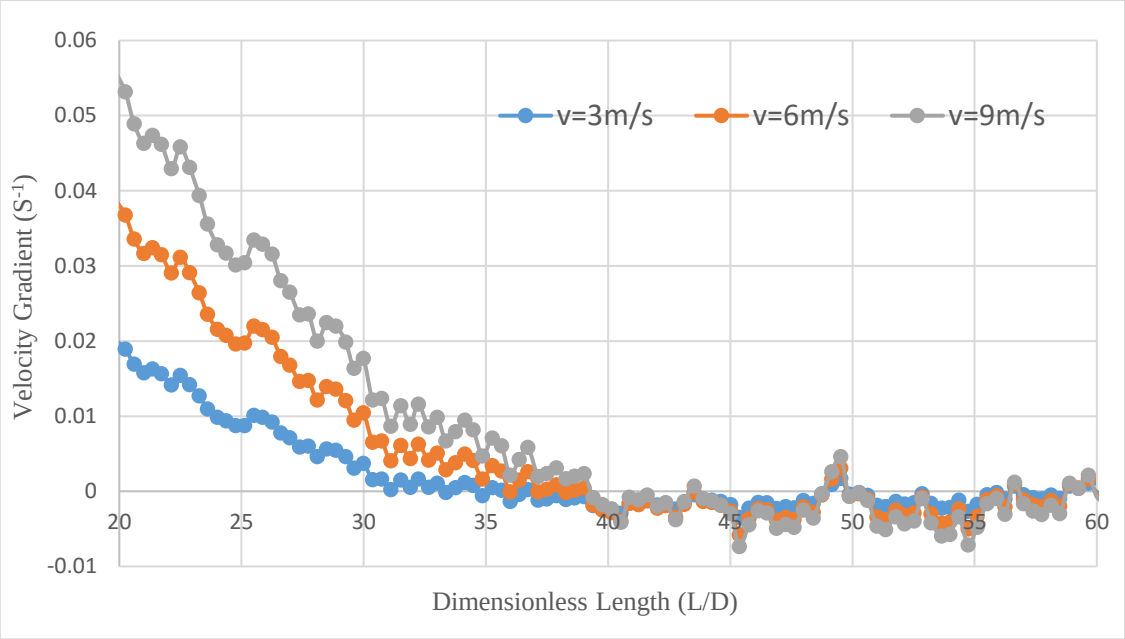

Figure 16. Enlarged velocity gradient profiles in a round duct with $d = 0.4$ m for different uniform inlet velocities.

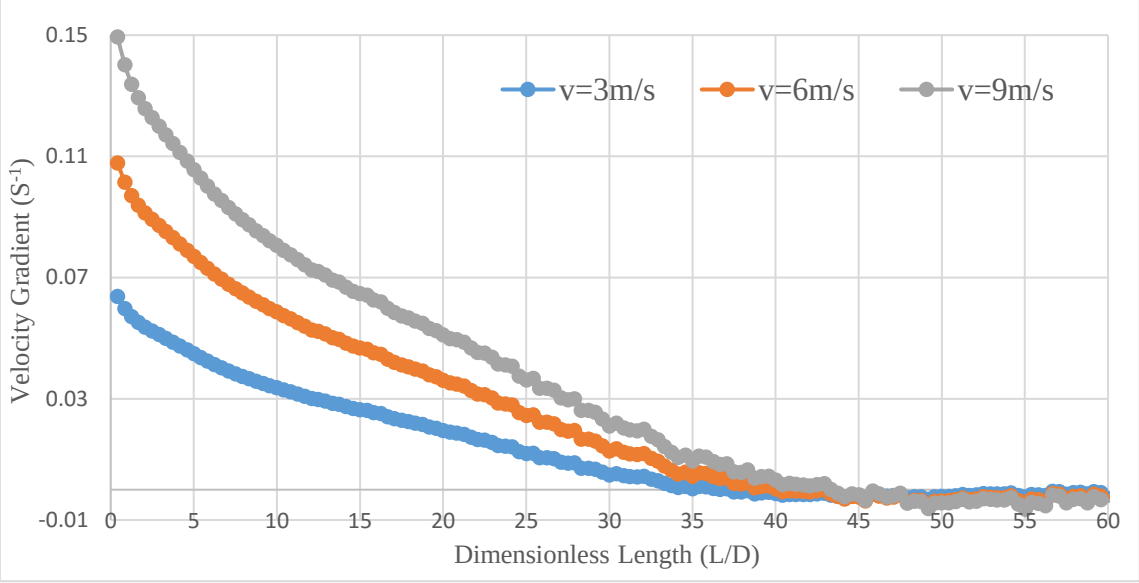

Figure 17. Velocity gradient profiles in a round duct with $d = 0.6$ m for different uniform inlet velocities.

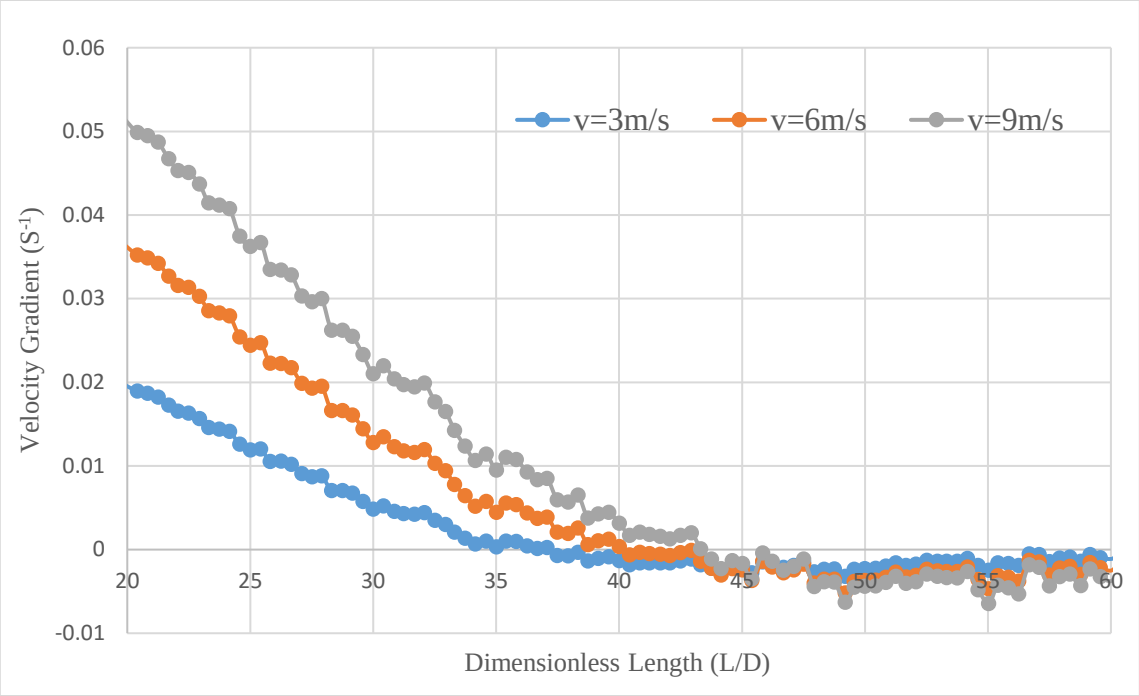

Figure 18. Enlarged velocity gradient profiles in a round duct with $d = 0.6$ m for different uniform inlet velocities.

The above $\left(\frac{L}{D}\right)_{FD}$ results are plotted as function of Reynolds number for each case as shown in Figure 19, and then by using a curve fitting procedure, a velocity-based CFD correlation for the fully developed flow location is developed for room temperature air flowing inside a round duct.

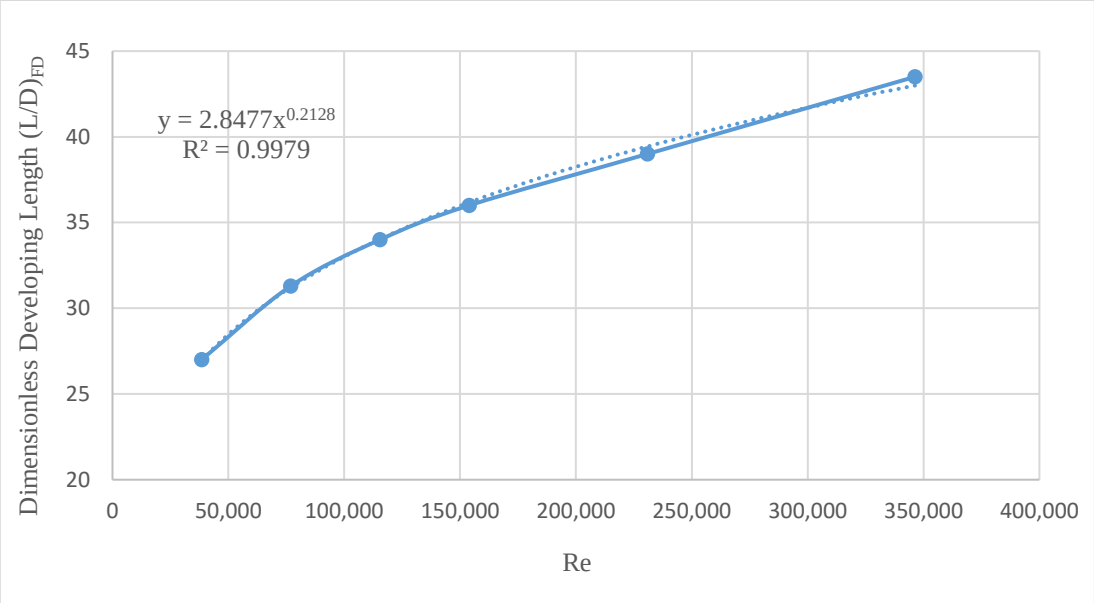

Figure 19. Curve fitting profile (velocity-based correlation) of round duct.

The resulting correlation based on the curve fitting can be expressed as

$$(\frac{L}{D})_{FD_V} = 2.8477 * Re^{0.2128} \quad (4.2)$$

A similar analysis based on the pressure profiles was carried out to investigate the developing length and then compared to the velocity based results at each flow Reynolds number. By using the fully developed flow criteria mentioned earlier, the dimensionless developing length $\left(\frac{L}{D}\right)_{FD}$ based on pressure gradient profiles was found to be 21 with an inlet velocity of 3 m/s, 26 with an inlet velocity of 6 m/s, and 29 with the highest velocity of 9 m/s for the round duct size with 0.2 m diameter.

For the round duct with 0.4 m, the dimensionless developing length $\left(\frac{L}{D}\right)_{FD}$ was 26 with an inlet velocity of 3 m/s, 31 with an inlet velocity of 6 m/s, and 36 with a 9 m/s velocity. For the largest round duct size with 0.6 m, the dimensionless developing lengths $\left(\frac{L}{D}\right)_{FD}$ are 29 , 36, and 38.7 for uniform flow velocities of 3 m/s, 6 m/s, and 9 m/s, respectively.

Similar to the velocity analysis, the results show that the pressure-based dimensionless developing lengths $\left(\frac{L}{D}\right)_{FD}$ increase with increasing Reynolds number of the flow, while it remains almost constant with different flow velocities and duct sizes that share an identical Reynolds number. All of the above results are tabulated in Table 11 and plotted in Figures 20 through 22.

Table 11 Summary of dimensionless developing length $(L/D)_{FD}$ for all round duct cases based on pressure profiles with their corresponding Reynolds numbers

P-based Profile	**v= 3m/s**		**v= 6m/s**		**v= 9m/s**	
$\boldsymbol{D}$ **(m)**	**Re**	**$(L/D)_{FD}$**	**Re**	**$(L/D)_{FD}$**	**Re**	**$(L/D)_{FD}$**
0.2	38,480	21	76,960	26	115,430	29
0.4	76,960	26	153,910	31	230,870	36
0.6	115,430	29	230,870	36	346,300	38.7

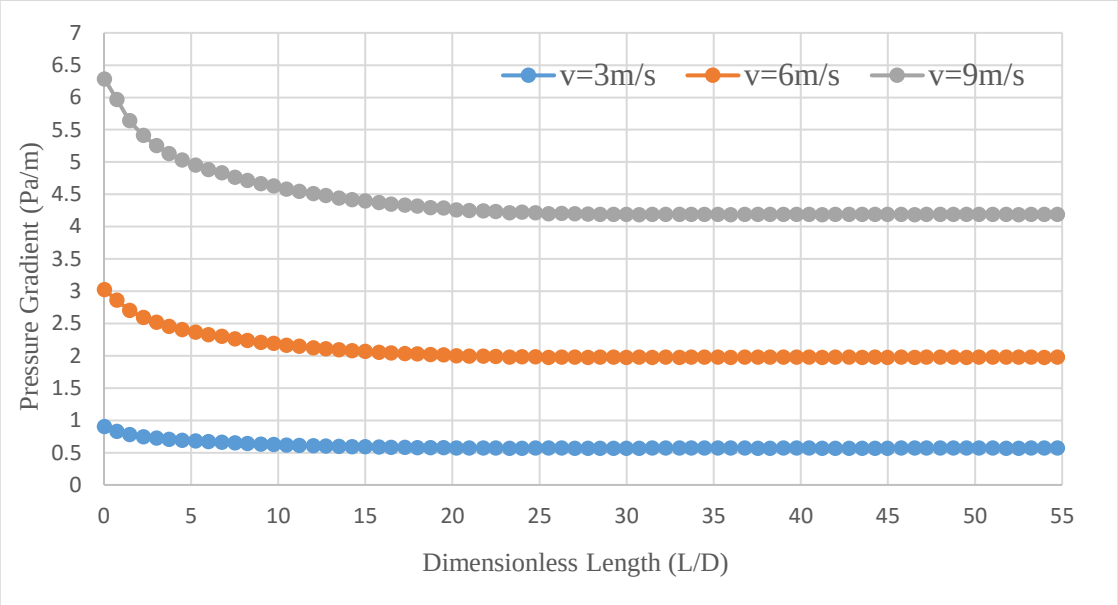

Figure 20. Pressure gradient profiles in a round duct with $d = 0.2$ m for different uniform inlet velocities.

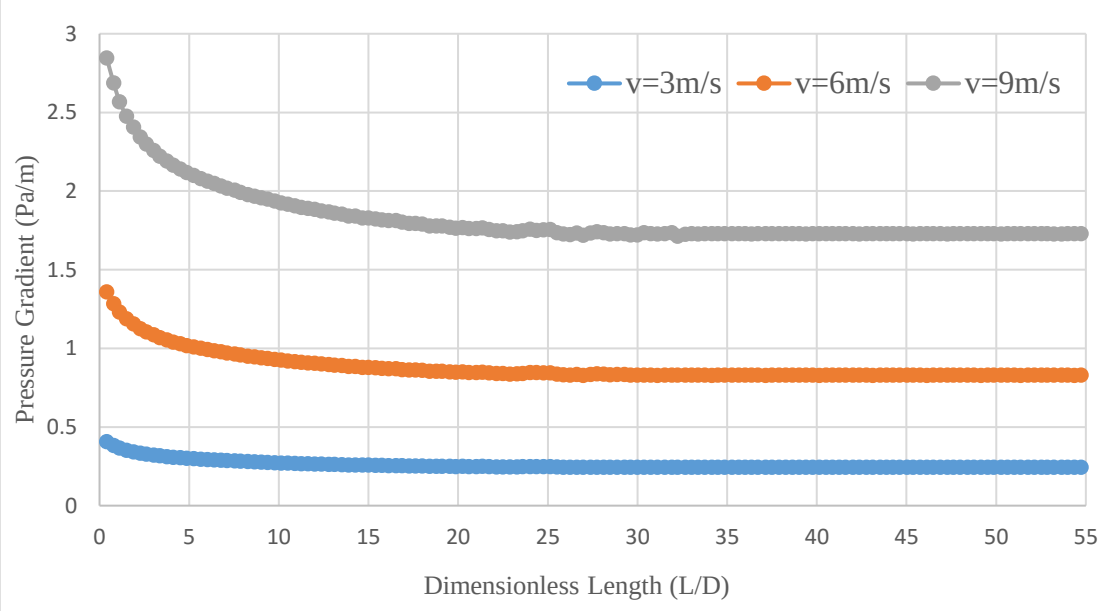

Figure 21. Pressure gradient profiles in a round duct with $d = 0.4$ m for different uniform inlet velocities.

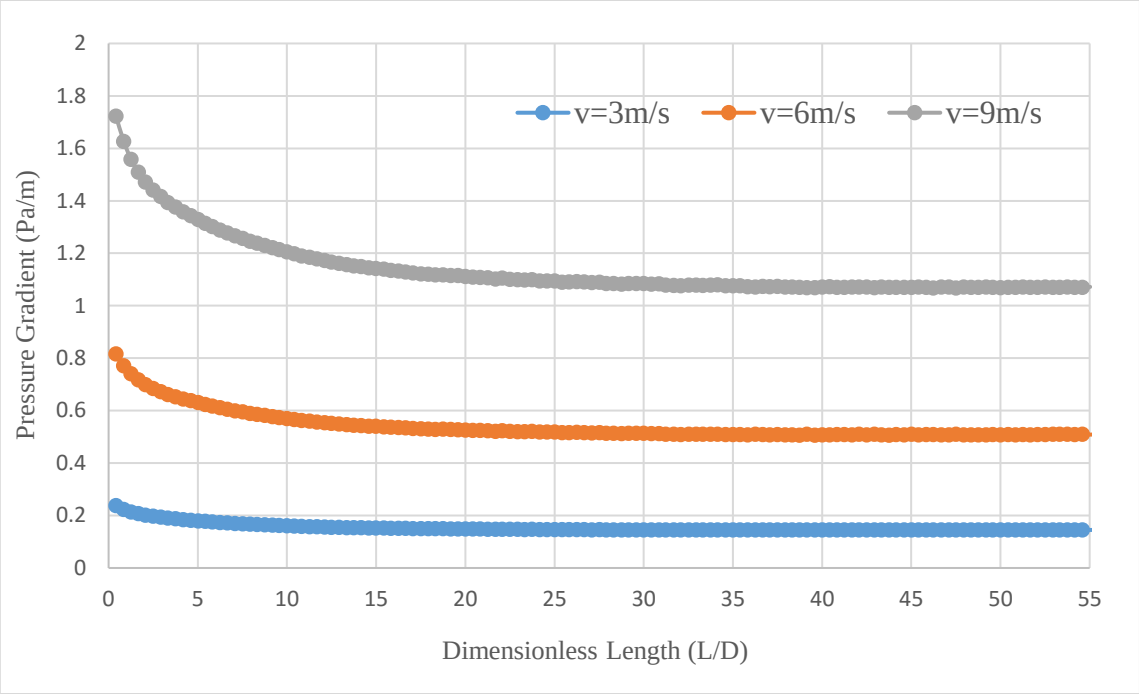

Figure 22. Pressure gradient profiles in a round duct with $d = 0.6$ m for different uniform inlet velocities.

The above $\left(\frac{L}{D}\right)_{FD}$ results are plotted as function of Reynolds number for each case in Figure 23, and then by using a curve fitting procedure, a pressure-based CFD correlation for the fully the developed flow location is developed for room temperature air flowing inside a round duct.

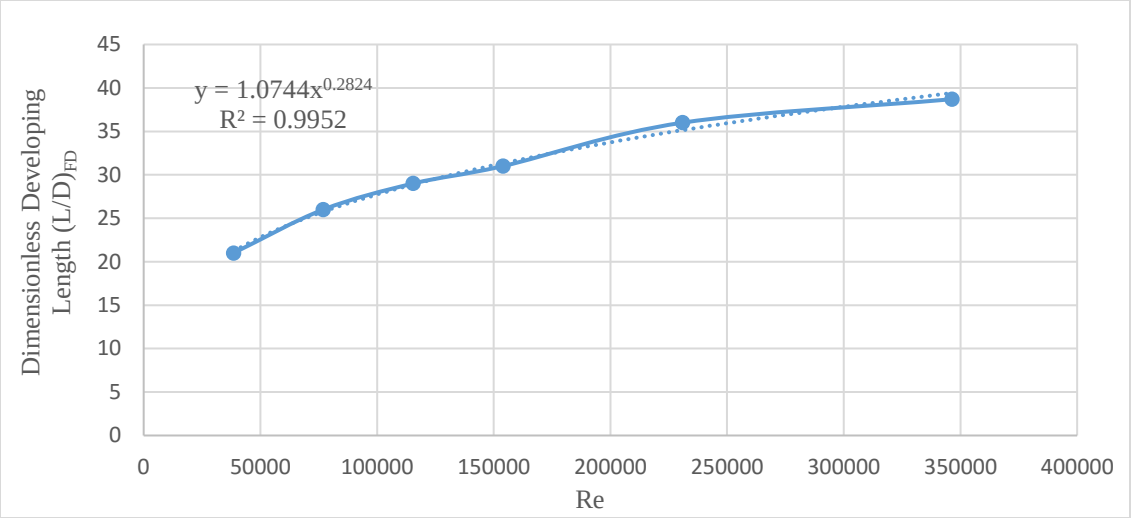

Figure 23. Curve fitting profile (pressure-based correlation) of round duct.

The resulting correlation based on the curve fittings can be expressed as

$$(\frac{L}{D})_{FDF_P} = 1.0744 * Re^{0.2824} \quad (4.3)$$

Table 12 Comparison of velocity-based and pressure-based developing length $(\frac{L}{D})_{FD}$ values in round ducts flow at different Reynolds numbers

Re	$(L/D)_{FDF_V}$	$(L/D)_{FDF_P}$	**(L/D)P/(L/D)V**
38,480	27	21	0.78
76,960	31.3	26	0.83
115,430	34	29	0.85
153,910	36	31	0.86
230,870	39	36	0.92
346,300	43.5	39	0.9

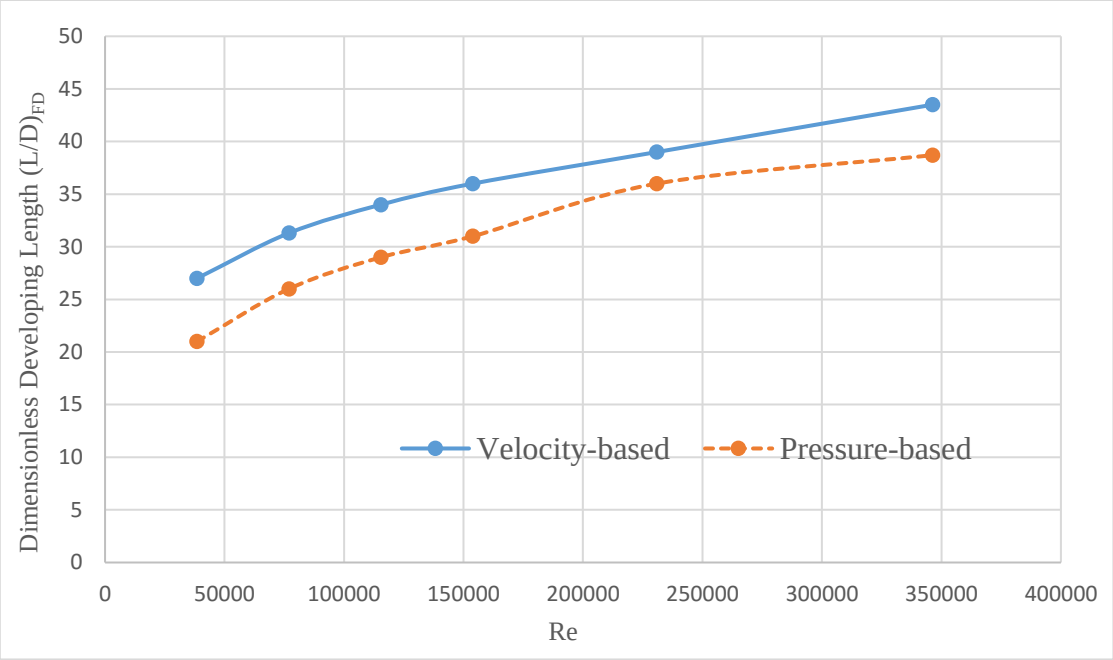

Figure 24. Comparison of velocity-based and pressure-based dimensionless developing $(L/D)_{FD}$ values in round ducts flow at different Reynolds numbers.

As shown in the analysis and results above, there are two distinct approaches that can be used to quantify the developing length in turbulent flow round duct, namely velocity-based and pressure based approaches. The two approaches are directly compared in Table 12 and Figure 24 where the developing lengths are shown at the same Reynolds number.

As can be seen in Table 12 and Figure 24, the pressure-developing length is on average shorter than the velocity-developing length by around 14%, and therefore, it might be more conservative to go with the velocity based correlation for all the simulated cases. Because the two correlations have similar behavior as shown in Figure 24, by using Equations 4.2 and 4.3, a ratio of the pressure-based correlation and velocity-based correlation can be expressed as follows

$$\frac{(\frac{L}{D})_P}{(\frac{L}{D})_v} = 0.0377\ Re^{0.0696} \tag{4.4}$$

$$(\frac{L}{D})_P \approx 0.86 * (\frac{L}{D})_v \tag{4.5}$$

Table 12 presented developing length ratios for Reynolds number range from 40,000 to 350,000, in which the ratio values show slight changes over the Reynolds number range, with an average value being around 0.86, which signifies only a weak function of Reynolds number.

4.5 Comparing Numerical with Analytical and Experimental Results

4.5.1 Comparison of CFD and Experimental Results

Because analytical solutions are not available for velocity profiles in developing turbulent flows inside round ducts, experimental correlations were developed by Bhatti and Shah (1987) and Munson, Okiishi, and Huebsch (2009) are compared against the CFD results for dimensionless developing length, based on the velocity profile as shown in Equation (4.6) below.

$$(\frac{L}{D})_{Exp} = 4.4\ Re^{(\frac{1}{6})} \tag{4.6}$$

The experimental correlation shown in Equation (4.6) is compared to the velocity-based developing length correlation found by using CFD result, Equation (4.2), and the results are shown in Table 13 and Figure 25.

Table 13 Comparison of Experimental and Numerical Developing Length Values $(L/D)_{FD}$ in all Round Ducts Cases

Re	$(L/D)_{Exp}$	$(L/D)_{CFD}$	$(L/D)_{EX}$ / $(L/D)_{CFD}$
38,480	25.6	27	0.95
76,960	28.7	31.3	0.92
115,430	30.7	34	0.90
153,910	32.2	36	0.89
230,870	34.7	39	0.89
346,300	36.9	43.5	0.85

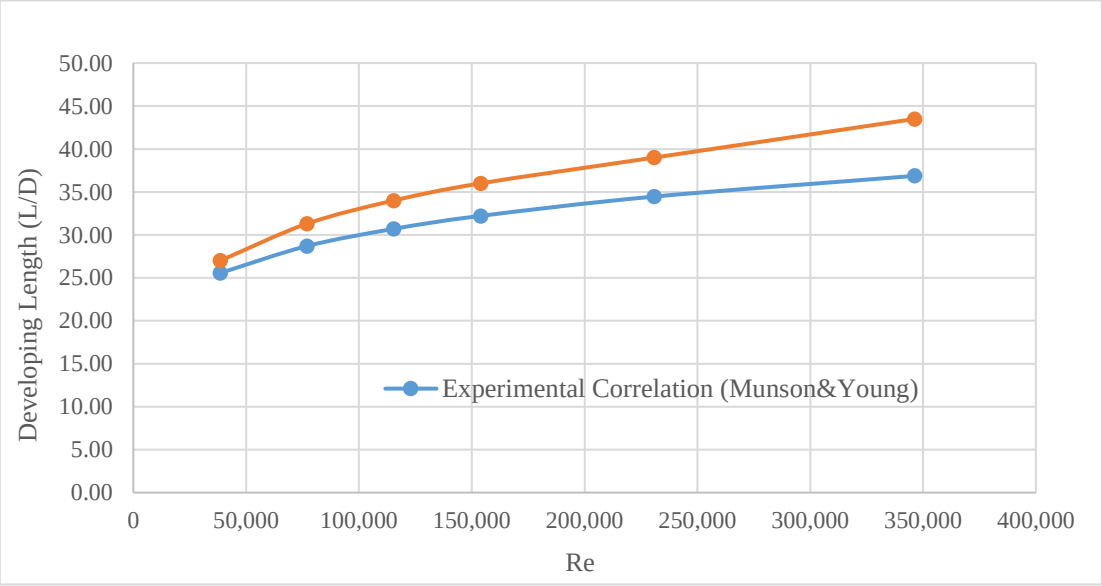

Figure 25. Comparison of experimental and numerical dimensionless developing length $(L/D)_{FD}$ at different Reynolds numbers.

The two approaches are quite similar at low and moderate Reynolds numbers. However, they diverge at high Reynolds number, as shown in Figure 25 above, which may indicate that either the experimental correlation is only valid on low and moderate Reynolds number range or a different fully developed flow criteria was used in the experiment, etc. By using Equations (4.2) and (4.6), a ratio of the experimental-developing length and the velocity-based developing length can be expressed as

$$\frac{(\frac{L}{D})_{Exp}}{(\frac{L}{D})_{CFD}} = 1.55 * Re^{-0.046} \quad (4.7)$$

$$(\frac{L}{D})_{Exp} \approx 0.9 * (\frac{L}{D})_{CFD} \quad (4.8)$$

Table 13 presented the CFD and experimental developing length ratios for Reynolds number range from 40,000 to 350,000, in which the ratio values show slight changes over the Reynolds number range, with an average value being around 0.9, which signifies only a weak function of Reynolds number.

4.5.2 Comparison of CFD and Analytical Pressure Gradients

In addition to the comparison of numerical results with experimental results, the numerical pressure gradient values in the fully developed region can be compared to values from the Darcy–Weisbach equation, which can be expressed as follow

$$\frac{dP}{dx} = \frac{\rho\, v^2\, f}{2\, D} \quad (4.9)$$

with the friction factor f for turbulent flow inside round ducts beings calculated by using the Colebrook equation as follow

$$\frac{1}{\sqrt{f}} = -2\log(\frac{\varepsilon/_D}{3.7} + \frac{2.51}{Re\sqrt{f}}) \quad (4.10)$$

CFD and analytical comparison shows that the difference percentage for all duct flows CFD models is relatively small and hence the CFD results are found to be in a good agreement with the Darcy-equation results. In a round duct with 0.2 m diameter, the

percentage difference is 1.7% for a flow velocity of 3 m/s, 2% for a flow velocity of 6 m/s, and 2.5% for a flow velocity of 9 m/s. For the middle duct size with 0.4 m, the percentage difference is 2% for 3 m/s inlet velocity, 2.2% for 6 m/s inlet velocity, and 3.3% for 9 m/s inlet velocity. In a round duct with 0.6 m, the percentage difference was found to be; 3.3%, 3.8%, and 4.4%, for inlet velocities of 3 m/s, 6 m/s, and 9 m/s, respectively. These results are all presented in tabulated form in Table 14 and graphical form in Figures 26 through 28.

Table 14 Comparison of Analytical and Numerical Pressure Gradient values in all Round Duct Flow Cases

D(m)	v(m/s)	Re	f	$\frac{dP}{dx}_{Darcy}$ (Pa/m)	$\frac{dP}{dx}_{CFD}$ (Pa/m)	% Difference
0.2	3	38,480	0.022	0.58	0.57	1.7%
	6	76,960	0.019	2.02	1.98	2%
	9	115,430	0.018	4.30	4.19	2.5%
0.4	3	76,960	0.019	0.25	0.245	2%
	6	153,910	0.016	0.85	0.83	2.2%
	9	230,870	0.015	1.79	1.73	3.3%
0.6	3	115,430	0.017	0.15	0.145	3.3%
	6	230,870	0.015	0.53	0.51	3.8%
	9	346,300	0.014	1.12	1.07	4.4%

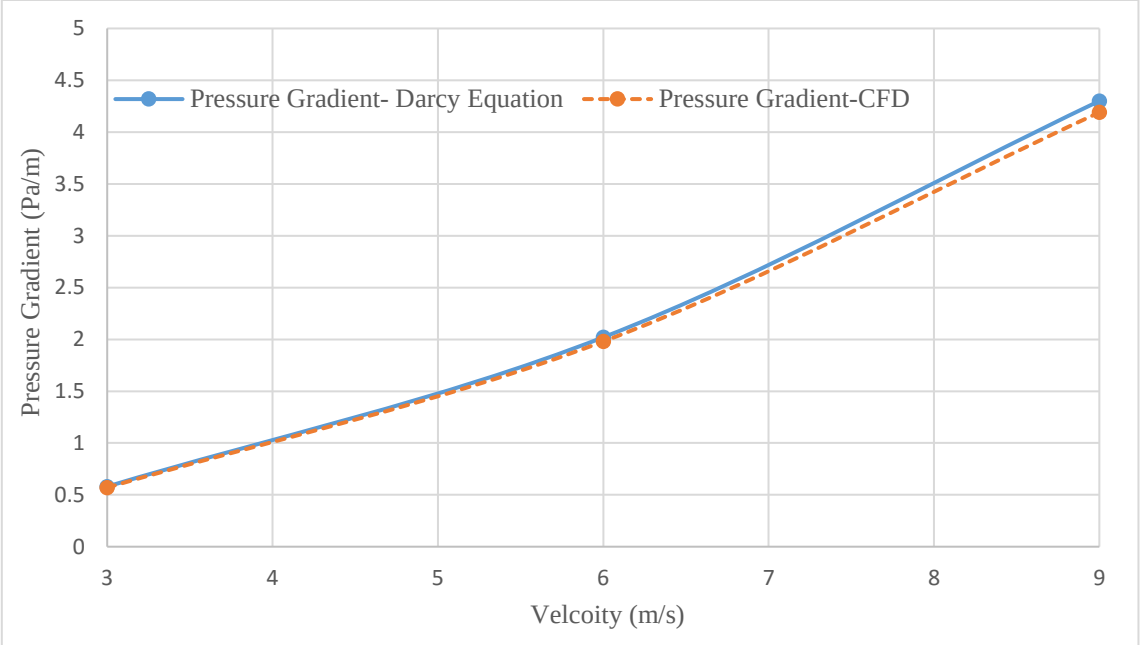

Figure 26. Comparison of analytical and numerical pressure gradient profiles in a round duct with $d = 0.2$ m.

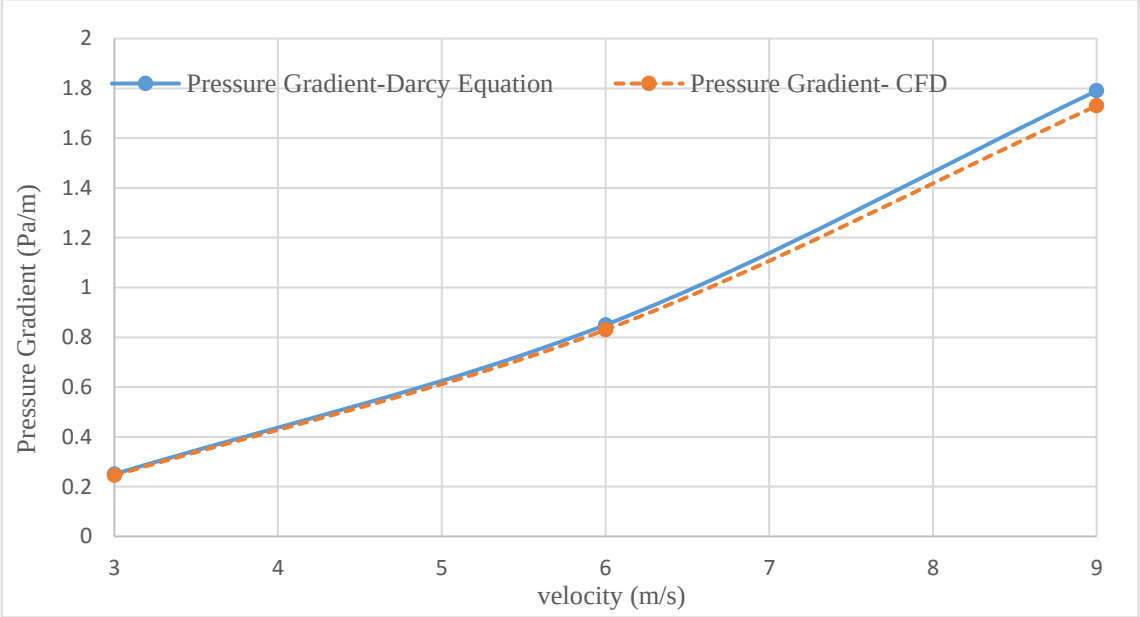

Figure 27. Comparison of analytical and numerical pressure gradient profiles in a round duct of $d = 0.4$ m.

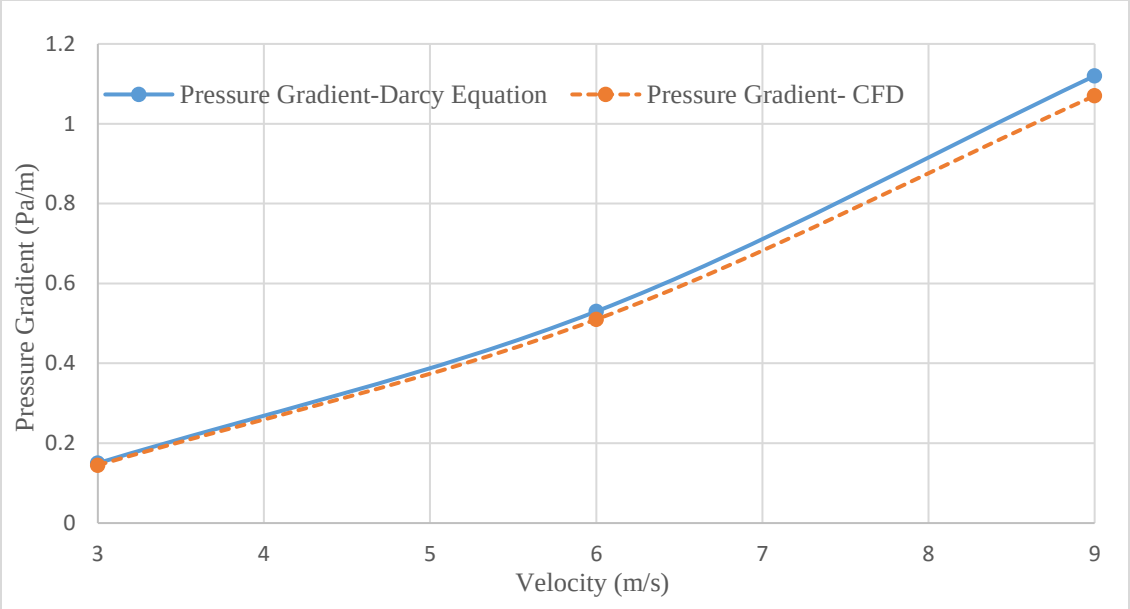

Figure 28. Comparison of analytical and numerical pressure gradient profiles in a round duct of $d = 0.6$ m.

4.6 Summary

This section presented a CFD analysis of turbulent flow in round ducts and analyzed the velocity and pressure profiles for several duct sizes and flow conditions that represent a range of Reynolds numbers. The results revealed for both of the velocity and pressure approaches that the developing length of the flow increases with increasing the velocity and/or increasing duct size. Moreover, in flow cases with identical Reynolds numbers, the developing length of the flow appeared to be the same. As a result, the developing length of the flow is a Reynolds number dependent variable such that larger Reynolds number requires larger developing length to achieve the fully developed flow condition in round ducts.

Based on using the velocity gradient profiles, the dimensionless developing length was found to be $27, 31.3, 34, 36, 39$, and 43.5 for increasing flow Reynolds numbers of $(38{,}480)$, $(76{,}960)$, $(115{,}430)$, $(153{,}910)$, (230.870), and $(346{,}300)$, respectively.

Similarly, by analyzing the pressure gradient profiles, the dimensionless developing length was found to be 21 for a Reynolds number of $(38{,}480)$, 26 for Reynolds number of (76960), 29 for Reynolds number of (115,430), 31 for Reynolds number of (153,910), 36 for Reynolds number of (230,870), and 38.7 for Reynolds number of (346,300).

Using the above numerical results, velocity-based and pressure-based correlations were developed to calculate the required developing length (or the entrance length) in turbulent round duct flow with any Reynolds number. Also, a well-known experimental correlation was compared to CFD results for a range of Reynolds numbers with the experimental to CFD ratio being about 0.9, signifying a shorter entrance length for experiments. Moreover, a comparison of velocity-based developing length and pressure-based developing length for a range of Reynolds number show a pressure-length to velocity length ratio being around 0.86, signifying a shorter pressure- entrance length.

Last but not least, the CFD model results show a good agreement when compared against the Darcy equation with a maximum error of 4.4% for the high turbulent flow case with Reynolds number of $346{,}300$.

V. SQUARE DUCT CASE

5.1 Introduction

This section continues the numerical modelling and CFD analysis of the internal turbulent flow in ducts. Square ducts are commonly used in many engineering practice especially in HVAC applications, and hence it made sense to study and investigate them just after the round ducts. In this section, CFD models of different square duct diameters with different uniform inlet velocities will be simulated in order to investigate the flow behavior in developing region of the duct, identity the parameters effecting the flow developing length, and also to derive numerical correlations to locate where the fully developed flow is achieved inside the square ducts based on both velocity and pressure profiles. Last but not least, a comparison of the round and the square ducts flow is presented to investigate the differences between these two designs and how that may relate to the developing length of the flow.

5.2 Problem Description

- The working fluid is air at room temperature and atmospheric pressure with thermophysical presented in Table 15.

Table 15 Thermophysical properties of air in square ducts

Thermophysical Property	Value
$\boldsymbol{T}(\mathbf{K})$	300
$\boldsymbol{\mu}\ (\frac{\mathbf{Kg}}{\mathbf{m.s}})$	1.84×10^{-5}
$\boldsymbol{\rho}\ (\frac{\boldsymbol{Kg}}{\boldsymbol{m^3}})$	1.18

- Three ducts dimeters are chosen representing a range of practical applications; 0.2 m 0.4 m, and 0.6 m.
- Air enters the channel at different uniform velocity representing a range used in industry practice; 3 m/s, 6 m/s, and 9 m/s.
- Assumptions applied to this analysis are
    - Steady incompressible flow.
    - Smooth stainless steel square ducts.
    - Negligible gravity effects on fluid flow.
    - Square duct is completely filled with the fluid being transported.

5.3 Modelling and Simulation

Similar to the round ducts, the square duct geometry was created using SOLIDWORKS software, and then imported to the STAR CCM+ commercial software in order to simulate the fluid flow. As explained earlier, STAR CCM+ uses control volume based finite volume method to solve the coupled, non-linear partial differential governing equations for the fluid, as shown in Figure 29 below.

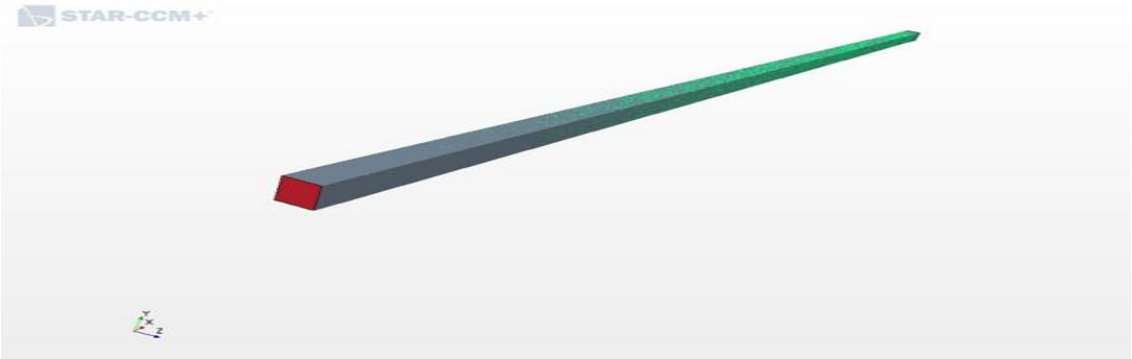

Figure 29. Computational domain of a square duct flow.

5.3.1 Mesh Generation

Similar to the round duct simulations, we started the numerical simulation of the square ducts by generating a mesh, or grid that represents the square duct geometry. In order to do so, the below mesh models were chosen in STAR CCM+ to most accurately simulate the turbulent fluid flow inside the square duct.

- Surface Remesher.
- Polyhedral Mesher.
- Embedded Thin Mesher.
- Prism Layer Mesher.

By following the user guide in STAR CCM+ for channel flow applications, the geometry mesh base size is selected as 5 cm with a surface growth rate of 1.7. Also, two layers of the thin mesh model and nine layers of prism mesh are applied for all duct sizes. Table 16 below summarizes all of the selected mesh parameter values.

Table 16 Summary of mesh parameter values used in square duct models

Mesh Parameters	Input Value
Base Size	0.05 m
Number of Prism Layers	9
Surface Growth Rate	1.7
Thin Mesh Layers	2
Relative Maximum Size	40
Relative Minimum Size	60

For the prism layer mesh model, the prism layer absolute thickness and the near wall thickness values are selected for each duct size in order to accurately capture the near wall velocity profiles and viscous sublayer of the turbulent flow. The absolute prism

layer thickness values selected are 8.903 mm, 13.35 mm, and 17.80 mm for square duct sizes of 0.2 m, 0.4 m, and 0.6 m , respectively. Moreover, the near wall prism layer thickness selected are 0.053 mm, 0.079 mm, and 0.106 mm for square duct sizes with 0.2 m, 0.4 m, and 0.6 m, respectively. Once the volume mesh was generated, the overall number of cells found to be 2,206,856 cells for the 0.2 m diameter duct, 2,654,000 cells for the 0.4 m diameter duct, and 5,049,373 cells for the 0.6 m diameter duct, as shown in Table 17 and Figure 30 through 32.

Table 17 Detailed prism layer mesh specifications and overall cells number for all square duct sizes

Square Duct Diameter (m)	Prism Layer Absolute Thickness (mm)	Thickness of Near Wall Prism Layers (mm)	Overall Number of Cells
D_h=0.2	8.903	0.053	2,206,856
D_h=0.4	13.35	0.079	2,654,000
D_h=0.6	17.80	0.106	5,049,373

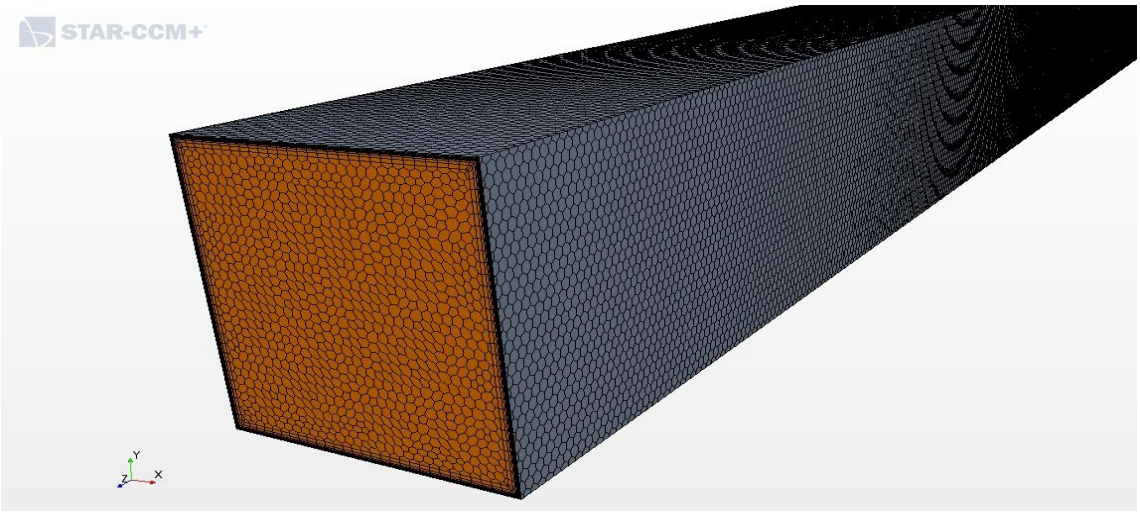

Figure 30. Generated volume mesh for a square duct of $d_h = 0.2$ m

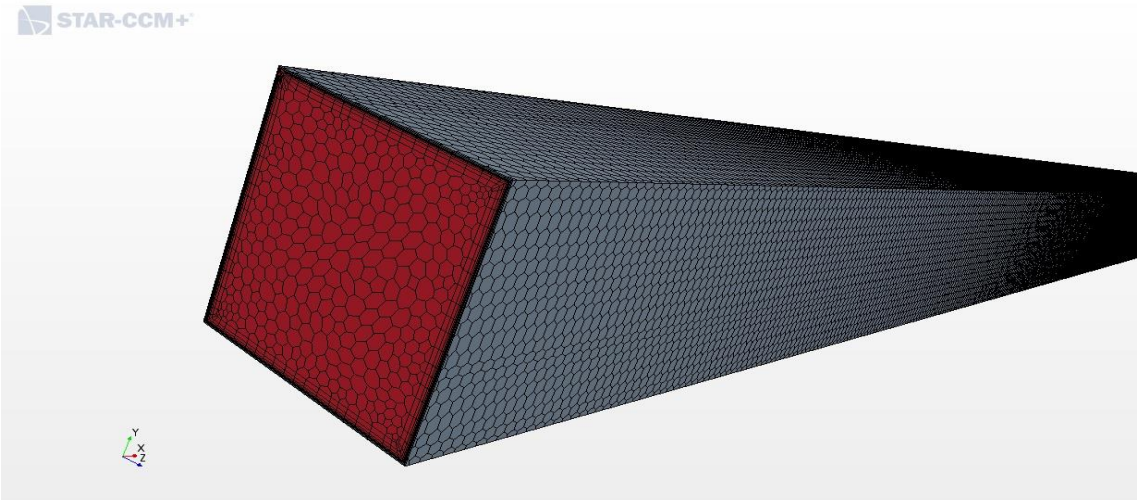

Figure 31. Generated volume mesh for a square duct of $d_h = 0.4$ m.

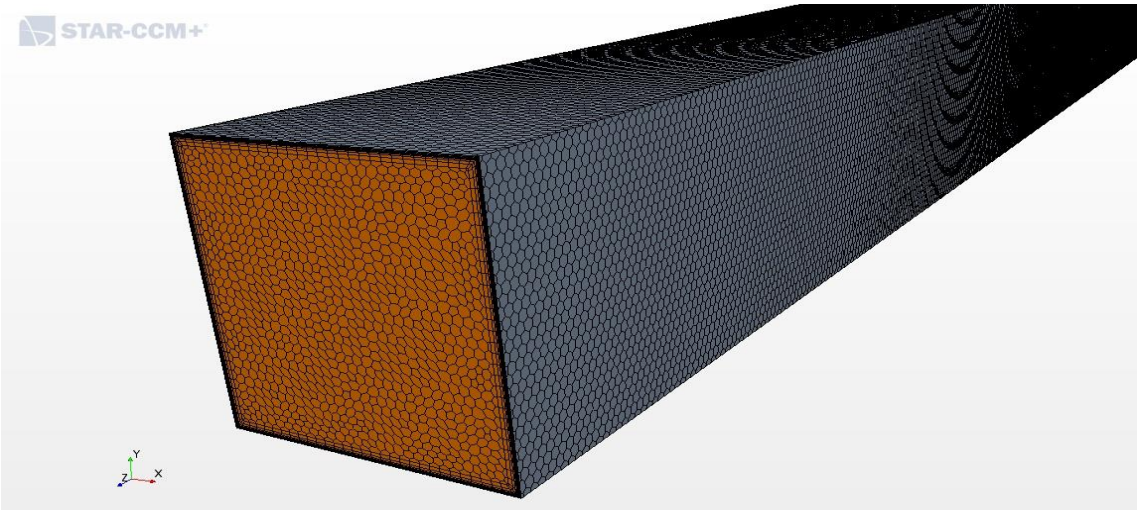

Figure 32. Generated volume mesh for a square duct of $d_h = 0.6$ m.

5.3.2 Fluid Physical Properties

Once the mesh or grid was established for each square duct size, the next step was to choose the appropriate physical models to accurately simulate the fluid flow. The recommended physical models for turbulent airflow inside a channel are listed below.

- Three dimensional steady flow.
- Constant Air Density.
- Turbulent Flow.
- K − ω Turbulence Model.
- All $y+$ wall treatment.
- Reynolds-Averaged Navier-Stokes
- Segregated Flow Model.
- Turbulence Suppression Transition Model.
- Cell Quality Remediation.

5.3.3 Boundary Conditions

The next step was to identify and specify the boundary conditions of the flow at duct inlet, $\frac{L}{D}$ of 0 , and exit, $\frac{L}{D}$ of 100, with the exit being an arbitrary chosen value that assured achieving the fully developed in all cases. For all duct sizes, the flow was assumed to enter with uniform flow velocities of 3 m/s, 6 m/s, and 9 m/s. The duct is considered long enough to assume atmospheric pressure at the duct outlet, which corresponds to zero gage pressure.

In this analysis, the turbulence parameters are quantified by the turbulent intensity of the flow and the turbulence length scale. At the inlet, the turbulence intensity is mainly a function of the upstream history of the flow and the nature of the flow application. For our case of turbulent flow in HVAC ducts, and as we did with the pipe flow simulations, a turbulent intensity of 5% was assumed at the square duct inlet. However, at the exit in the fully developed region, the turbulent intensity is estimated by using Equation (3.12) below.

$$TI_{FDF} = 0.16 * Re^{-\frac{1}{8}} \tag{3.12}$$

For the turbulence length scale, which is a quantity related to the size of large eddies that contain the turbulent energy. Equation (4.1) can be used as an approximation in the fully developed region of the flow.

$$l_{FDF} = 0.07 * D_h \tag{4.1}$$

In addition to the inlet and outlet boundary conditions, a stationary wall boundary condition with no-slip assumption is applied at the wall of the round duct, such that the velocity increases from zero at the wall to a maximum velocity in the middle of the duct. A symmetry boundary condition is applied on the other side of the square duct to accelerate the computation process. Moreover, for this model, a wall function method is used for the near wall treatment in order to accurately simulate the flow inside the square

duct. Figure 33 and Tables 18 through 21 illustrate all of boundary conditions types used and their input values.

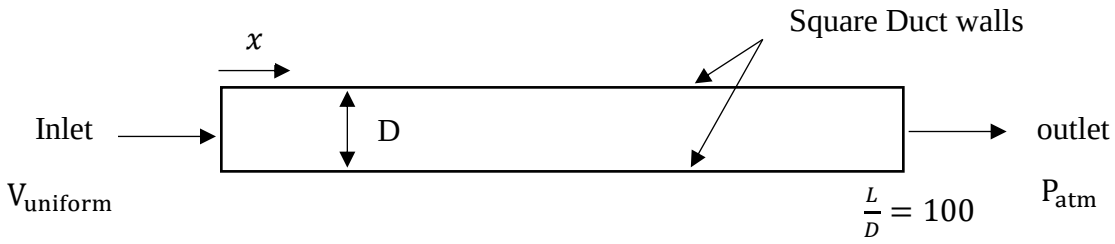

Figure 33. Types of boundary conditions used in square duct models.

Table 18 Summary of boundary conditions for all square duct sizes

Uniform Inlet Velocity (m/s)	3, 6 , 9
Outlet gage Pressure (Pa)	Zero

Table 19 Summary of turbulence parameters boundary conditions for a square duct of $d_h = 0.2$ m

Turbulence Parameters	**V=3m/s**	**V=6m/s**	**V=9m/s**
TI_{in} **(Intensity)**	5%		
l_{in} **(Length scale)**	0.02 m		
TI_{FD} **(Intensity)**	4.3%	3.9%	3.7%
l_{FD} **(Length Scale)**	0.014 m		

Table 20 Summary of turbulence parameters boundary conditions for square duct of $d_h = 0.4$ m

Turbulence Parameters	V=3m/s	V=6m/s	V=9m/s
TI_{in} (Intensity)	5%		
l_{in} (Length scale)	0.031 m		
TI_{FD} (Intensity)	3.9%	3.6%	3.4%
l_{FD} (Length Scale)	0.028 m		

Table 21 Summary of turbulence parameters boundary conditions for square duct of $d_h = 0.6$ m

Turbulence Parameters	V=3m/s	V=6m/s	V=9m/s
TI_{in} (Intensity)	5%		
l_{in} (Length scale)	0.05 m		
TI_{FD} (Intensity)	3.7%	3.4%	3.2%
l_{FD} (Length Scale)	0.042 m		

5.4 Results and Discussion

After the simulations have been set up for all the nine square ducts models, consisting of three different duct sizes with three different uniform inlet velocity inlet, STAR CCM+ was used to determine velocity and pressure profiles for each case. Then, by using these plots, velocity gradient profiles dv/dx and pressure gradient profiles dp/dx were developed as function of dimensionless duct length $\left(\frac{L}{D}\right)$ for each Reynolds number case, which is a necessary step to locate where the fully developed flow occurs.

Similar to what we did for round ducts models earlier, The criteria used to define where the fully developed flow is reached inside the ducts is to assume that the flow will be fully developed where the (dv/dx) value is around 99% of the fully developed region (dv/dx),which is $(dv/dx)_{FD}$equals to 0. Similarly, by using the pressure gradient

profiles, the flow is assumed to be fully developed where (dp/dx) reaches 99% of the (dp/dx) in the fully developed region, assuming that $(dp/dx)_{FD}$ is constant.

For a square duct of 0.2 m diameter, by using the above approach and criteria, the dimensionless developing length $\left(\frac{L}{D}\right)_{FD}$ was found to be 30.8 with an inlet velocity of 3 m/s, 36 with an inlet velocity of 6 m/s, and 39 with an inlet velocity of 9 m/s. For a square duct of 0.4 m diameter, the dimensionless developing length $\left(\frac{L}{D}\right)_{FD}$ was 36 with an inlet velocity of 3 m/s, 41.6 with an inlet velocity of 6 m/s, and 46 with 9 m/s inlet velocity. For the largest duct size of 0.6 m, the dimensionless developing length $\left(\frac{L}{D}\right)_{FD}$ were 39.6, 46, and 50 with inlet velocities of 3 m/s, 6 m/s, and 9 m/s, respectively.

The above results show that the dimensionless developing lengths $\left(\frac{L}{D}\right)_{FD}$ increase with the increasing Reynolds number of the flow, while it remain almost constant with different flow velocity and duct sizes, which they have an identical Reynolds number. These results are presented in both tabular and graphical forms in Table 22 and Figures 34 through 39.

Table 22 Summary of dimensionless developing length $(L/D)_{\mathrm{FD}}$ for all square duct cases based on velocity profiles with their corresponding Reynolds numbers.

V-based Profile	**v= 3m/s**		**v= 6m/s**		**v= 9m/s**	
D_h **(m)**	**Re**	**(L/D)FD**	**Re**	**(L/D)FD**	**Re**	**(L/D)FD**
0.2	38,480	30.8	76,960	36	115,430	39.6
0.4	76,960	36	153,910	41.6	230,870	46
0.6	115,430	39	230,870	46	346,300	50

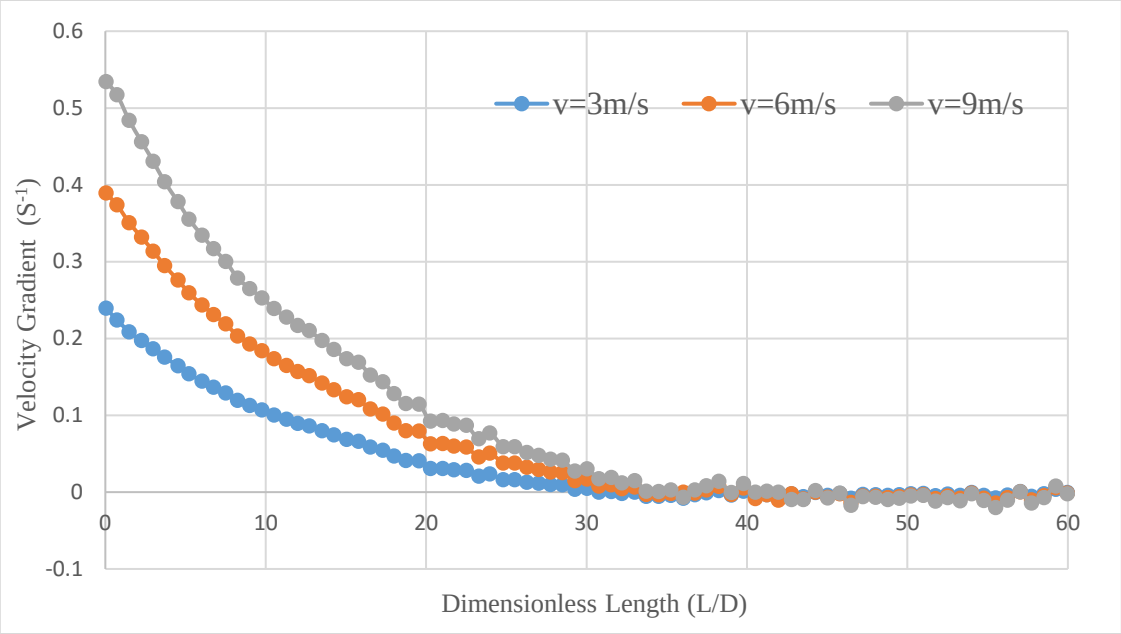

Figure 34. Velocity gradient profiles for different uniform inlet velocities in a square duct of $d_h = 0.2$ m.

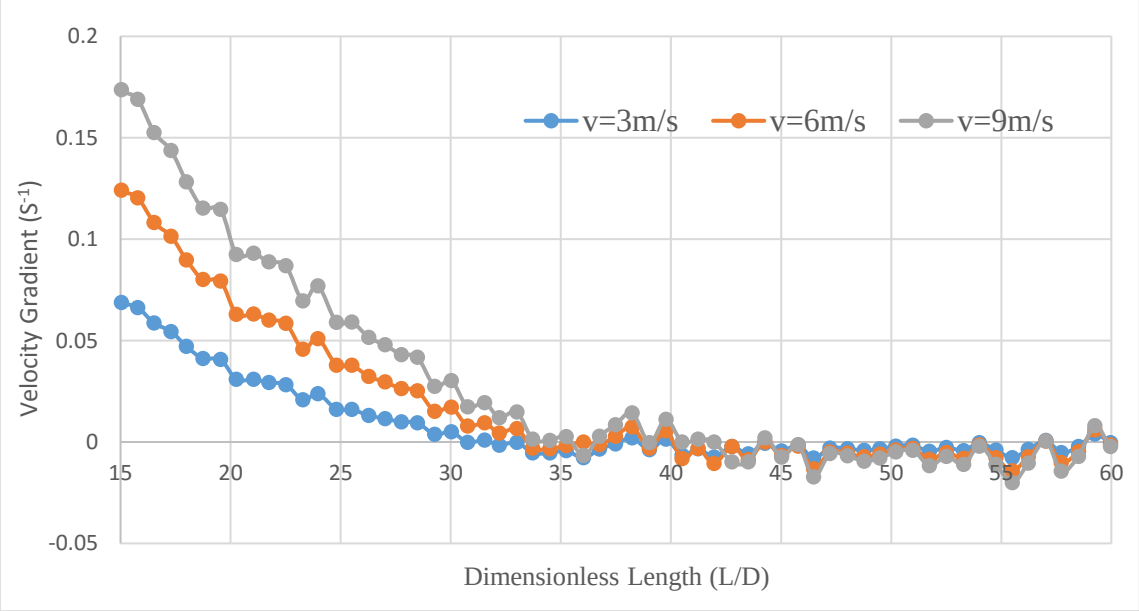

Figure 35. Enlarged velocity gradient profiles for different uniform inlet velocities in a square duct of $d_h = 0.2$ m.

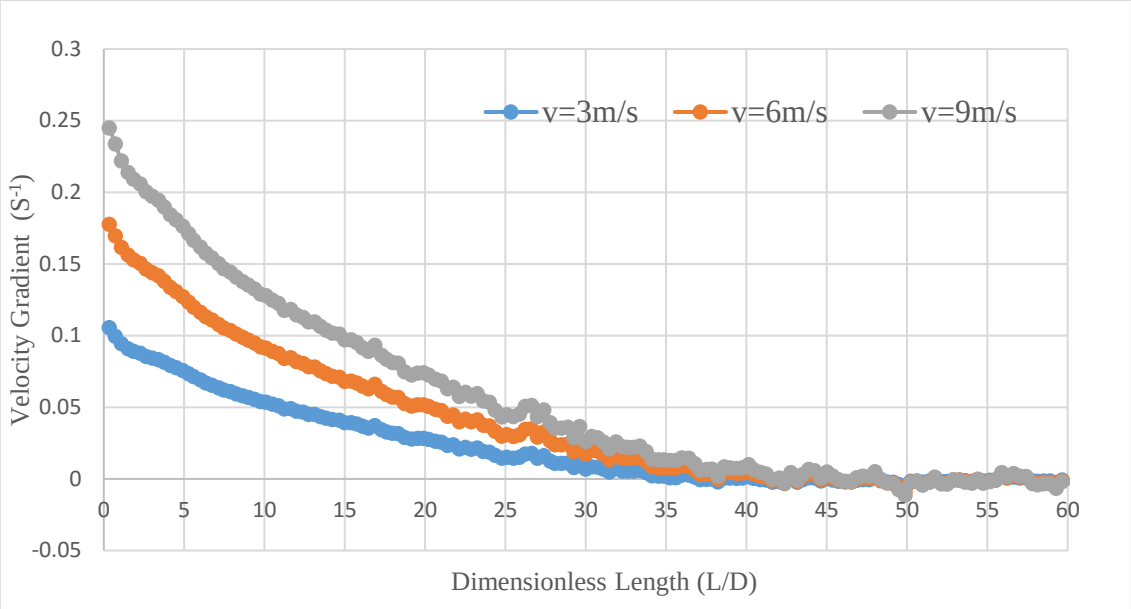

Figure 36. Velocity gradient profiles for different uniform inlet velocities in a square duct of $d_h = 0.4$ m.

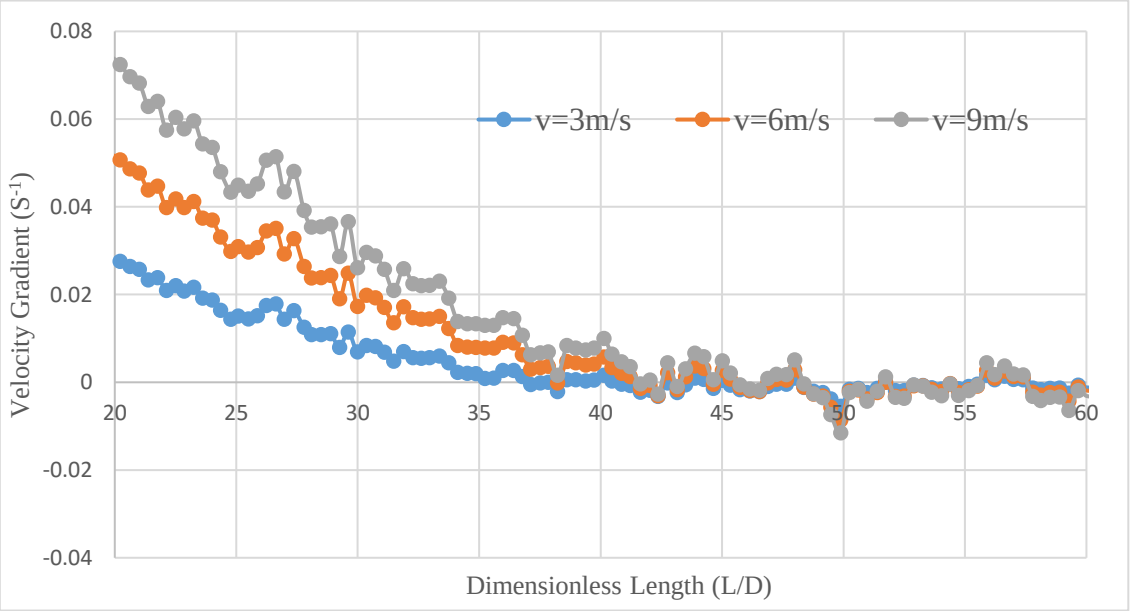

Figure 37. Enlarged velocity gradient profiles for different uniform inlet velocities in a square duct of $d_h = 0.4$ m.

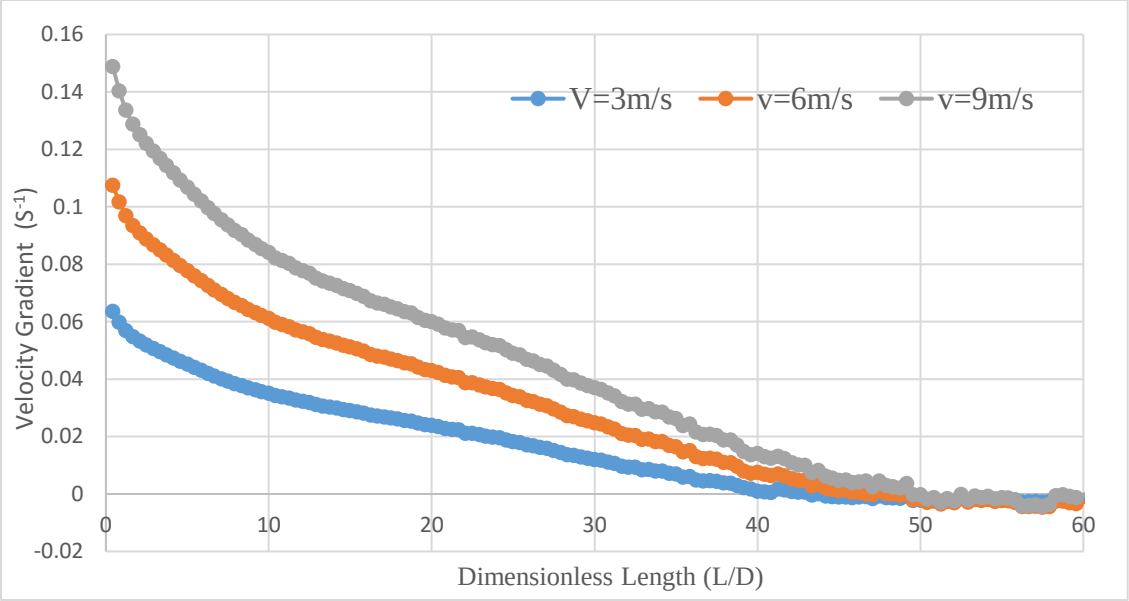

Figure 38. Velocity gradient profiles for different uniform inlet velocities in a square duct of $d_h = 0.6$ m.

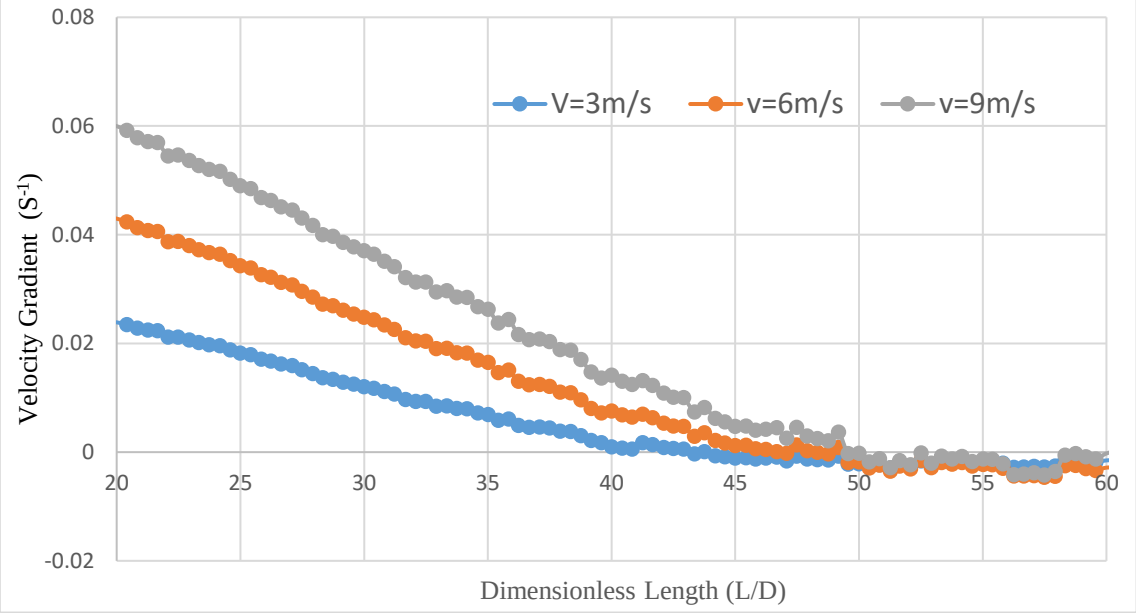

Figure 39. Enlarged velocity gradient profiles for different uniform inlet velocities in a square duct of $d_h = 0.6$ m.

The above $\left(\frac{L}{D}\right)_{FD}$ results are plotted as function of Reynolds number for each case in Figure 40, and then by using a curve fitting procedure, a velocity-based CFD correlation for the fully developed flow location is developed for room temperature air flowing inside a square duct.

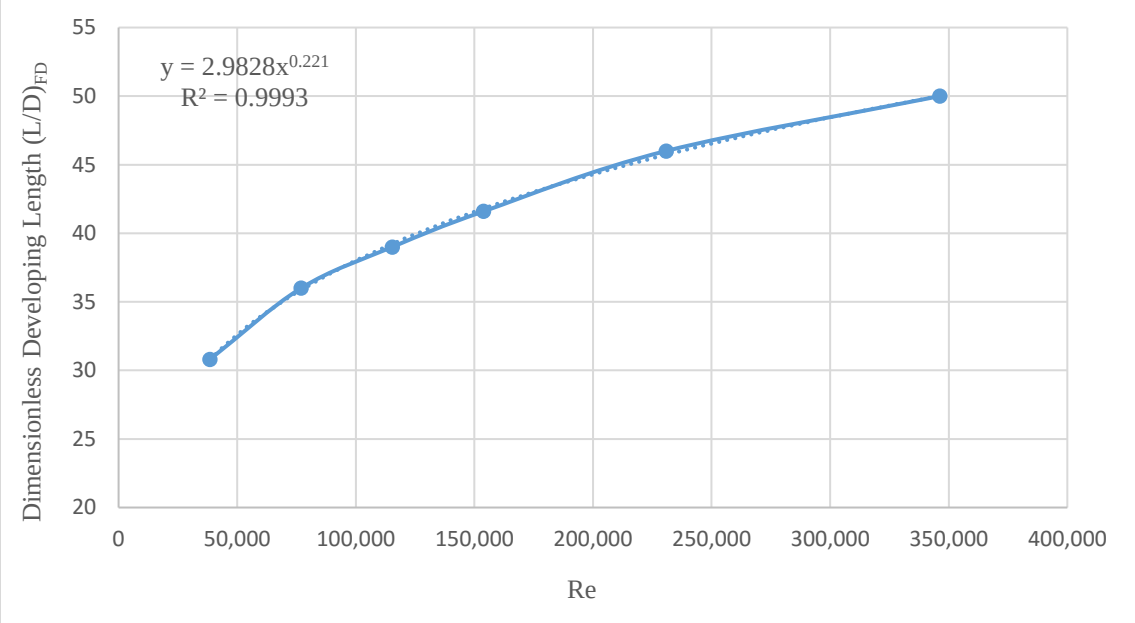

Figure 40. Curve fitting profile (velocity-based correlation) of square ducts.

The resulting correlation based on the curve fitting can be expressed as

$$(\frac{L}{D})_{FDF_V} = 2.9828 * Re^{0.221} \quad (5.1)$$

A similar analysis based on the pressure profiles was carried out to investigate the developing length and then compared to the velocity based results at each flow Reynolds number. By using the fully developed flow criteria mentioned earlier, the dimensionless developing length $\left(\frac{L}{D}\right)_{FD}$ based on the pressure gradient profiles was found to be 25.5 with an inlet velocity of 3 m/s, 31 with an inlet velocity of 6 m/s, and 36.5 with highest velocity of 9 m/s in a square duct with 0.2 m diameter. For a square duct of 0.4 m diameter, the dimensionless developing length $\left(\frac{L}{D}\right)_{FD}$ was 31 with an inlet velocity of 3 m/s, 39 with an inlet velocity of 6 m/s, and 45 with 9 m/s inlet velocity. For the largest duct with 0.6 m, the dimensionless developing length $\left(\frac{L}{D}\right)_{FD}$ were 36.5, 45, and 48.3 for flow with uniform inlet velocities of 3 m/s, 6 m/s, and 9 m/s, respectively.

The above results show that the dimensionless developing lengths $\left(\frac{L}{D}\right)_{FD}$ increase with the increasing Reynolds number of the flow, while it remains almost constant with different flow velocity and duct sizes, which they have an identical Reynolds number. These results are presented in both tabular and graphical forms in Table 23 and Figures 41 through 43.

Table 23 Summary of dimensionless developing length $\left(\frac{L}{D}\right)_{FD}$ for all square duct cases based on pressure profiles with their corresponding Reynolds numbers

P-based Profile	**v=3m/s**		**v=6m/s**		**v=9m/s**	
D **(m)**	**Re**	**$(L/D)_{FD}$**	**Re**	**$(L/D)_{FD}$**	**Re**	**$(L/D)_{FD}$**
0.2	38,480	25.5	76,960	31	115,430	36.5
0.4	76,960	31	153,910	39	230,870	45
0.6	115,430	36.5	230,870	45	346,300	48.3

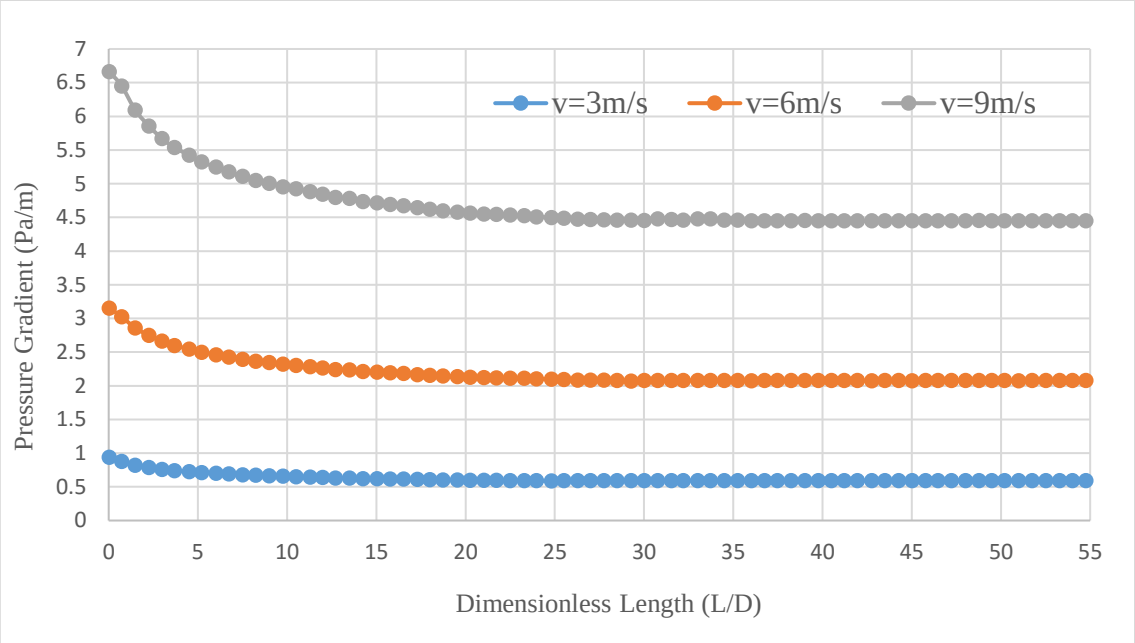

Figure 41. Pressure gradient profiles for different uniform inlet velocities in a square duct of $d_h = 0.2$ m.

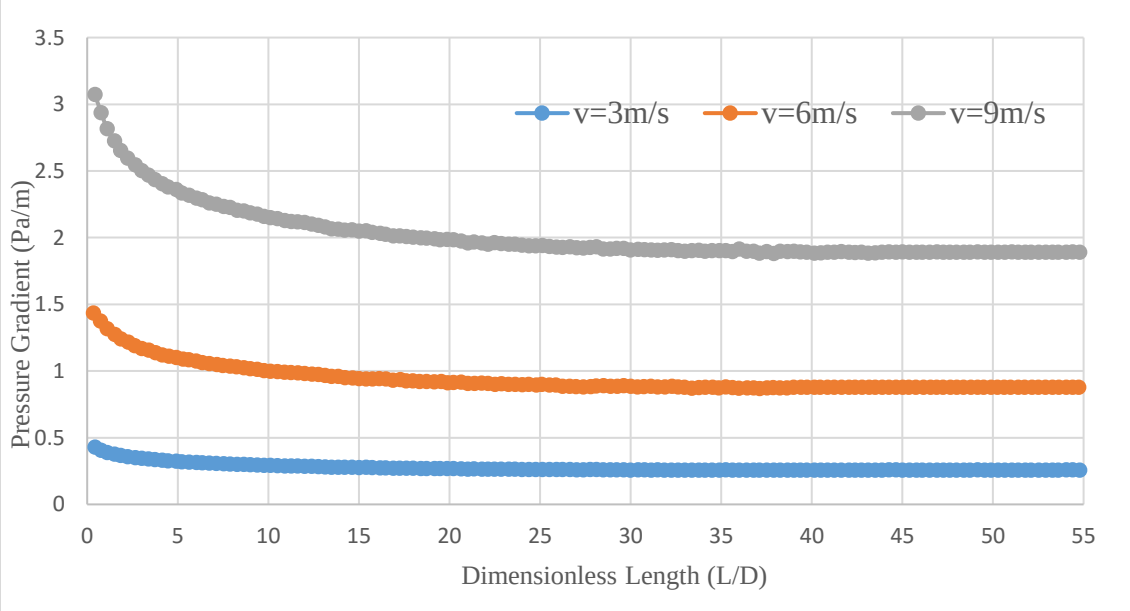

Figure 42. Pressure gradient profiles for different uniform inlet velocities in a square duct of $d_h = 0.4$ m.

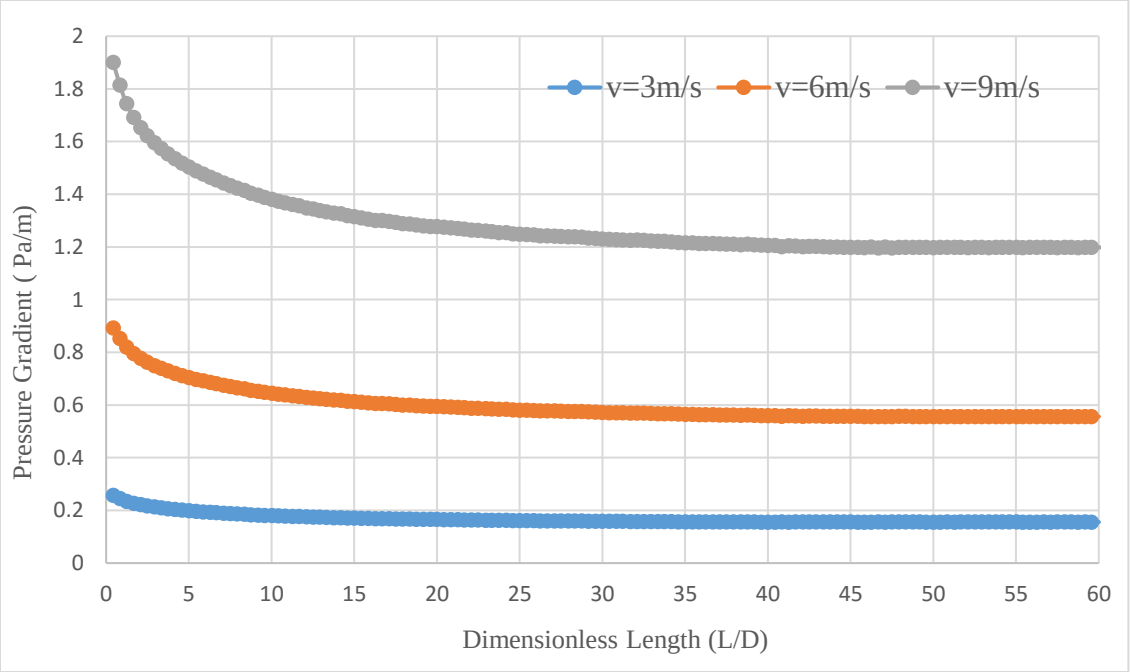

Figure 43. Pressure gradient profiles for different uniform inlet velocities in a square duct of $d_h = 0.6$ m.

The above $\left(\frac{L}{D}\right)_{FD}$ results are plotted as function of Reynolds number for each case in Figure 44, and then by using a curve fitting procedure, a pressure-based CFD correlation for the fully developed flow location is developed for room temperature air flowing inside a square duct.

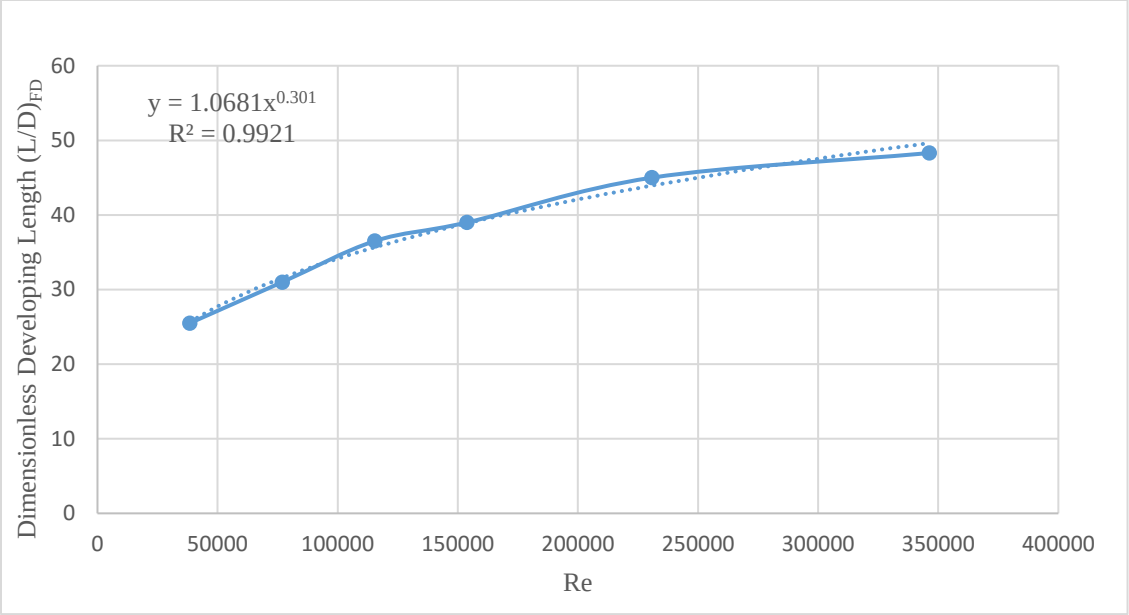

Figure 44. Curve fitting profile (pressure-based correlation) of square ducts.

The resulting correlation based on the curve fitting is

$$(\frac{L}{D})_{FDF_P} = 1.0681 * Re^{0.301} \quad (5.2)$$

Table 24 Comparison of velocity-based and pressure-based developing $(L/D)_{FD}$ values in square ducts flow at different Reynolds numbers

Re	$(L/D)_{FDF_V}$	$(L/D)_{FDF_P}$	**$(L/D)_P$ / $(L/D)_V$**
38,480	30.8	25.5	0.83
76,960	36	31	0.86
115,430	39	36.5	0.94
153,910	41.6	39	0.94
230,870	46	45	0.98
346,300	50	48.3	0.97

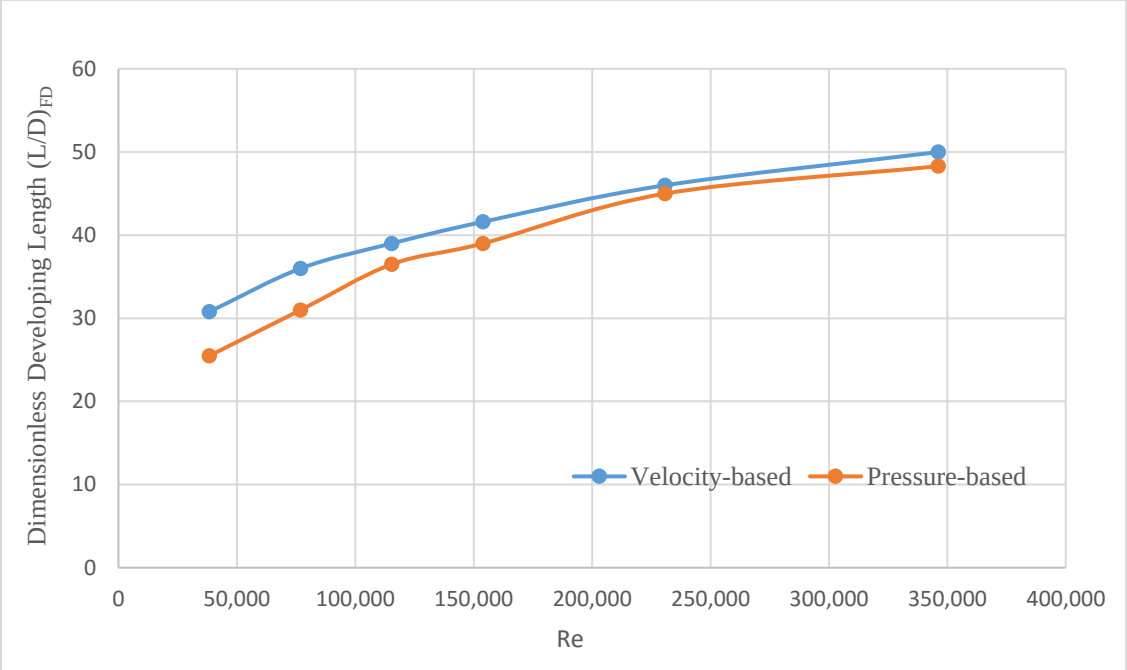

Figure 45. Comparison of velocity-based and pressure-based developing $(L/D)_{FD}$values in square ducts flow at different Reynolds numbers.

As shown in the above analysis and results, there are two distinct approaches that can be used to quantify the developing length in turbulent flow square duct, namely velocity-based and pressure based approaches. The two approaches are directly compared in Table 24 and Figure 45 where the two developing lengths are shown at the same Reynolds number. However, and unlike the round duct case, the pressure-based correlation approaches the velocity correlation and they become almost identical at high Reynolds numbers values. Using Equations (5.1) and (5.2) below, a ratio of the pressure-based correlation and velocity-based correlation can be obtained.

$$\frac{(\frac{L}{D})_P}{(\frac{L}{D})_V} = 0.36\, Re^{0.08} \tag{5.3}$$

$$(\frac{L}{D})_P = 0.92 * (\frac{L}{D})_V \tag{5.4}$$

Table 24 presented developing length ratios for Reynolds number range from 40,000 to 350,000, in which the ratio values show slight changes over the Reynolds number range, with an average value being around 0.92, which signifies only a weak function of Reynolds number.

5.5 Comparison of CFD and Analytical Pressure Gradients

Similar to the round duct analysis, the numerical and CFD solutions obtained for square ducts can be compared against either analytical or experimental solutions to assure the accuracy of simulated results, the assumptions that have been made in simulation, and types of mesh and physical models implemented in the analysis. Unfortunately, since there is not yet a comprehensive experimental correlation for turbulent square duct flow that covers wide range of Reynolds numbers, the square ducts simulations presented in this section are compared against the Darcy–Weisbach equation.

Similar to round ducts models, Colebrook equation is used to estimate the friction factor for the turbulent flow inside a square duct.

$$\frac{dP}{dx} = \frac{\rho\, v^2\, f}{2\, D} \tag{4.9}$$

$$\frac{1}{\sqrt{f}} = -2\log\left(\frac{\varepsilon/_D}{3.7} + \frac{2.51}{Re\sqrt{f}}\right) \quad (4.10)$$

One interesting finding may worth pointing out is that Darcy–Weisbach equation assumes that both round ducts and square ducts will experience the same pressure gradients at same flow velocity and duct size. However, the CFD results presented earlier shown that square ducts experience higher pressure gradients compared to the round ducts at a given Reynolds number, which do make sense as one would expect higher pressure gradient with square ducts due to their larger area.

CFD and analytical comparison shows that the percentage difference for all the square duct flows is relatively small and hence the CFD results are found to be in a good agreement with the Darcy-equation results, but with higher errors compared to round ducts as one would have expected. In a square duct with 0.2 m diameter, the percentage difference is 2.2% for a velocity of 3 m/s, 2.9% for 6 m/s, and 3.5% for 9 m/s. In the middle duct size with 0.4 m, the percentage difference is 2.8% for 3 m/s velocity, 3.3% for 6 m/s, and 4.9% for 9 m/s. In square duct with 0.6 m diameter, the percentage difference was found to be; 4%, 4.9%, and 7%, for an inlet velocities of 3 m/s, 6 m/s, and 9 m/s, respectively. These results are all tabulated in Table 25 and plotted in Figures 46 through 48.

Table 25 Comparison of analytical and numerical pressure gradient values in all square duct flow cases

D_h(m)	v (m/s)	Re	f	dP/dx_{Darcy} (Pa/m)	dP/dx_{CFD} (Pa/m)	% Difference
0.2	3	38,480	0.022	0.58	0.593	2.2%
	6	76,960	0.019	2.02	2.078	2.9%
	9	115,430	0.018	4.30	4.45	3.5%
0.4	3	76,960	0.019	0.25	0.257	2.8%
	6	153,910	0.016	0.85	0.878	3.3%
	9	230,870	0.015	1.79	1.877	4.9%
0.6	3	115,430	0.017	0.15	0.156	4%
	6	230,870	0.015	0.53	0.556	4.9%
	9	346,300	0.014	1.12	1.198	7%

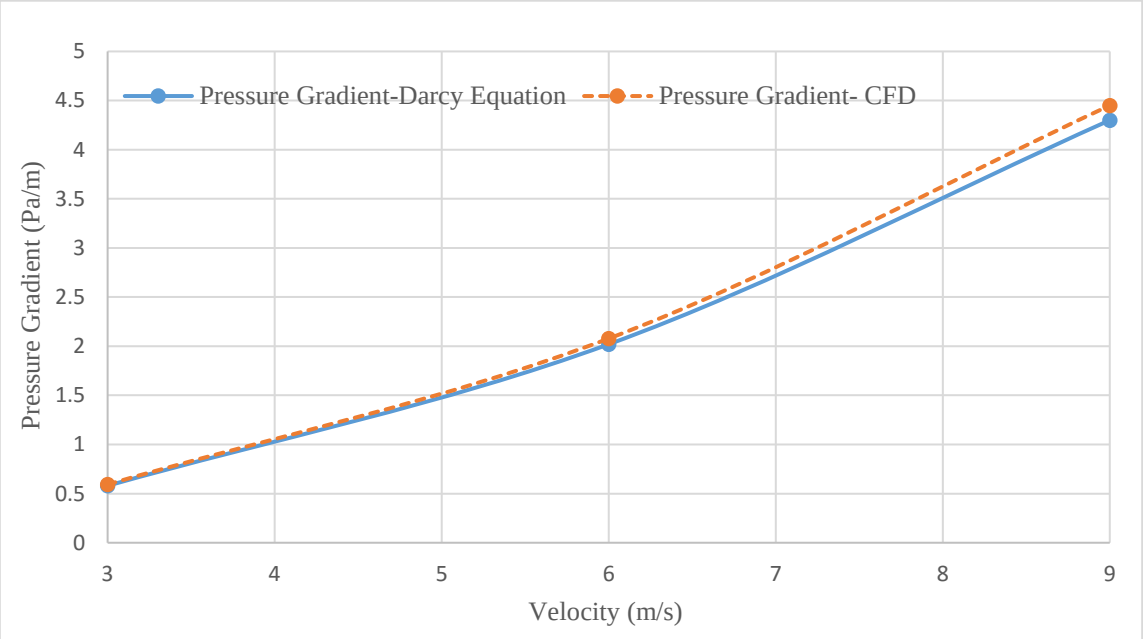

Figure 46. Comparison of analytical and numerical pressure gradient profiles in a square duct of $d_h = 0.2$ m.

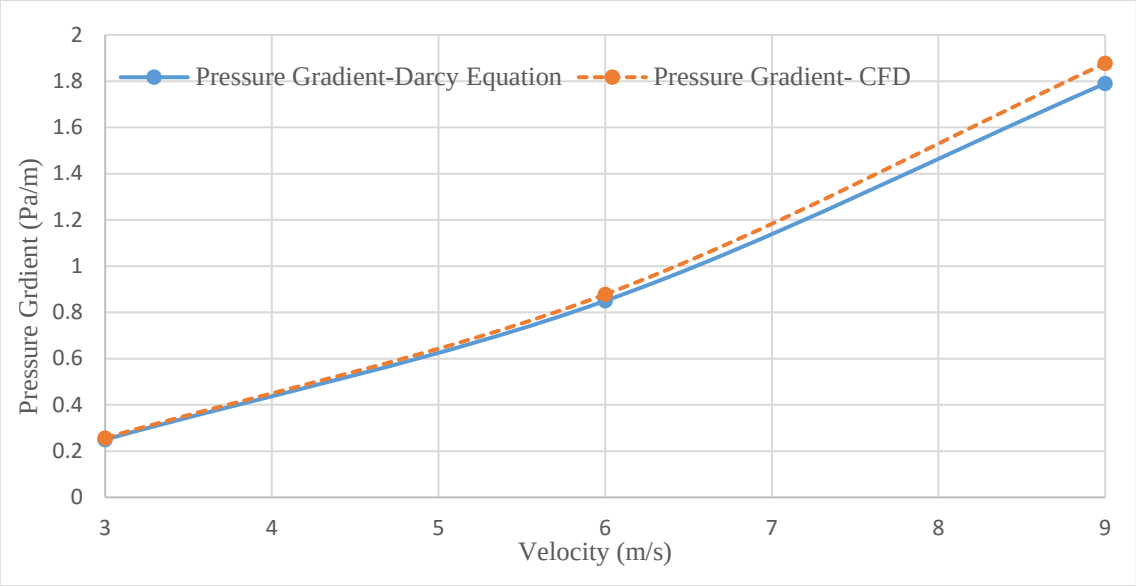

Figure 47. Comparison of analytical and numerical pressure gradient profiles in a square duct of $d_h = 0.4$ m.

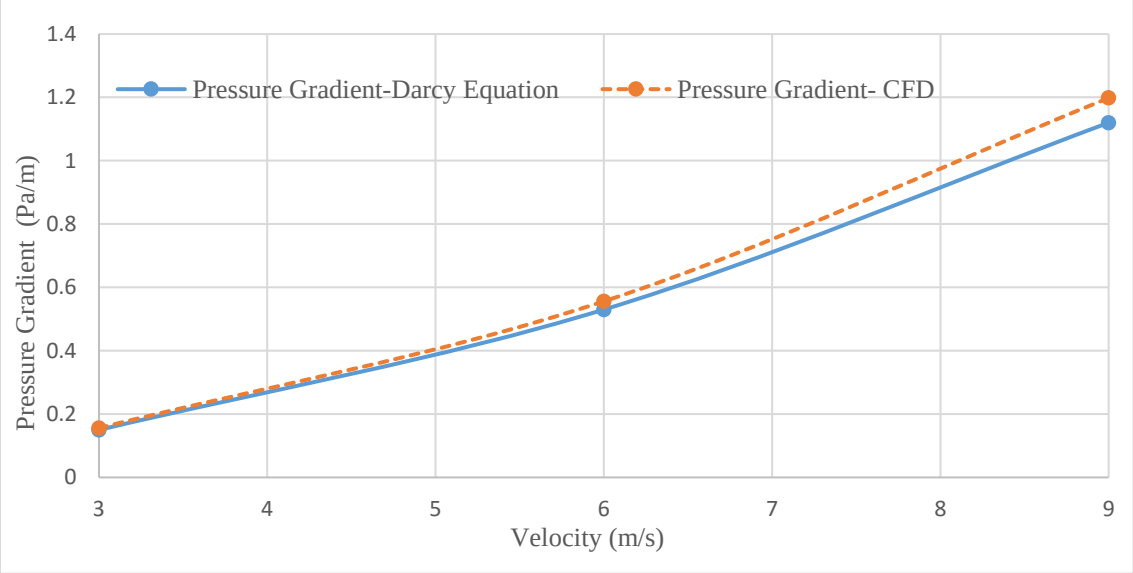

Figure 48. Comparison of analytical and numerical pressure gradient profiles in a square duct of $d_h = 0.6$ m.

5.6 Comparison of Round Ducts and Square Ducts

A comparison of results in Sections IV and V shows that there are some differences between the round and square ducts for both velocity and pressure profiles at any Reynolds number, which in turn leads to different turbulent flow developing length correlations. As one would expect, the round duct models experience lower pressure drops compared to square duct models and shorter flow developing lengths at all Reynolds numbers. These differences are due to the different geometry configuration between round and square ducts, especially at the corners of the square ducts where zero (or near zero) velocity might occurs, which in turn effects the velocity distribution across the duct cross-sectional area.

5.6.1 Effect of Dead Zones

The corners "dead zones" on the square duct cross-section are worth investigating, as they directly affect the velocity profile and even pressure profile of the flow and possibly causing some delay in flow development. One way to tackle such an issue is to compare the cross-section velocity profile at a given point along the duct, and compare that to a diagonal velocity profile at the same location, as shown in Figure 49 below.

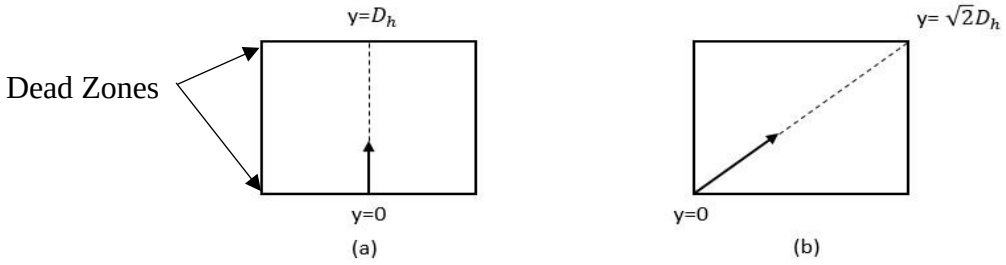

Figure 49. Schematic of cross-section velocity profile (a) and diagonal velocity profile (b).

For a flow velocity of 6 m/s in a $0.6m$ square duct, the cross-sectional velocity profile and the diagonal velocity profile are plotted in the developing length region at $\left(\frac{L}{D}\right)$ of 20 and in the fully developed region at $\left(\frac{L}{D}\right)$ of 60 as shown in Figures 50 and 51 below.

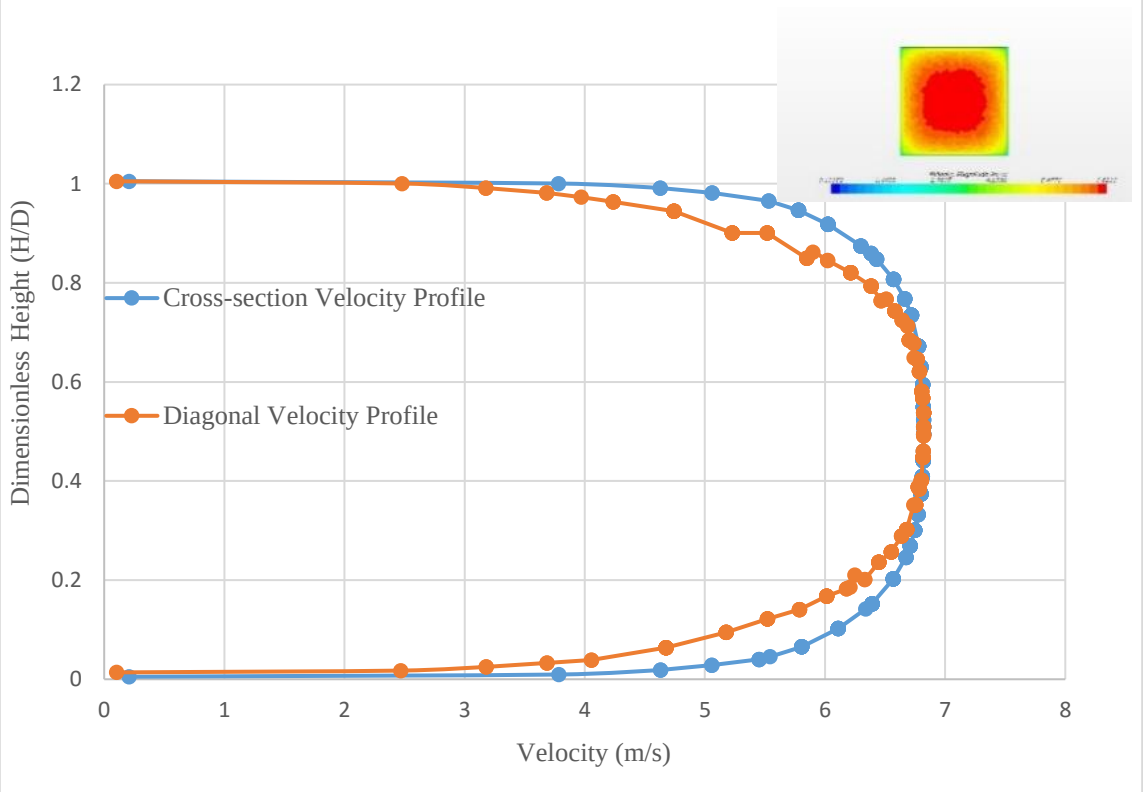

Figure 50. Comparison of cross-section velocity and diagonal velocity profiles at developing region (L/D) = 20 for $v = 6$ m/s flow inside a 0.6 m square duct.

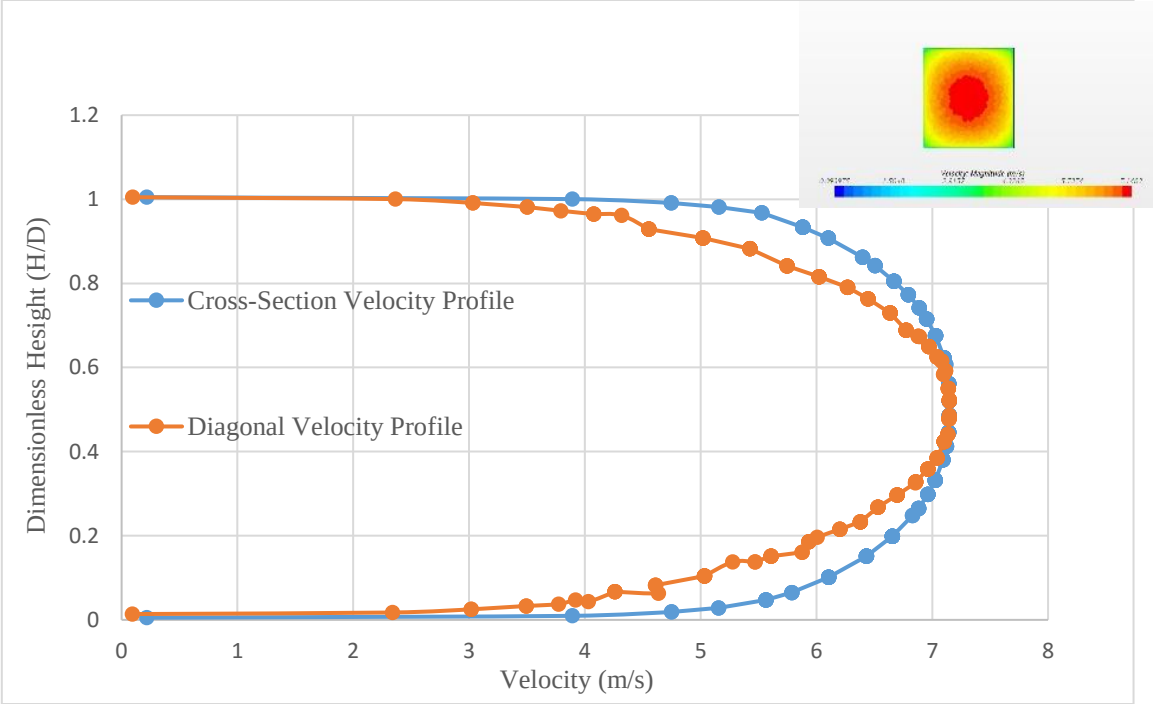

Figure 51. Comparison of cross-section velocity and diagonal velocity profiles at fully developed region $(\frac{L}{D}) = 60$ for $v = 6$ m/s flow inside a 0.6 m square duct.

The above charts clearly show the effect of a near-wall "dead zone" on velocity profiles. In the fully developed flow chart, at a dimensionless height of $(\frac{H}{D})$ of 0.2 , the cross-section velocity was 6.7 m/s while the diagonal velocity was only 6 m/s due to the dead zone effect on boundary layer growth, which can lead to a delay in developing the flow in the square duct compared to the round pipe.

5.6.2 Ratio Correlations

It might be more useful in engineering practice to have a developing length ratio based on the square duct to round duct correlation. By using Equations (4.2) and (5.1), the ratio correlation based on the velocity analysis is

$$\frac{(\frac{L}{D})_{Round}}{(\frac{L}{D})_{Square}} = 0.95 * Re^{-0.0082} \quad (5.5)$$

$$(\frac{L}{D})_{Round} \approx 0.87 * (\frac{L}{D})_{square} \quad (5.6)$$

Based on the pressure analysis, and by using Equations (4.3) and (5.2), the result is

$$\frac{(\frac{L}{D})_{Round}}{(\frac{L}{D})_{Square}} = 1.01 * Re^{-0.0186} \quad (5.7)$$

$$(\frac{L}{D})_{Round} \approx 0.81 * (\frac{L}{D})_{Square} \quad (5.8)$$

A comparison of round and square developing length correlations is tabulated in Tables 26 and 27 and plotted in Figures 52 and 53 below.

Table 26 Comparison of round and square developing length based on velocity profiles

Re	$(L/D)_{Round}$	$(L/D)_{Square}$	$(L/D)_{Round}/(L/D)_{Square}$
38,480	26.9	30.8	0.88
76,960	31.2	35.9	0.87
115,430	34	39.2	0.87
153,910	36.2	41.8	0.87
230,870	39.4	45.7	0.86
346,300	43	50	0.86

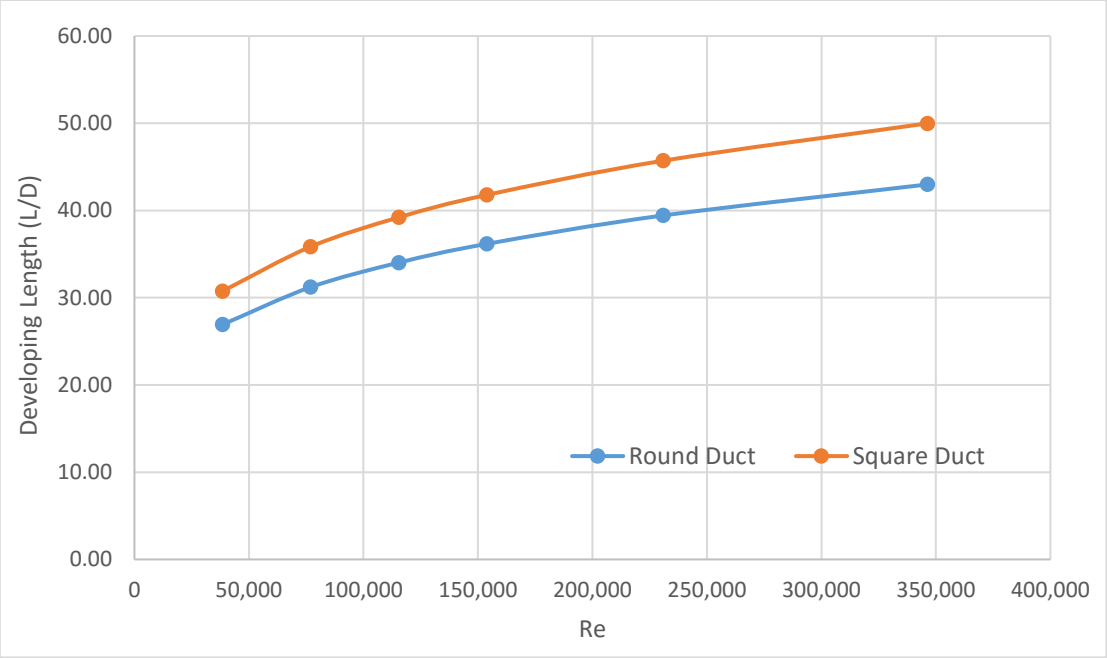

Figure 52. Comparison of round and square ducts developing length based on velocity profiles.

Table 27 Comparison of round and square developing length based on pressure profiles

Re	$(L/D)_{Round}$	$(L/D)_{Square}$	$(L/D)_{Round}/(L/D)_{Square}$
38,480	21.2	25.6	0.83
76,960	25.8	31.6	0.82
115,430	28.9	35.7	0.81
153,910	31.3	38.9	0.81
230,870	35.1	44	0.80
346,300	39.4	49.7	0.79

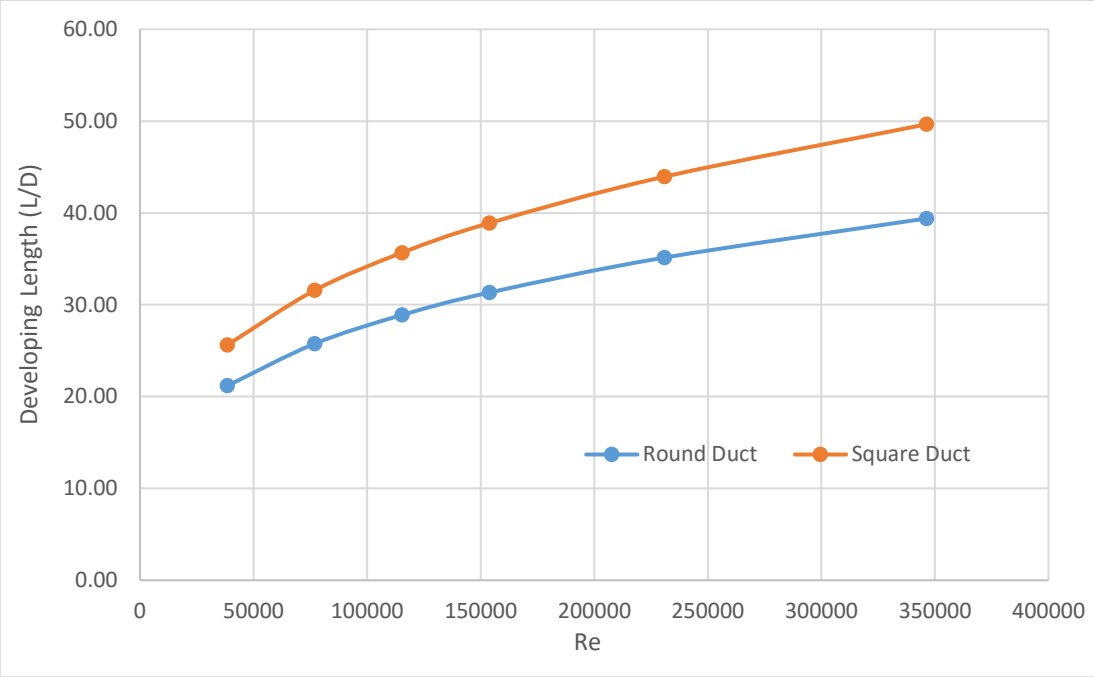

Figure 53. Comparison of round and square ducts developing length based on pressure profiles.

Tables 26 and 27 presented developing length ratios for Reynolds number range from 40,000 to 350,000 based on velocity and pressure approaches, respectively. In both approaches, the ratio values show slight changes over the Reynolds number range, with an average value being around 0.87 with the velocity approach and 0.81 with the pressure approach, which signify only a weak function of Reynolds number.

5.7 Summary

This section presented a CFD analysis of the turbulent flow in square ducts, and analyzed the velocity and pressure profiles for several square duct flow sizes and flow conditions that represent a range of Reynolds numbers. Similar to what we found in round ducts, the results show for both of the velocity and pressure analysis that the

developing length of the flow increases with increasing inlet velocity and/or increasing duct size. Moreover, in flow cases with identical Reynolds numbers, the developing length of the flow appeared to be the same. As a result, the developing length of the flow is a Reynolds number dependent variable such that larger Reynolds number requires a larger developing length to achieve the fully developed flow condition in square ducts.

Based on the velocity gradient profiles, the dimensionless developing length was found to be $30.8, 36, 39, 41.6, 46$, and 50 for increasing flow Reynolds numbers of $(38{,}480)$, $(76{,}960)$, $(115{,}430)$, $(153{,}910)$, (230.870), and $(346{,}300)$, respectively. Similarly, by analyzing the pressure gradient profiles, the dimensionless developing length was found to be 25.5 for a Reynolds number of $(38{,}480)$, 31 for (76960), 36.5 for $(115{,}430)$, 39 for $(153{,}910)$, 45 for $(230{,}870)$, and 48.3 for $(346{,}300)$.

Using thee above numerical results, velocity-based and pressure-based correlations were developed to calculate the required developing length (or the entrance length) in turbulent square duct flow with any Reynolds number. Moreover, a comparison of velocity-based developing length and pressure-based developing length for a range of Reynolds number show a pressure-length to velocity length ratio being around 0.92, signifying a shorter entrance length for pressure-developing length. In addition, the CFD model results show a good agreement when compared against the Darcy equation with a maximum error of 7% for the high turbulent flow case with Reynolds number of $346{,}300$.

Last but not least, square duct results were compared to their corresponded round duct results for a range of Reynolds number. This comparison shows that the developing length in the round duct was relatively shorter than the corresponded square duct by around 13% based on velocity profiles and 19% based on pressure profiles. Also, the round to square developing length ratio values show slight changes over the Reynolds number range, with an average value being around 0.87 with the velocity approach and 0.81 with the pressure approach, which signify only a weak function of Reynolds number.

VI. RECTANGULAR DUCT CASE

6.1 Introduction

This section presents the numerical modelling and CFD analysis of rectangular ducts, with aspect ratios other than one, to study the turbulent flow behavior in the developing region of the duct in order to identity the parameters that effect the developing length of the flow and to locate where fully developed flow is achieved for different Reynolds numbers. Moreover, similar to the round and square ducts, numerical correlations are developed to locate where the fully developed flow is achieved inside these rectangular ducts based on the velocity and pressure profile. Also, an overall comparison of the round, square, and rectangular ducts is presented to investigate the effect of the duct geometry on the developing length of the turbulent flow.

6.2 Problem Description

- The working fluid is air at room temperature and atmospheric pressure with thermophysical properties presented in Table 28.

Table 28 Thermophysical properties of air in rectangular ducts

Thermophysical Property	Value
$\boldsymbol{T}(\mathbf{K})$	300
$\boldsymbol{\mu}\ (\frac{\mathbf{Kg}}{\mathbf{m.s}})$	1.84×10^{-5}
$\boldsymbol{\rho}\ (\frac{\mathbf{Kg}}{\mathbf{m^3}})$	1.18

- Air enters the channel at different uniform velocities of $3\ m/s,\ 6\ m/s,$ and $9\ m/s$.
- Two different rectangular ducts representing aspect ratios of 1.5 and 2, which were chosen because they represent duct designs commonly used in engineering practice. The hydraulic dimeter of the two ducts are found to be 0.4 m as shown in Figure 54 below.

Figure 54. Rectangular ducts with aspect ratio of 1.5 (a), and 2 (b).

- Assumptions applied to this analysis are
    - Steady incompressible flow.
    - Smooth stainless steel rectangular ducts.
    - Negligible gravity effects on fluid flow.
    - Rectangular ducts are completely filled with the fluid being transported.

6.3 Modelling and Simulation

The rectangular duct geometry was created and imported to the STAR CCM+ software in order to simulate the fluid flow. As explained earlier, STAR CCM+ uses control volume based finite volume method to solve the coupled, non-linear partial differential governing equations for the fluid, as shown in Figures 55 and 56 below.

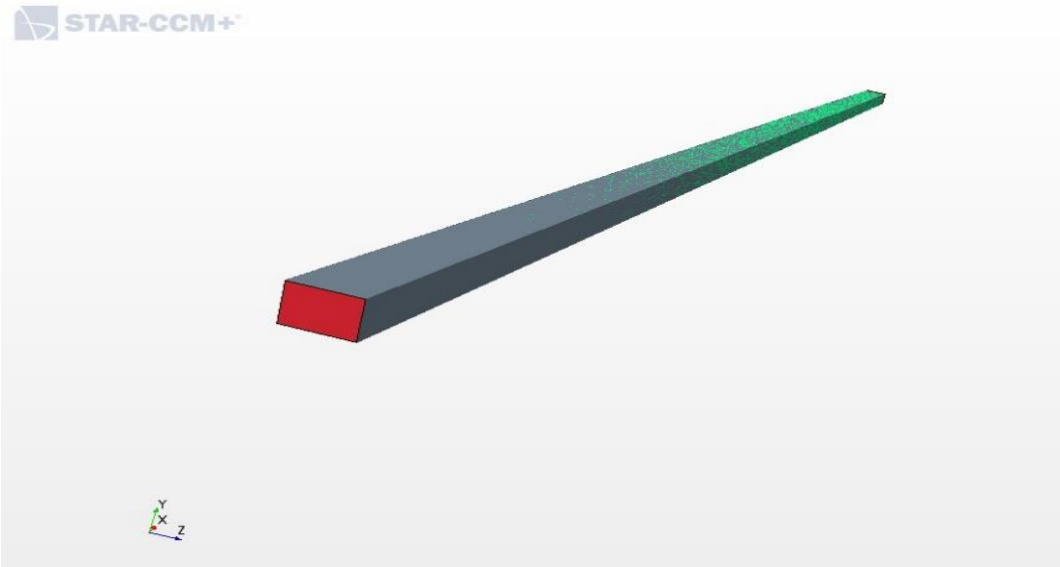

Figure 55. Computational domain of rectangular duct flow with aspect ratio of 1.5.

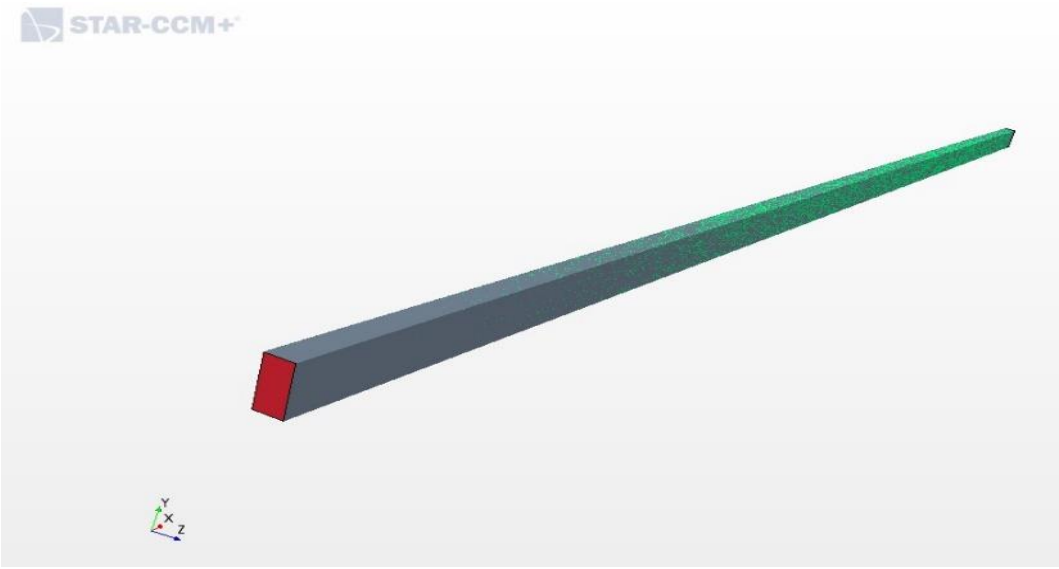

Figure 56. Computational domain of rectangular duct flow with aspect ratio of 2.

6.3.1 Mesh Generation

As we did with round and square ducts simulations, the first step in the CFD simulation of the fluid flow is to generate a mesh that represents the duct geometry. In order to do so, the below mesh models were chosen in STAR CCM+ to most accurately simulate the turbulent fluid flow inside the rectangular duct.

- Surface Remesher.
- Polyhedral Mesher.
- Embedded Thin Mesher.
- Prism Layer Mesher.

By following the user guide in STAR CCM+ for channel flow applications, the geometry mesh base size is selected as 5 cm with a surface growth rate of 1.7. Also, since both of the rectangular ducts have the same hydraulic diameter, two layers of the thin mesh model and nine layers of prism mesh are used in generating the volume mesh for both of the rectangular ducts. Table 29 below summarizes the volume mesh parameter values used in generating the rectangular duct mesh.

Table 29 Summary of mesh parameter values used in rectangular ducts models

Mesh Parameters	Input Value
Base Size	0.05 m
Number of Prism Layers	9
Surface Growth Rate	1.7
Thin Mesh Layers	2
Relative Maximum Size	40
Relative Minimum Size	60

For the prism layer mesh model, the prism layer absolute thickness and the near wall thickness values are selected for both rectangular ducts aspect ratios in order to

accurately capture the near wall velocity profiles and viscous sublayer of the turbulent flow. The absolute prism layer thickness values selected are 14.25 mm and 15.21 mm for rectangular ducts with aspect ratios of 1.5 and 2, respectively. Moreover, the near wall prism layer thickness selected are 0.056 mm and 0.06 mm for rectangular ducts with aspect ratios of 1.5 and 2, respectively. Once the volume mesh was generated, the overall number of cells found to be 2,733,620 cells for the rectangular duct with the aspect ratio of 1.5 and 2,979,646 cells for the rectangular duct with aspect ratio of 2, as tabulated in Table 30 and plotted in Figures 57 and 58 below.

Table 30. Detailed prism layer mesh specifications and overall cells number for all rectangular ducts aspect ratios

Aspect Ratio	Prism Layer Absolute Thickness (mm)	Thickness of Near Wall Prism Layers (mm)	Overall Number of Cells
1.5	14.25	0.056	2,733,620
2	15.21	0.060	2,979,646

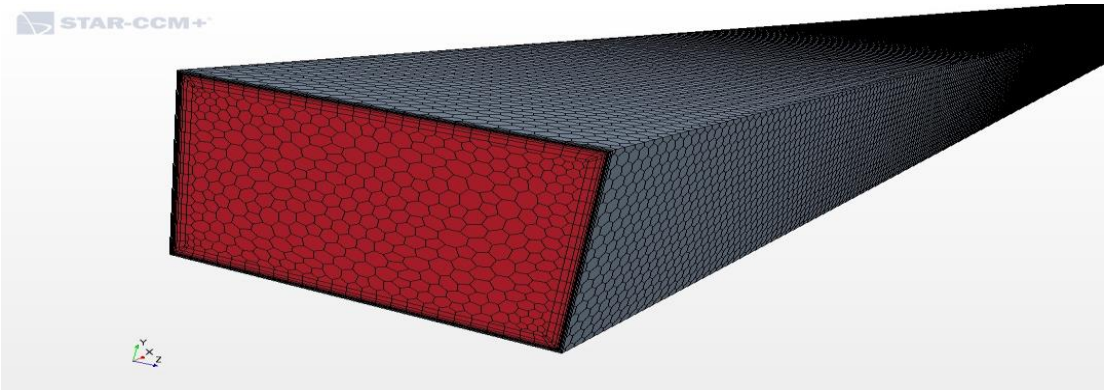

Figure 57. Generated volume mesh for rectangular duct with aspect ratio of 1.5 and hydraulic diameter of $d_h = 0.4$ m.

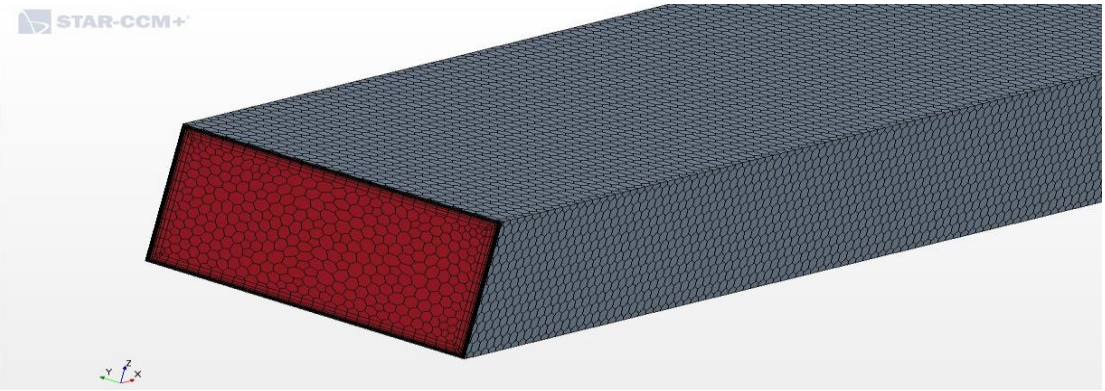

Figure 58. Generated volume mesh for rectangular duct with aspect ratio of 2 and hydraulic diameter of $d_h = 0.4$ m.

6.3.2 Fluid Physical Properties

Once the mesh or grid was established for each rectangular duct size, the next step was to choose the appropriate physical models to accurately simulate the fluid flow. By following the STAR CCM+ user guide, the fluid physical models recommended to use for the straight channel turbulent flow simulations are listed below.

- Three dimensional steady flow.
- Constant Air Density.
- Turbulent Flow.
- K − ω Turbulence Model.
- All $y+$ wall treatment.
- Reynolds-Averaged Navier-Stokes.
- Segregated Flow Model.
- Turbulence Suppression. Transition Model.
- Cell Quality Remediation.

6.3.3 Boundary Conditions

The next step was to identify and specify the appropriate boundary conditions of the flow at the duct inlet, $\frac{L}{D}$ of 0 and exit, $\frac{L}{D}$ of 100, with the exit being an arbitrary chosen value that assured achieving the fully developed flow in all cases. For all the rectangular ducts aspect ratios, the flow was assumed to enter with uniform flow velocities of $3\ \mathrm{m/s}, 6\ \mathrm{m/s}$, and $9\ \mathrm{m/s}$. The duct is considered long enough to assume atmospheric pressure at the duct outlet, which corresponds to zero gauge pressure.

In this analysis, the turbulence parameters are quantified by the turbulent intensity of the flow and the turbulence length scale. At the inlet, as stated earlier, the turbulence intensity is mainly a function of the upstream history of the flow and the nature of the flow application. For our case of turbulent flow in HVAC, it is usually reasonable to assume turbulent intensity of 5% at the duct inlet. However, as we did with other ducts, at the exit in the fully developed region, the turbulent intensity is estimated by using Equation (3.12) below.

$$I_{FDF} = 0.16 * Re^{-\frac{1}{8}} \tag{3.12}$$

For the turbulence length scale, which is a quantity related to the size of large eddies that contain the turbulent energy, Equation (4.1) may be used as an approximation in the fully developed region of the flow.

$$l_{FDF} = 0.07 * D_h \tag{4.1}$$

In addition to the inlet and outlet boundary conditions, a stationary wall boundary condition, namely a no-slip assumption, is applied at the walls of the rectangular ducts, such that velocity increases from zero at the wall to a maximum velocity in middle of the

duct. Moreover, as with the other round and square ducts simulations, a wall function method is used for near wall treatment in order to accurately simulate the flow inside the round duct, as plotted in Figure 59 and tabulated in Tables 31 and 32 below.

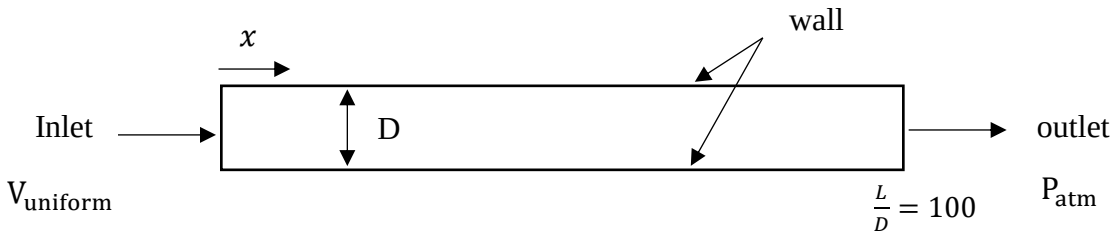

Figure 59. Types of boundary conditions used in rectangular duct models.

Table 31 Summary of inlet and outlet boundary conditions for all rectangular duct sizes

Uniform Inlet Velocity (m/s)	3, 6 , 9
Outlet gage Pressure (Pa)	Zero

Table 32 Summary of turbulence parameters boundary conditions for all rectangular aspect ratios

Turbulence Parameters	**V=3m/s**	**V=6m/s**	**V=9m/s**
TI_{in} **(Intensity)**	5%		
l_{in} **(Length Scale)**	0.031 m		
TI_{FD} **(Intensity)**	3.9%	3.6%	3.4%
l_{FD} **(Length Scale)**	0.028 m		

6.4 Results and Discussion

After the simulations have been set up for the rectangular ducts with the two aspect rations, the STAR CCM+ was used to determine velocity and pressure profiles for each case. By using these plots, the velocity gradient profiles dv/dx and pressure gradient profiles dp/dx were developed for each Reynolds number value and used to locate where the fully developed flow occurs in the rectangular ducts based on these velocity and pressure profiles.

Similar to what we did for round ducts models earlier, the criteria used to define where the fully developed flow is reached inside the ducts is to assume that the flow will be fully developed where the (dv/dx) value is around 99% of the fully developed region (dv/dx),which is $(dv/dx)_{FD}$ of 0. Similarly, by using the pressure gradient profiles, the flow is assumed to be fully developed where (dp/dx) reaches 99% of the (dp/dx) in the fully developed region, assuming that $(dp/dx)_{FD}$ is constant.

6.4.1 Rectangular Ducts with Aspect Ratio of One and Half

Three rectangular ducts models with aspect ratio of 1.5 and hydraulic diameter of $0.4m$ have been modeled and simulated with uniform inlet velocities of $3\ \mathrm{m/s}$,$6\ \mathrm{m/s}$, and $9\ \mathrm{m/s}$. By analyzing the obtained velocity profiles in each case, and by following the fully developed flow criteria stated above, the dimensionless developing length $\left(\frac{L}{D}\right)_{FD}$ found to be 44 with an inlet velocity of $3\ \mathrm{m/s}$, 49 with an inlet velocity of $6\ \mathrm{m/s}$, and 54 with an inlet velocity of $9\ \mathrm{m/s}$.

Similarly, and in order to investigate the duct size effect on the developing length of the flow, rectangular ducts with aspect ratio of 1.5 and hydraulic diameters of 0.2 m

and 0.6 m with uniform inlet velocity of 6 m/s have been modeled. The dimensionless developing length $\left(\frac{L}{D}\right)_{FD}$ revealed to be 43.7 and 54.2 for the rectangular ducts with diameters of 0.2 m and 0.6 m, respectively.

The above results show that the dimensionless developing lengths $\left(\frac{L}{D}\right)_{FD}$ increase with the increasing Reynolds number of the flow, while it remains almost constant with different flow velocity and duct sizes, which they share an identical Reynolds number. These findings are tabulated in Table 33 and plotted in Figures 60 and 61 below.

Table 33 Summary of dimensionless developing length $\left(\frac{L}{D}\right)_{FD}$ for all rectangular duct cases with aspect ratio of 1.5 based on velocity profiles with their corresponding Reynolds numbers

V-based Profile		**v=3m/s**		**v=6m/s**		**v=9m/s**	
Dimensions(m)	$\boldsymbol{D_h}$ **(m)**	**Re**	**$(L/D)_{FD}$**	**Re**	**$(L/D)_{FD}$**	**Re**	**$(L/D)_{FD}$**
a=0.25,b=0.17	0.2	38,480	*	76,960	43.7	115,430	*
a=0.5, b=0.33	0.4	76,960	44	153,910	49	230,870	54
a=0.75, b=0.5	0.6	115,430	*	230,870	54.2	346,300	*

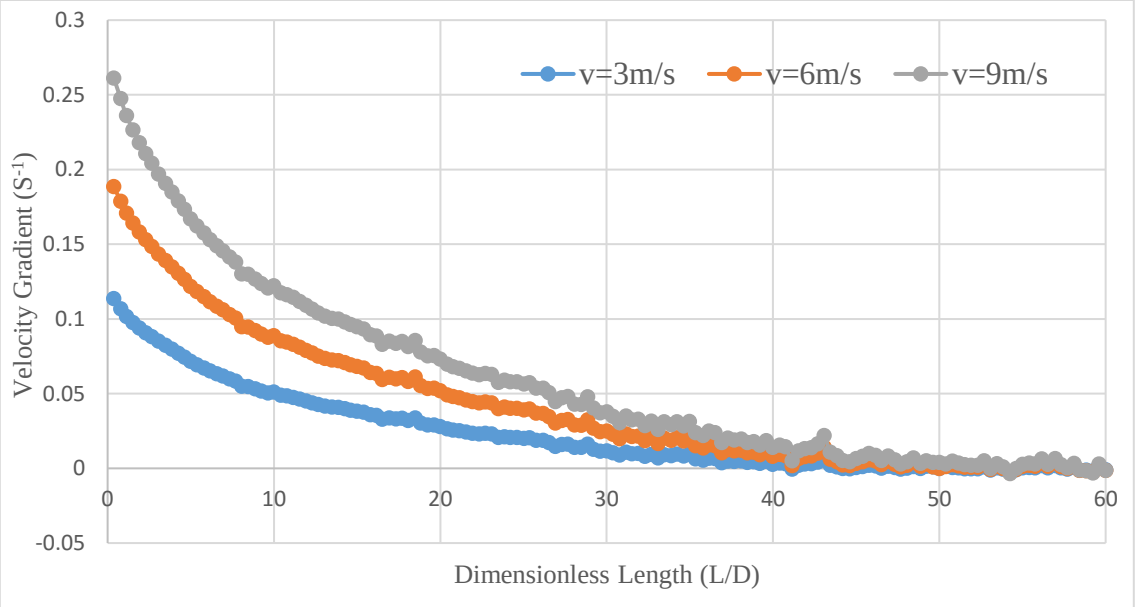

Figure 60. Velocity gradient profiles for different uniform inlet velocities in rectangular duct of $d_h = 0.4$ m with aspect ratio of 1.5.

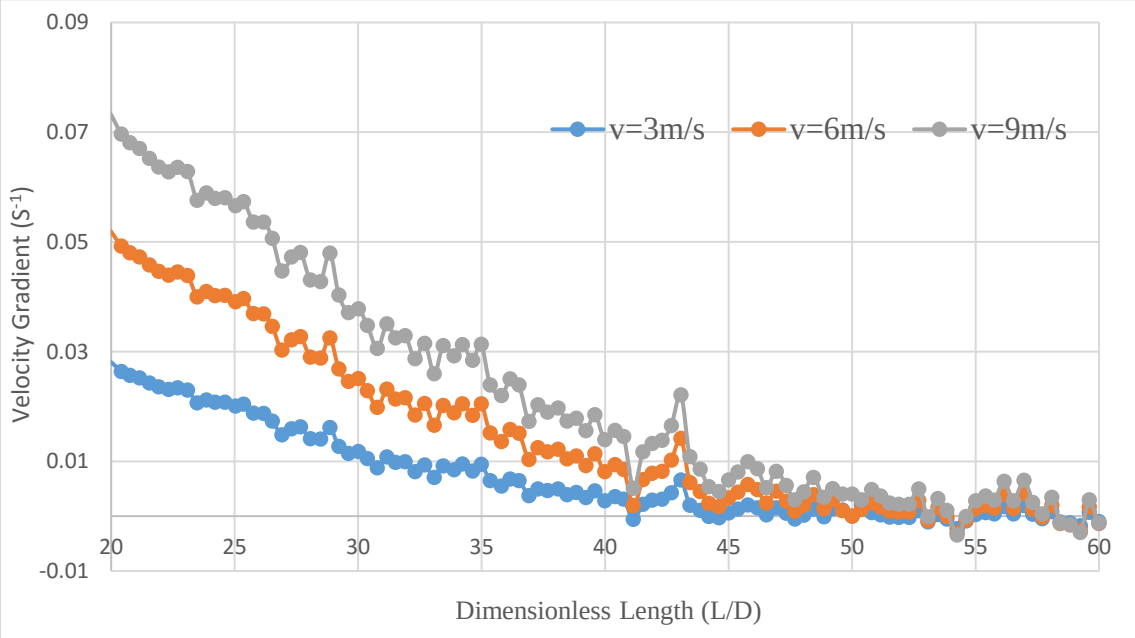

Figure 61. Enlarged velocity gradient profiles for different uniform inlet velocities in rectangular duct of $d_h = 0.4$ m with aspect ratio of 1.5.

The above $\left(\frac{L}{D}\right)_{FD}$ results are plotted as function of Reynolds number for each case in Figure 62, and by then using a curve fitting procedure, a velocity-based CFD correlation for the fully developed flow location is developed for room temperature air flowing inside a 1.5 aspect ratio rectangular duct.

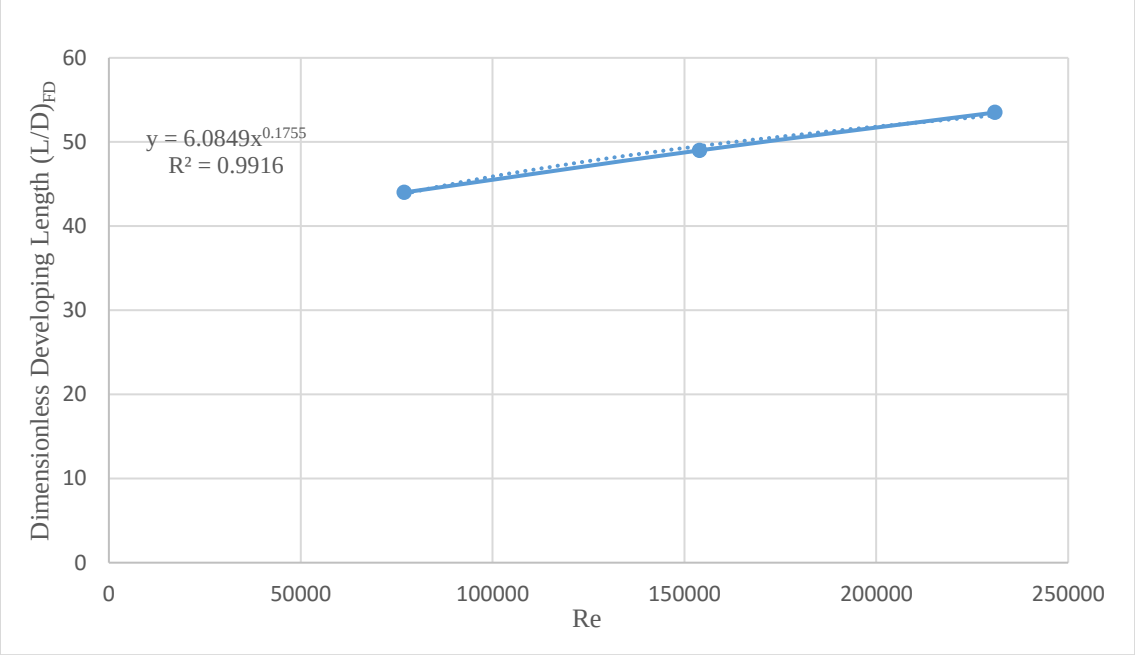

Figure 62. Curve fitting profile (velocity-based correlation) for rectangular duct with aspect ratio of 1.5.

The resulting correlation based on the curve fitting is

$$\left(\frac{L}{D}\right)_{FDF_V} = 6.0849 * Re^{0.1755} \tag{6.1}$$

A similar analysis based on the pressure profiles was carried out to investigate the developing length and then compared to the previous velocity based results at each flow Reynolds number. By using the fully developed flow criteria stated earlier, for rectangular duct of 0.4 m, the dimensionless developing length $\left(\frac{L}{D}\right)_{FD}$ based on the pressure gradient profiles was found to be 38 with an inlet velocity of 3 m/s, 46 with an inlet velocity of 6 m/s, and 53 with 9 m/s inlet velocity. In rectangular ducts of 0.2 m and 0.6 m with a uniform inlet velocity of 6 m/s , the dimensionless developing length $\left(\frac{L}{D}\right)_{FD}$ found to be 37.3 and 54.1, respectively.

Similar to the velocity analysis results, the results show that the pressure-based dimensionless developing lengths $\left(\frac{L}{D}\right)_{FD}$ increase with the increasing Reynolds number of the flow, while it remains almost constant with different flow velocity and duct sizes that have an identical Reynolds number. Table 34 and Figure 63 below show these findings.

Table 34 Summary of dimensionless developing length $\left(\frac{L}{D}\right)_{FD}$ for all rectangular duct cases with aspect ratio of 1.5 based on pressure profiles with their corresponding Reynolds numbers

P-based Profile		**v=3m/s**		**v=6m/s**		**v=9m/s**	
Dimensions(m)	$\boldsymbol{D}$ **(m)**	**Re**	**$(L/D)_{FD}$**	**Re**	**$(L/D)_{FD}$**	**Re**	**$(L/D)_{FD}$**
a=0.25,b=0.17	0.2	38,480	*	76,960	37.3	115,430	*
a=0.5, b=0.33	0.4	76,960	38	153,910	46	230,870	53
a=0.75, b=0.5	0.6	115,430	*	230,870	54.1	346,300	*

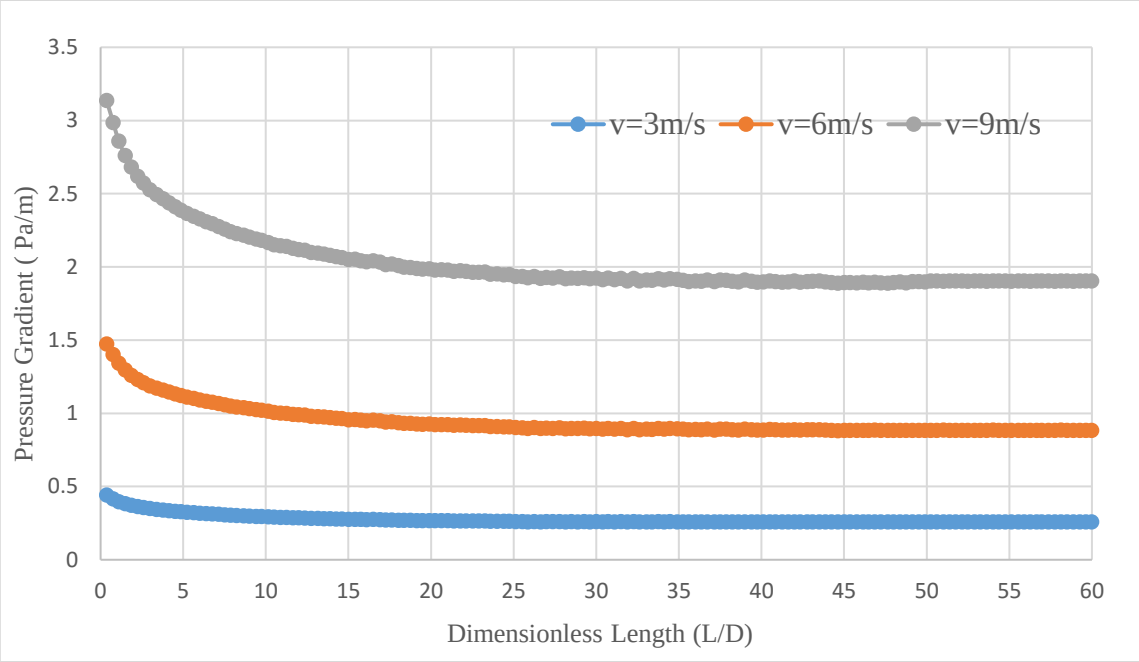

Figure 63. Pressure gradient profiles for different uniform inlet velocity in rectangular duct of $d_h = 0.4$ m and aspect ratio of 1.5.

The above $\left(\frac{L}{D}\right)_{FD}$ results are plotted as function of Reynolds number for each case in Figure 64, and then by using a curve fitting procedure, a pressure-based CFD correlation for the fully developed flow location is developed for room temperature air flowing inside a 1.5 aspect ratio rectangular duct.

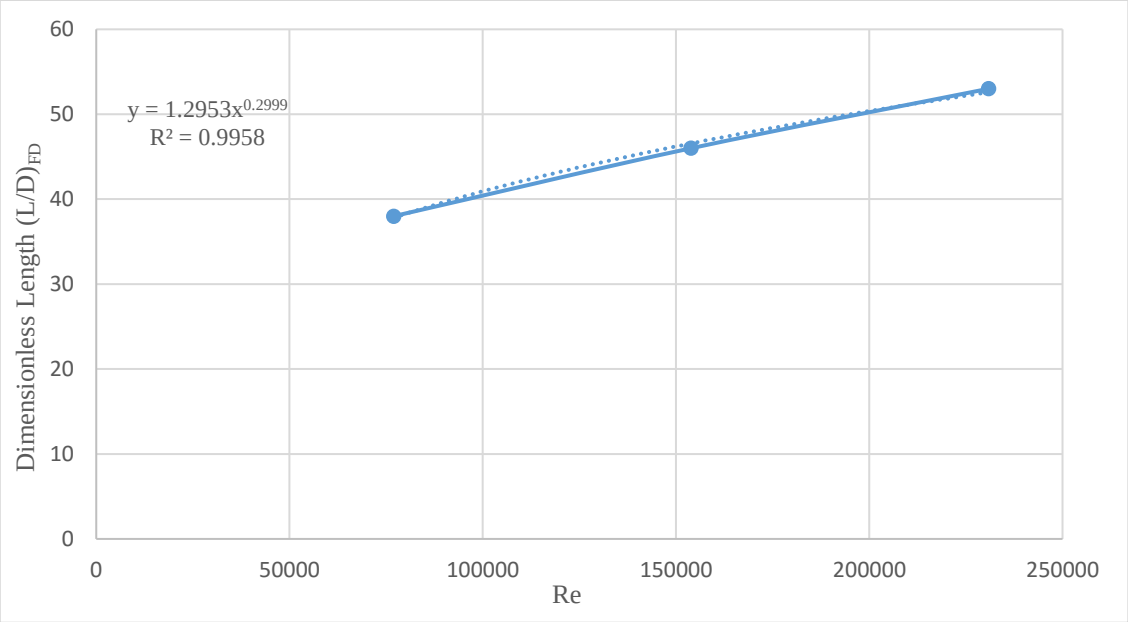

Figure 64. Curve fitting profile (pressure-based correlation) in rectangular duct with aspect ratio of 1.5.

The resulting correlation based on the curve fitting graph is

$$(\frac{L}{D})_{FDF_P} = 1.2953 * Re^{0.3} \quad (6.2)$$

Table 35 Comparison of velocity-based and pressure-based developing $(L/D)_{FD}$ values in rectangular ducts with aspect ratio of 1.5 at different Reynolds numbers

Re	$\mathbf{(L/D)_{FDF_V}}$	$\mathbf{(L/D)_{FDF_P}}$	**(L/D)P/(L/D)V**
76,960	44	38	0.86
153,910	49	46	0.94
230,870	54	53	0.98

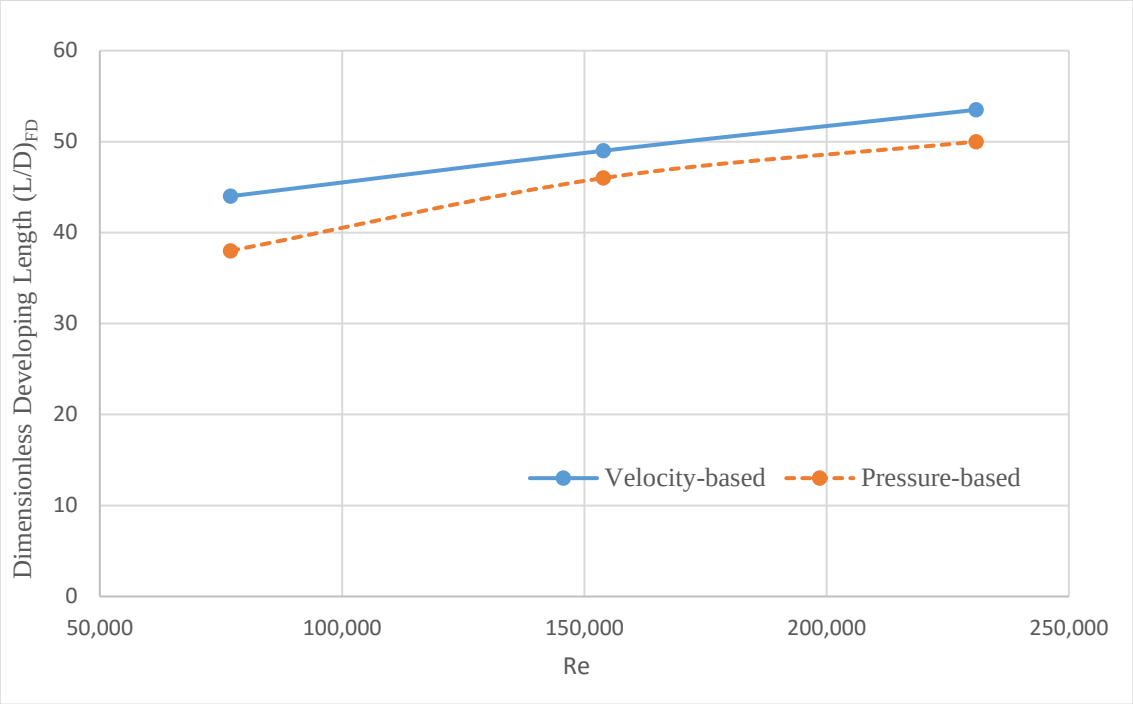

Figure 65. Comparison of velocity-based and pressure-based developing $(L/D)_{FD}$ values in rectangular duct with aspect ratio of 1.5 at different Reynolds numbers.

As shown in above analysis and results, there are two distinct approaches that can be used to quantify the developing length in turbulent flow rectangular duct, namely velocity-based and pressure based correlations. The two approaches are directly compared in Table 35 and Figure 65 where the two developing lengths are shown and plotted at the same Reynolds number. Using Equation (6.1) and (6.2), a ratio of the pressure-based correlation and velocity-based correlation was obtained as follow

$$\frac{(\frac{L}{D})_P}{(\frac{L}{D})_V} = 0.213\ Re^{0.1245} \tag{6.3}$$

$$(\frac{L}{D})_P = 0.93 * (\frac{L}{D})_V \quad (6.4)$$

Table 35 presented developing length ratios for Reynolds number range from 40,000 to 350,000, in which the ratio values show slight changes over the Reynolds number range, with an average value being around 0.93, which signifies only a weak function of Reynolds number.

6.4.2 Rectangular Ducts with Aspect Ratio of Two

Three rectangular ducts models with aspect ratio of 2 and hydraulic diameter of $0.4m$ have been modeled and simulated with uniform inlet velocities of $3\ \mathrm{m/s}$,$6\ \mathrm{m/s}$, and $9\ \mathrm{m/s}$. By analyzing the obtained velocity profiles in each case, and by following the fully developed flow criteria stated above, the dimensionless developing length $\left(\frac{L}{D}\right)_{FD}$ found to be 50 with an inlet velocity of $3\ \mathrm{m/s}$, 56.5 with an inlet velocity of $6m/s$, and 62 with an inlet velocity of $9\ \mathrm{m/s}$.

Similarly, and in order to investigate the duct size effect on the developing length of the flow, rectangular ducts with aspect ratio of 2 and hydraulic diameters of $0.2\ \mathrm{m}$

and $0.6\ \mathrm{m}$ with uniform inlet velocity of $6\ \mathrm{m/s}$ have been modeled. The dimensionless developing length $\left(\frac{L}{D}\right)_{FD}$ revealed to be 49.2 and 63 for rectangular ducts of $0.2\ \mathrm{m}$ and $0.6\ \mathrm{m}$, respectively.

Similar to rectangular ducts with 1.5 aspect ratio, the above results show that the dimensionless developing length $\left(\frac{L}{D}\right)_{FD}$ increases with the increasing Reynolds number of the flow, while it remains almost constant with different flow velocity and duct sizes,

which they share an identical Reynolds number. These findings are tabulated in Table 36 and plotted in Figures 66 and 67 below.

Table 36 Summary of dimensionless developing length $\left(\frac{L}{D}\right)_{FD}$ for all rectangular duct cases with aspect ratio of 2 based on velocity profiles with their corresponding Reynolds numbers

V-based Profile		**v=3m/s**		**v=6m/s**		**v=9m/s**	
Dimensions(m)	**D_h (m)**	**Re**	**$(L/D)_{FD}$**	**Re**	**$(L/D)_{FD}$**	**Re**	**$(L/D)_{FD}$**
a=0.3,b=0.15	0.2	38,480	*	76,960	49.2	115,430	*
a=0.6, b=0.3	0.4	76,960	50	153,910	56.5	230,870	62
a=0.9, b=0.45	0.6	115,430	*	230,870	63	346,300	*

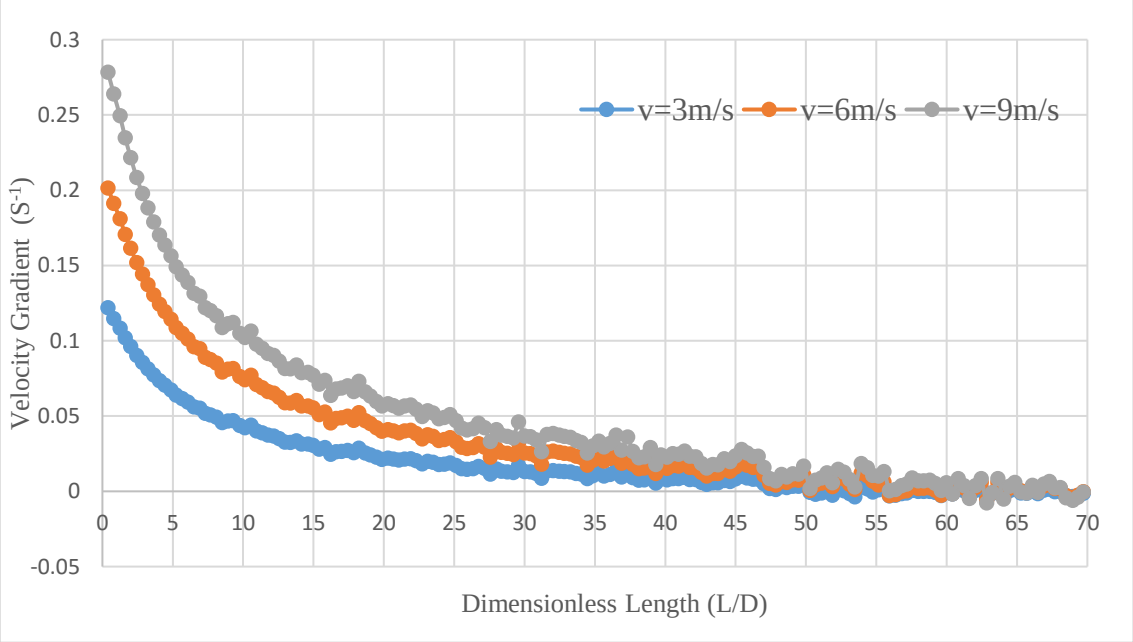

Figure 66. Velocity gradient profiles for different uniform inlet velocities in rectangular duct of $d_h = 0.4$ m and aspect ratio of 2.

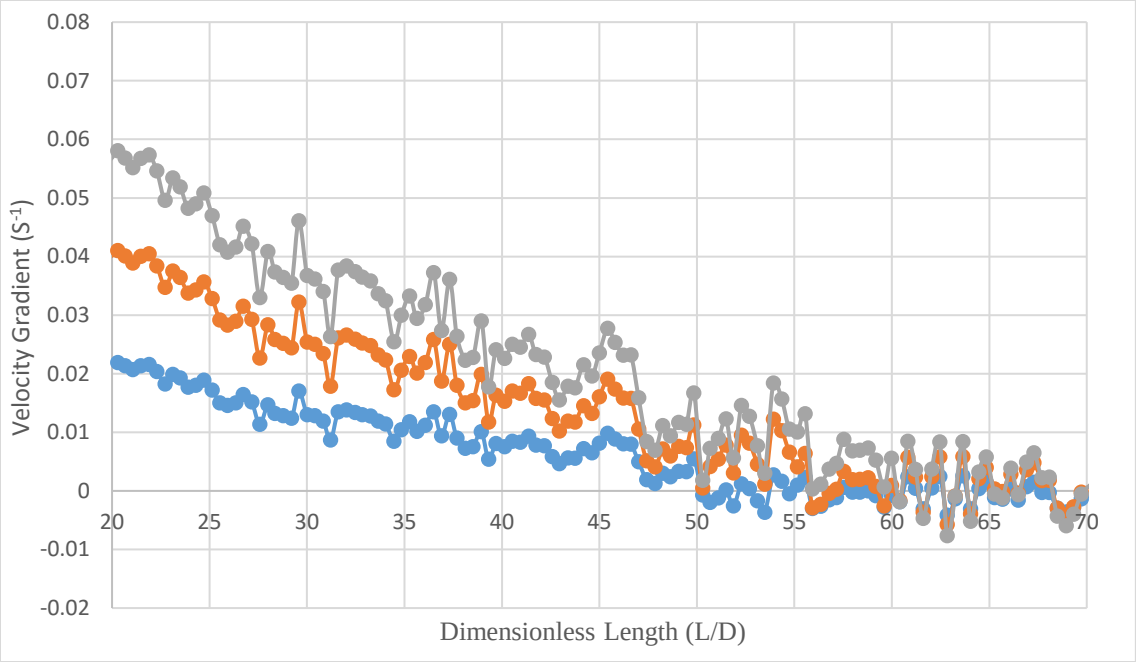

Figure 67. Enlarge velocity gradient profiles for different uniform inlet velocities in rectangular duct of $d_h = 0.4$ m and aspect ratio of 2.

The above $\left(\frac{L}{D}\right)_{FD}$ results are plotted as function of Reynolds number for each case in Figure 68, and then by using a curve fitting procedure, a velocity-based CFD correlation for the fully developed flow location is developed for room temperature air flowing inside a rectangular duct with aspect ratio of 2.

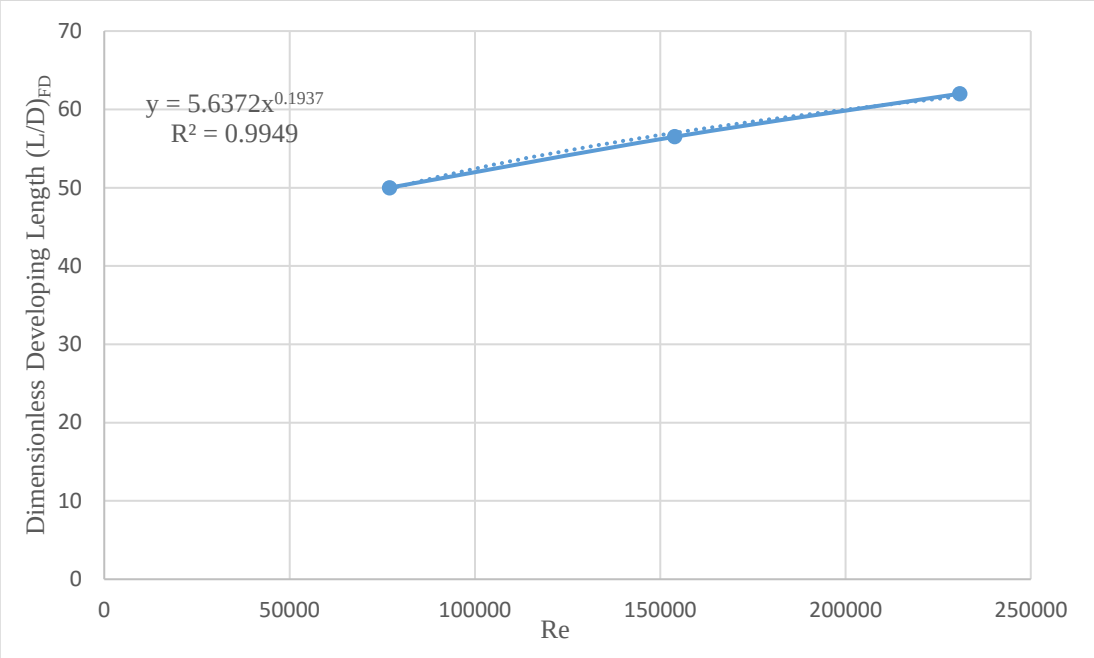

Figure 68. Curve fitting profile (velocity-based correlation) in rectangular ducts with aspect ratio of 2.

The resulting correlation based on the curve fitting graph above can be expressed as

$$(\frac{L}{D})_{FDF_V} = 5.6372 * Re^{0.1937} \quad (6.5)$$

Similar analysis based on the pressure profiles was carried out to investigate the developing length and then compared to the previous velocity based result at each flow Reynolds number. By using the fully developed flow criteria stated earlier, for a rectangular duct of 0.4 m, the dimensionless developing length $\left(\frac{L}{D}\right)_{FD}$ based on the pressure gradient profiles was 43.5 with an inlet velocity of 3 m/s, 52.5 with an inlet velocity of 6 m/s, and 60 with an inlet velocity of 9 m/s. For rectangular ducts of 0.2 m

and 0.6 m with uniform inlet velocity of 6 m/s , the dimensionless developing length $\left(\frac{L}{D}\right)_{FD}$ found to be 42.6 and 62, respectively.

Similar to the velocity analysis results, the pressure-based dimensionless developing length $\left(\frac{L}{D}\right)_{FD}$ increases with the increasing Reynolds number of the flow, while it remains almost constant with different flow velocity and duct sizes that share an identical Reynolds number. These results are tabulated in Table 37 and plotted in Figure 69.

Table 37 Summary of dimensionless developing length $\left(\frac{L}{D}\right)_{FD}$ for all rectangular duct cases with aspect ratio of 2 based on pressure profiles with their corresponding Reynolds numbers

P-based Profile		**v=3m/s**		**v=6m/s**		**v=9m/s**	
Dimensions(m)	D_h (m)	**Re**	**$(L/D)_{FD}$**	**Re**	**$(L/D)_{FD}$**	**Re**	**$(L/D)_{FD}$**
a=0.3,b=0.15	0.2	38,480	*	76,960	42.6	115,430	*
a=0.6, b=0.3	0.4	76,960	43.5	153,910	52.5	230,870	60
a=0.9, b=0.45	0.6	115,430	*	230,870	62	346,300	*

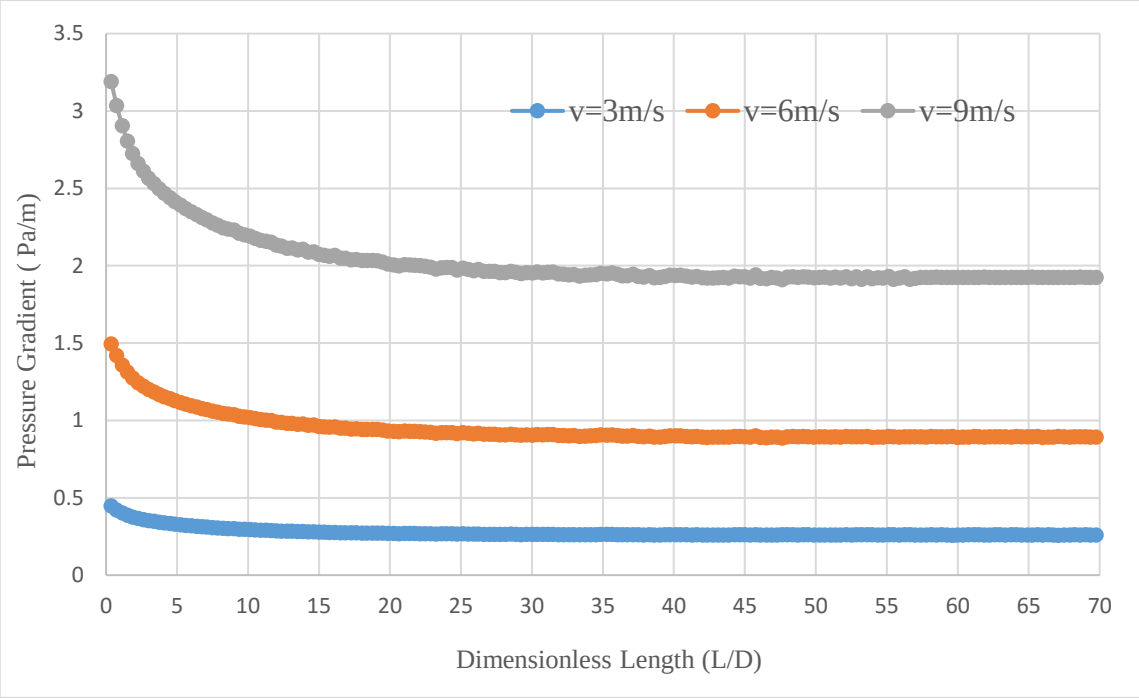

Figure 69. Pressure gradient profiles for different uniform inlet velocities in rectangular duct of $d_h = 0.4$ m and aspect ratio of 2.

The above $\left(\frac{L}{D}\right)_{FD}$ results are plotted as function of Reynolds number for each case in Figure 70, and then by using a curve fitting procedure, a pressure-based CFD correlation for the fully developed flow location is developed for room temperature air flowing inside rectangular duct with aspect ratio of 2.

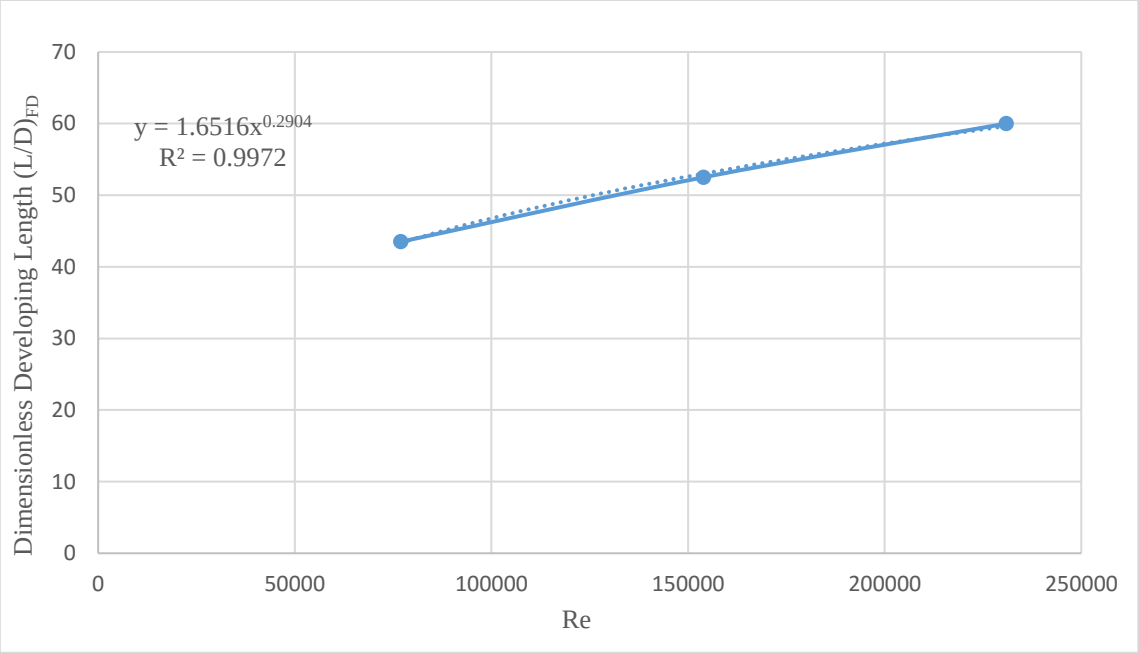

Figure 70. Curve fitting profile (pressure-based correlation) for rectangular duct with aspect ratio of 2.

The resulting correlation based on the curve fitting graph can be expressed as

$$(\frac{L}{D})_{FDF_P} = 1.6516 * \ Re^{0.2904} \tag{6.6}$$

Table 38 Comparison of velocity-based and pressure-based developing $(L/D)_{FD}$ values in rectangular ducts with aspect ratio of 2 at different Reynolds numbers

Re	$(L/D)_{FDF_V}$	$(L/D)_{FDF_P}$	**(L/D)P / (L/D)V**
76,957	50	43.5	0.87
153,913	56.5	52.5	0.93
230,870	62	60	0.97

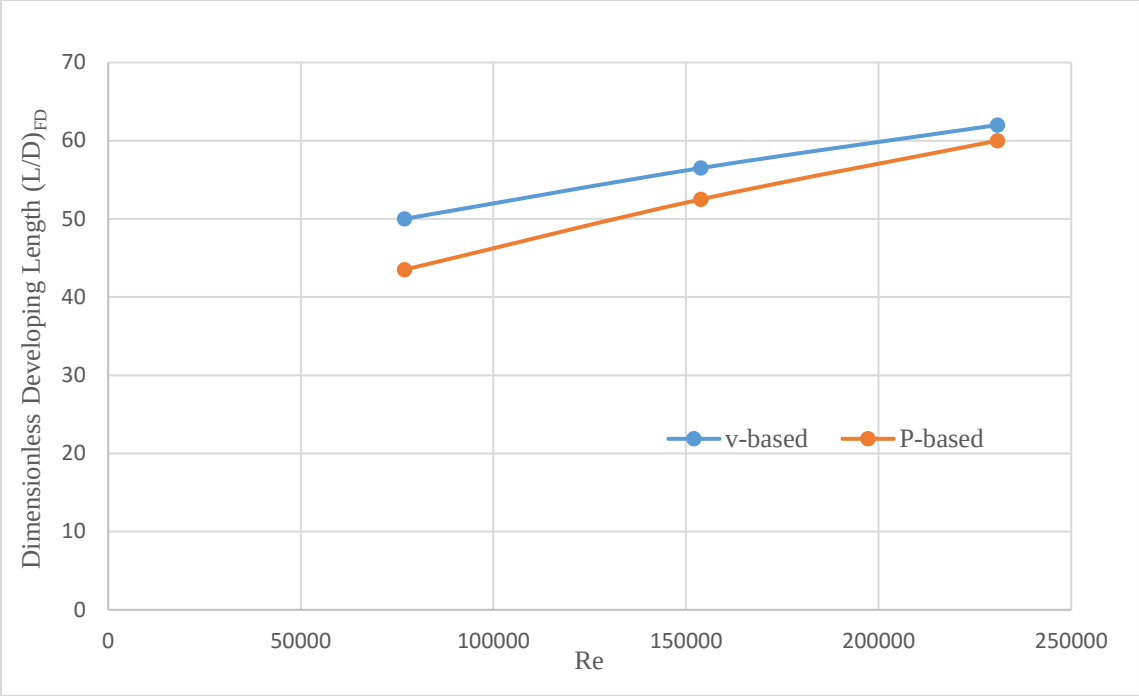

Figure 71. Comparison of velocity-based and pressure-based developing $(L/D)_{FD}$ values in rectangular ducts with aspect ratio of 2 at different Reynolds numbers.

Similar to rectangular ducts with aspect ratio of 1.5, the results and analysis above show that there are two distinct approaches that can be used to quantify the developing length in turbulent flow rectangular duct with aspect ratio of 2, namely velocity-based and pressure based approaches. The two approaches are directly compared in Table 38 and Figure 71 where the two developing lengths are shown and plotted at the same Reynolds number value. Using Equations (6.5) and (6.6), a ratio of the pressure-based correlation and velocity-based correlation can be expressed as follow

$$\frac{(\frac{L}{D})_P}{(\frac{L}{D})_V} = 0.293\ Re^{0.0967} \tag{6.7}$$

$$(\frac{L}{D})_P \approx 0.92 * (\frac{L}{D})_V \quad (6.8)$$

Table 38 presented developing length ratios for Reynolds number range from 40,000 to 350,000, in which the ratio values show slight changes over the Reynolds number range, with an average value being around 0.92, which signifies only a weak function of Reynolds number.

6.5 Comparison of CFD and Analytical Pressure Gradients

Similar to other straight duct analysis presented earlier, CFD results of the rectangular ducts flow with aspect ratios of 1.5 and 2 are compared against the Darcy-equation, Equation (4.9), and by using Colebrook equation, Equation (4.10), as shown below.

$$\frac{dP}{dx} = \frac{\rho\, v^2\, f}{2\, D} \quad (4.9)$$

$$\frac{1}{\sqrt{f}} = -2\log(\frac{\varepsilon/_D}{3.7} + \frac{2.51}{Re\sqrt{f}}) \quad (4.10)$$

CFD and analytical comparison shows that the percentage difference for rectangular duct is relatively small and hence the CFD results are found to be in a good agreement with the Darcy-equation results, but with higher errors compared to round and square ducts as one would have expected. In 0.4 m diameter rectangular ducts with aspect ratio of one and half, the percentage difference is 3.8% for a velocity of 3 m/s, 4.7% for 6 m/s, and 6.7% for 9 m/s velocity. These errors go up a little bit with 0.4 m diameter rectangular ducts with aspect ratio of 2, such that the percentage error found to be; 5%, 6.2%, and 8.3%, for inlet velocities of 3 m/s, 6 m/s, and 9 m/s, respectively. These results are tabulated in Tables 39 and 40 and plotted in Figures 72 and 73 below.

Table 39 Comparison of analytical and numerical pressure gradient values in 0.4 m diameter rectangular duct with aspect ratio of 1.5

$D(\mathrm{m})$	$v(\mathrm{m/s})$	Re	f	dP/dx_{Darcy} $(\mathrm{Pa/m})$	dP/dx_{CFD} $(\mathrm{Pa/m})$	% Difference
0.4	3	76,957	0.019	0.25	0.259	3.8%
	6	153,913	0.016	0.85	0.890	4.7%
	9	230,870	0.015	1.79	1.910	6.7%

Table 40 Comparison of analytical and numerical pressure gradient values in 0.4 m diameter rectangular duct with aspect ratio of 2

$D(\mathrm{m})$	$v(\mathrm{m/s})$	Re	f	dP/dx_{Darcy} $(\mathrm{Pa/m})$	dP/dx_{CFD} $(\mathrm{Pa/m})$	% Difference
0.4	3	76,957	0.019	0.25	0.263	5%
	6	153,913	0.016	0.85	0.903	6.2%
	9	230,870	0.015	1.79	1.944	8.3%

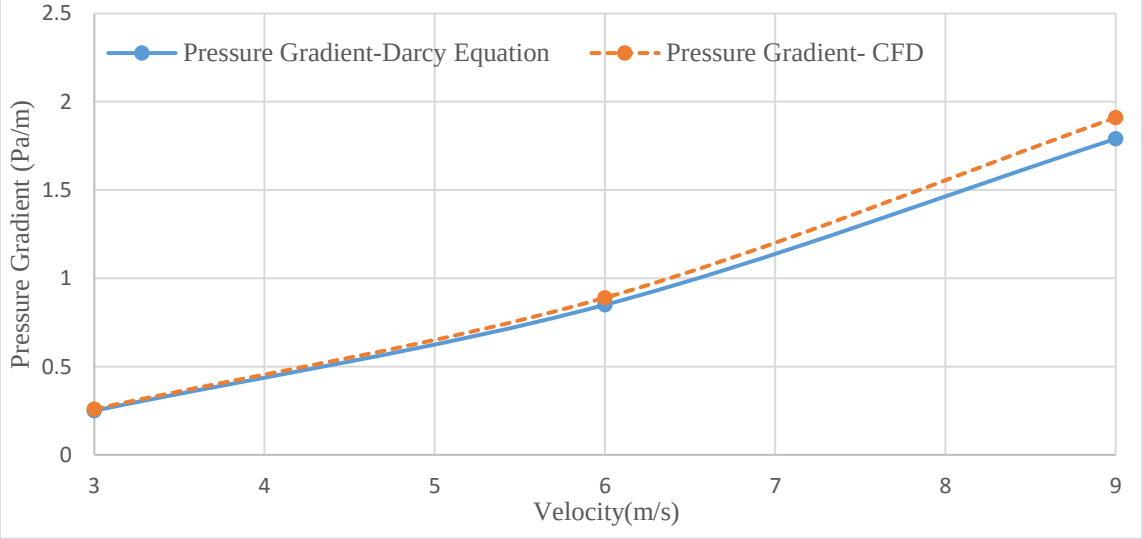

Figure 72. Comparison of analytical and numerical pressure gradient profiles in rectangular duct of $d_h = 0.4$ m with aspect ratio of 1.5.

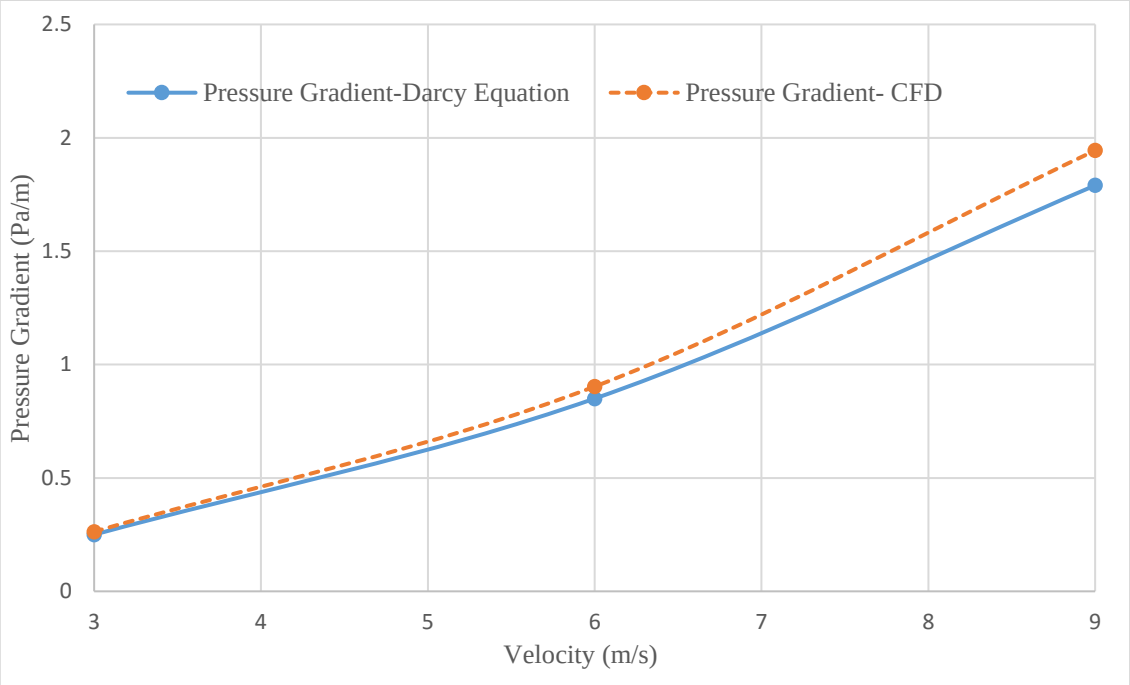

Figure 73. Comparison of analytical and numerical pressure gradient profiles in rectangular duct of $d_h = 0.4$ m with aspect ratio of 2.

6.6 Comparison of Different Ducts Flow

So far, the analysis of round, square, and two different aspect ratios of rectangular ducts models have been presented and their developing length correlations have been developed. This section presents an overall comparison of the round, square, and rectangular ducts developing length in order to investigate the geometry effect of the developing length. Also, generalized developing length correlations of any rectangular ducts are developed based on velocity and pressure profiles.

6.6.1 Developing Length based on Velocity Profile

As seen in previous analysis, dimensionless developing length is mainly function of Reynolds number of the flow, and duct geometry and design. Figure 74 compares the velocity-based developing length of round and rectangular ducts with aspect ratio of 1, 1.5, and 2 over wide range of Reynolds number.

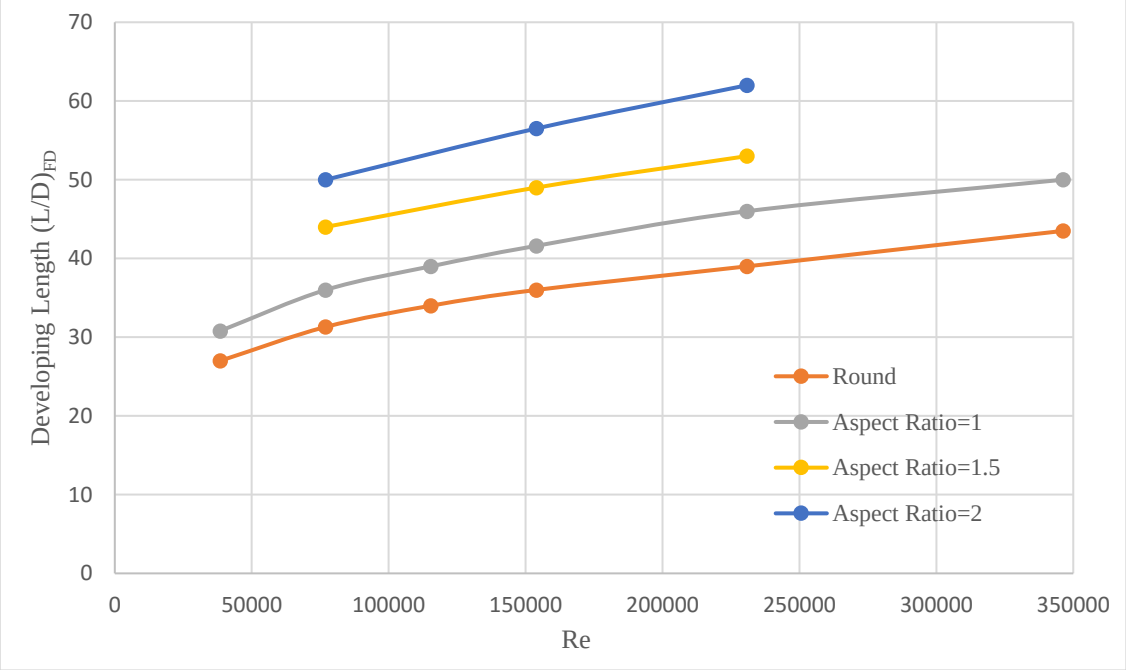

Figure 74. Comparison of numerical developing length of round and rectangular ducts to experimental round duct.

By taking the round duct correlation as a reference, the resulted developing length correlation ratio can be plotted as shown in Figure 75.

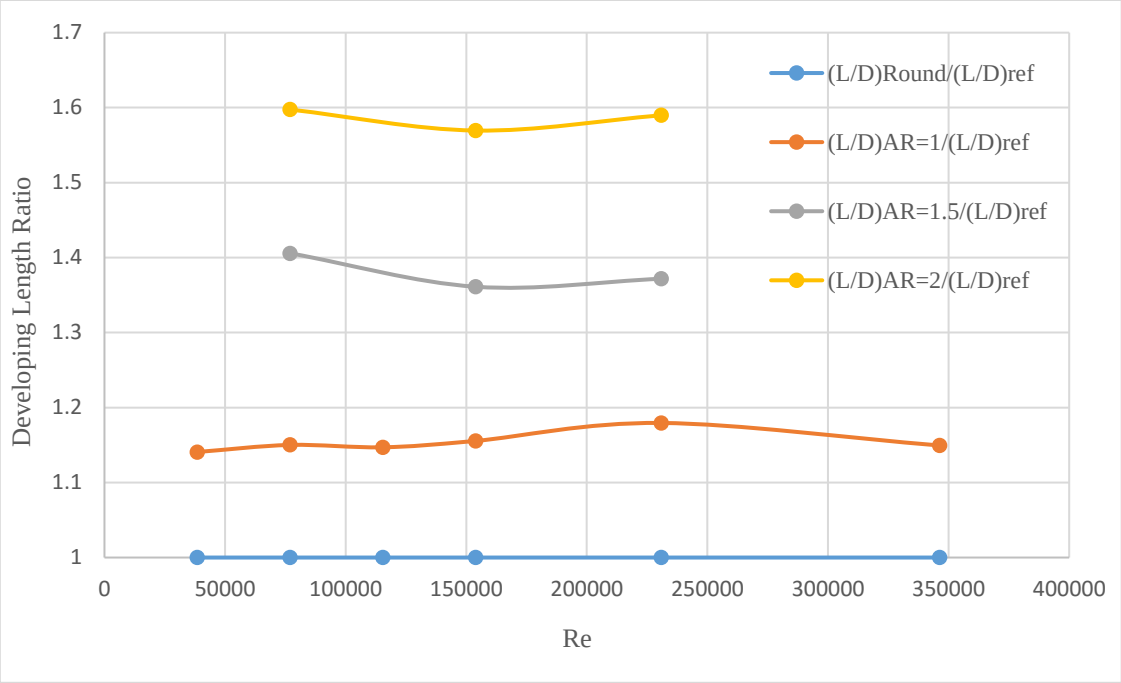

Figure 75. Comparison of the developing length ratio of round and rectangular ducts to the numerical round duct reference-velocity profiles.

Based on Figure 75 above, the below velocity based- developing length correlations ratios are developed to related each duct design to the reference round duct correlation.

$$\left(\frac{L}{D}\right)_{Square} = 1.05 * Re^{0.0082} * \left(\frac{L}{D}\right)_{Round} \approx 1.15 * \left(\frac{L}{D}\right)_{Round} \quad (6.9)$$

$$\left(\frac{L}{D}\right)_{Rect,Ar=1.5} = 2.14 * Re^{-0.0373} * \left(\frac{L}{D}\right)_{Round} \approx 1.37 * \left(\frac{L}{D}\right)_{Round} \quad (6.10)$$

$$\left(\frac{L}{D}\right)_{Rect,Ar=2} = 1.98 * Re^{-0.0191} * \left(\frac{L}{D}\right)_{Round} \approx 1.58 * \left(\frac{L}{D}\right)_{Round} \quad (6.11)$$

By using Equations (6.9) through (6.11), a generalized rectangular duct correlation can be derived, which can be used to find the velocity- developing length of any rectangular duct aspect ratio, as shown in Figure 76 and Equation (6.12).

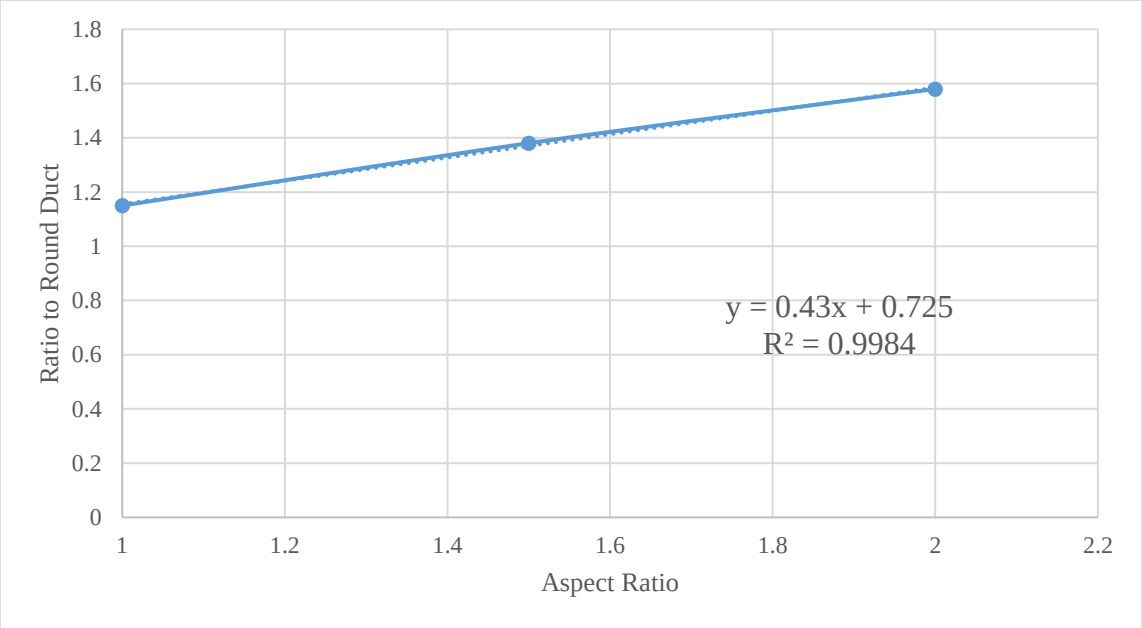

Figure 76. Derivation of the generalized velocity- developing length correlation for rectangular duct.

$$\frac{\left(\frac{L}{D}\right)_{AR}}{\left(\frac{L}{D}\right)_{Round}} = 0.43 * AR + 0.725 \qquad (6.12)$$

6.6.2 Developing Length based on Pressure Profile

As seen in all ducts design analysis earlier, and similar to the velocity profile analysis presented above, developing length of the flow based on pressure profile mainly depends on Reynolds number of the flow as well as duct design, but with shorter developing length compared to velocity-based analysis at a given Reynolds number. Figure 77 below compares the dimensionless developing length for the round, square, and rectangular ducts over wide range of Reynolds number.

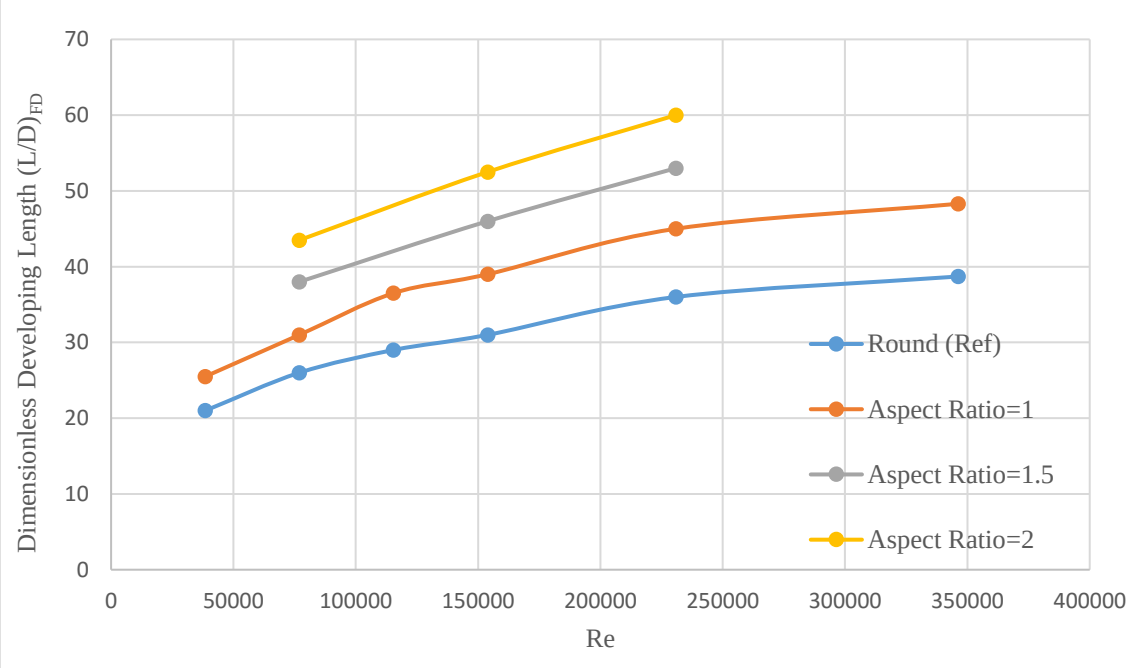

Figure 77. Comparison of numerical developing length of round and rectangular ducts to the experimental round duct.

By taking the round duct correlation as a reference, the resulted developing length correlation ratio can be plotted as shown in Figure 78 below.

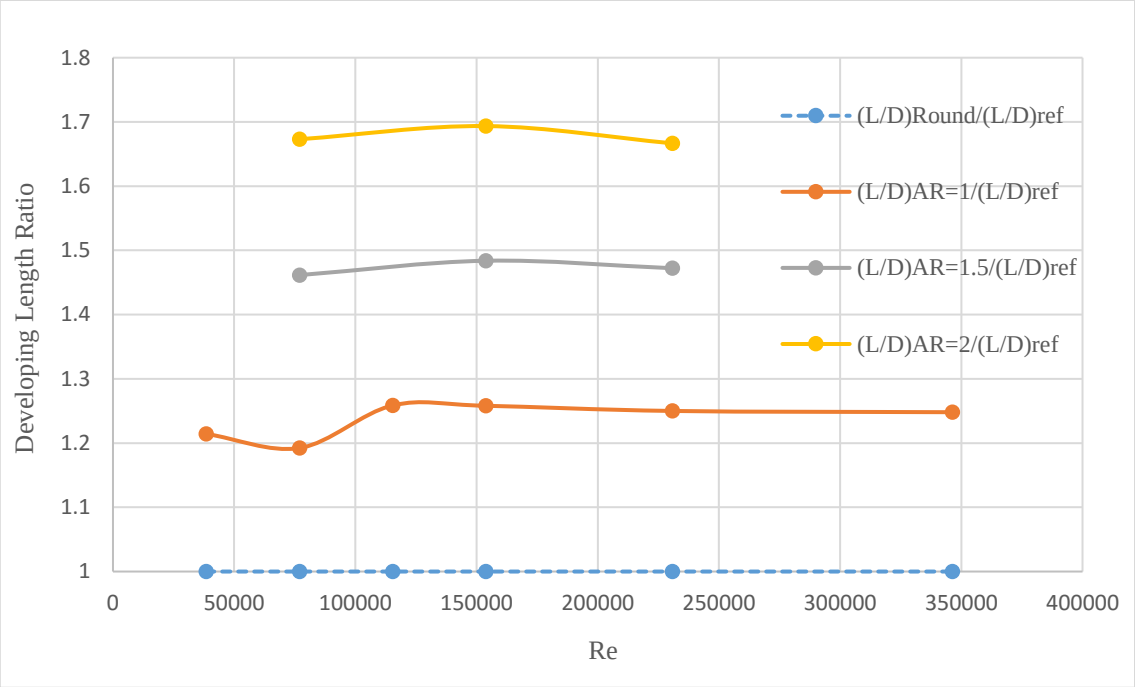

Figure 78. Comparison of the developing length ratio of round and rectangular ducts to the numerical round duct reference-pressure profiles.

Based on Figure 78 above, the below pressure-based developing length correlations ratios are developed, to related each duct design to the reference correlation of round duct

$$\left(\frac{L}{D}\right)_{Square} = 0.994 * Re^{0.0186} * \left(\frac{L}{D}\right)_{Round} \approx 1.24 * \left(\frac{L}{D}\right)_{Round} \quad (6.13)$$

$$\left(\frac{L}{D}\right)_{Rect,Ar=1.5} = 1.21 * Re^{0.0176} * \left(\frac{L}{D}\right)_{Round} \approx 1.49 * \left(\frac{L}{D}\right)_{Round} \quad (6.14)$$

$$\left(\frac{L}{D}\right)_{Rect,Ar=2} = 1.54 * Re^{0.008} * \left(\frac{L}{D}\right)_{Round} \approx 1.69 * \left(\frac{L}{D}\right)_{Round} \quad (6.15)$$

Similar to the velocity analysis, by using Equations (6.13) through (6.15), a generalized rectangular duct correlation can be derived, which can be used to find the pressure-developing length of any rectangular duct aspect ratio, as shown in Figure 79 and Equation (6.16).

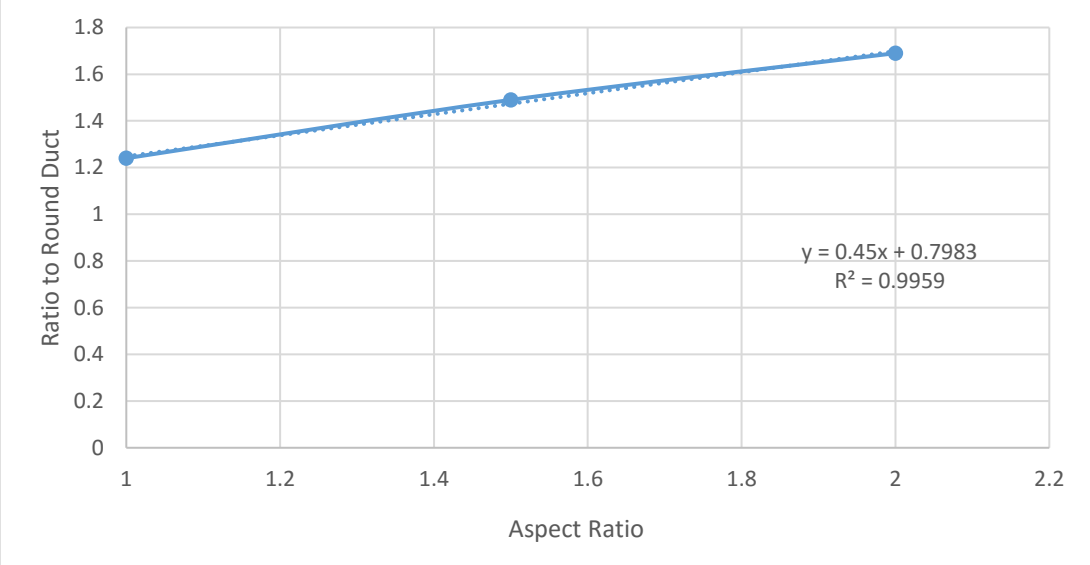

Figure 79. Derivation of the generalized pressure-developing length correlation for rectangular duct.

$$\frac{\left(\frac{L}{D}\right)_{AR}}{\left(\frac{L}{D}\right)_{Round}} = 0.45 * AR + 0.8 \qquad (6.16)$$

6.6.3 Comparison of Numerical and Analytical Pressure Gradients

We have presented in some details earlier how the resulted numerical or CFD pressure gradient compared or validated against Darcy–Weisbach equation for each individual duct design which includes the round, square, and two rectangular ducts. However, it is also interesting to compare these ducts against Darcy equation over wide range of Reynolds numbers. As shown in Figure 80 below, and as one would have expected, the numerical pressure gradient in round duct is the closest to the analytical one for all Reynolds number values, which corresponds to the lowest percentage errors, followed by square duct, rectangular duct with aspect ratio one and half, and then the rectangular duct with aspect ratio of two. Also, for all ducts, the higher the Reynolds number of the flow, the more the numerical pressure gradient deviates from the analytical results, which produced a higher error percentage.

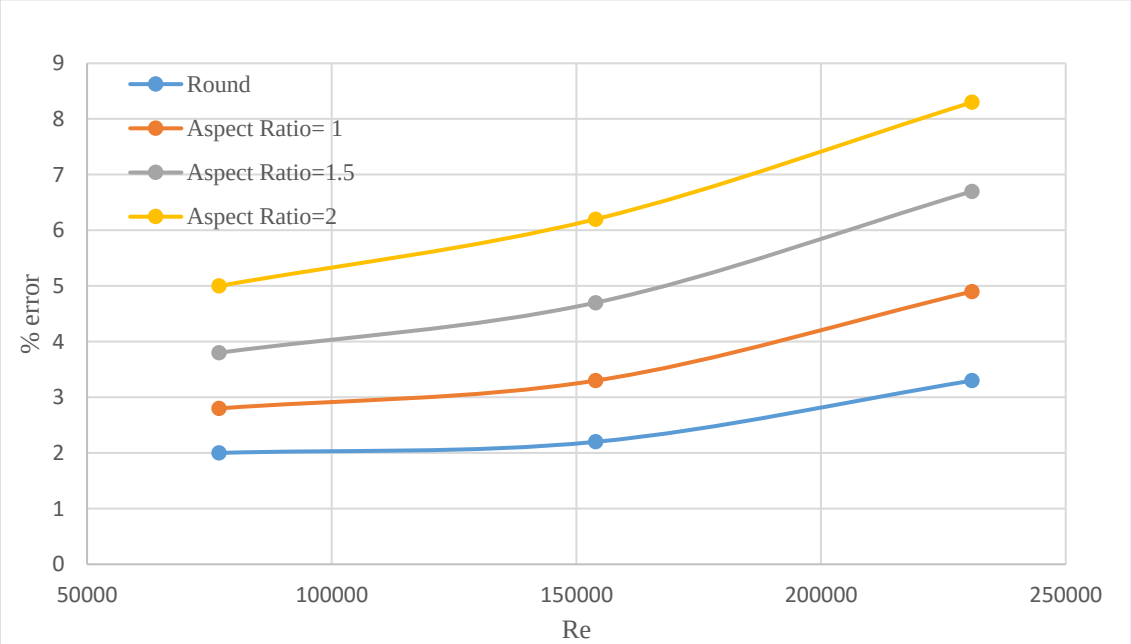

Figure 80. Comparison of the numerical round and rectangular ducts deviations from Darcy-Weisbach equation.

6.7 Summary

This section presented a CFD analysis of the turbulent flow in rectangular ducts with aspect ratio of 1.5 and 2. The velocity and pressure profiles were obtained for each flow case, and by employing the fully developed flow criteria stated earlier, the dimensionless developing length were determined based on the velocity and pressure profiles for each flow Reynolds number.

The results show for both of the rectangular ducts aspect ratios that the developing length of the flow increases with increasing inlet velocity and/or increasing duct size. Moreover, in flow cases with identical Reynolds numbers, the developing length of the flow appeared to be almost constant. As a result, the velocity-based and pressure-based developing length of the flow is a Reynolds number dependent variable such that larger Reynolds number requires longer developing length to achieve the fully developed flow condition in rectangular ducts.

For rectangular duct with aspect ratio of 1.5, the dimensionless developing length based on the velocity gradient profiles were found to be $44, 49$ and 53.5 for increasing flow Reynolds number of $(76{,}960)$, $(153{,}910)$, and $230{,}870$ respectively. Also, based on pressure gradient profiles, the dimensionless developing length were found to be $38, 46,$ and 53 for flow Reynolds number of $(76{,}960)$, $(153{,}910)$, and $(230{,}870)$ respectively.

For rectangular duct with aspect ratio of 2, the dimensionless developing length and based on the velocity gradients profiles were found to be $50, 56.5$ and 62 for increasing flow Reynolds number of $(76{,}960)$, $(153{,}910)$, and $230{,}870$ respectively. Similarly, based on the pressure gradient profiles, the dimensionless developing length were found to be $43.5, 52.5,$ and 60 for increasing flow Reynolds number of $(76{,}960)$, $(153{,}910)$, and $(230{,}870)$ respectively.

Using thee above numerical results, velocity-based and pressure-based correlations were developed to calculate the required developing length (or the entrance length) in

turbulent rectangular duct flow with any Reynolds number. Moreover, for rectangular duct with aspect ratios of 1.5 and 2, a comparison of velocity-based developing length and pressure-based developing length for a range of Reynolds number show a pressure-developing length to a velocity-developing length ratio being around 0.93, signifying a shorter entrance length for pressure-developing length.

In addition, the CFD model results show a good agreement when compared against the Darcy equation with a percentage difference of 6.7% and 8.3% with 1.5 and 2 aspect ratios, respectively for high turbulent flow with Reynolds number of 230,870.

Last but not least, an overall comparison of round, square, and rectangular duct flows were presented. The comparison shows that the developing length in the round duct was shorter than the corresponded rectangular duct with 1.5 aspect ratio by around 25% based on the velocity profiles and 30% based on the pressure profiles. Similarly, the developing length in the round duct was shorter than the corresponded rectangular duct with aspect ratio of 2 by around 36 % based on the velocity profiles and 40% based on the pressure profiles.

VII. SQUARE DUCT DOWNSTREAM OF A RIGHT-ANGLE ELBOW CASE

7.1 Introduction

This section continues the CFD modelling and numerical analysis of internal turbulent flow beyond straight duct geometries to include fluid flow through right-angle elbows. So far, air flow has been analyzed in a straight duct for geometries of round ducts, square ducts, and rectangular ducts. However, the ducting systems in many engineering practice are more complicated with these straight ducts often beings placed on the upstream or downstream side of an elbow or bend and also connected to duct fittings fittings devices such as dampers, tees, and flanges. Consequently, these complications in the ducting systems can be expected to disturb the flow, and thus affecting the developing length of the flow inside these ducts. This section presents a CFD modelling of a straight, square duct located downstream of a right-angle elbow type with a uniform inlet velocity entering the elbow. The resulting velocity and pressure profiles are analyzed and used to derive the developing length correlation downstream of the elbow. Moreover, a comparison of this elbow-duct system with the regular square ducts flow analyzed and discussed in Section V is presented in order to quantify the effect on the flow developing length of installing a right-angle elbow into a ducting system. In addition to the case of uniform flow entering the elbow, a similar analysis is performed for the case of a fully developed flow entering the elbow. Also, a comparison is performed of the developed flow length downstream of the elbow for the two different flow entering the elbow, namely, the uniform inlet flow and the fully developed inlet flow.

7.2 Problem Description

- The working fluid is air at room temperature and atmospheric pressure with thermophysical properties presented in Table 41 below.

Table 41 Thermophysical properties of air in elbow-duct system

Thermophysical Property	Value
$\boldsymbol{T}(\mathbf{K})$	300
$\boldsymbol{\mu}\ (\frac{\mathbf{Kg}}{\mathbf{m.s}})$	1.84×10^{-5}
$\boldsymbol{\rho}\ (\frac{\mathbf{Kg}}{\mathbf{m^3}})$	1.18

- Three ducts dimeters are chosen representing a range of practical applications; 0.2 m, 0.4 m, and 0.6 m.
- Air enters the elbow-duct system at different uniform velocities representing a range used in industry practice; 3 m/s, 6 m/s, and 9 m/s.
- Assumptions applied to this analysis are
    - Steady incompressible flow in smooth stainless steel elbow-duct system.
    - Elbow-duct system is completely filled with the fluid being transported.

7.3 Modelling and Simulation

The elbow-duct system geometry was created using SOLIDWORKS software, and then imported to the STAR CCM+ CFD commercial software in order to simulate the fluid flow. As explained earlier, STAR CCM+ uses a control volume based finite volume method to solve the coupled, non-linear partial differential governing equations for the fluid, as shown in Figures 81 and 82 below.

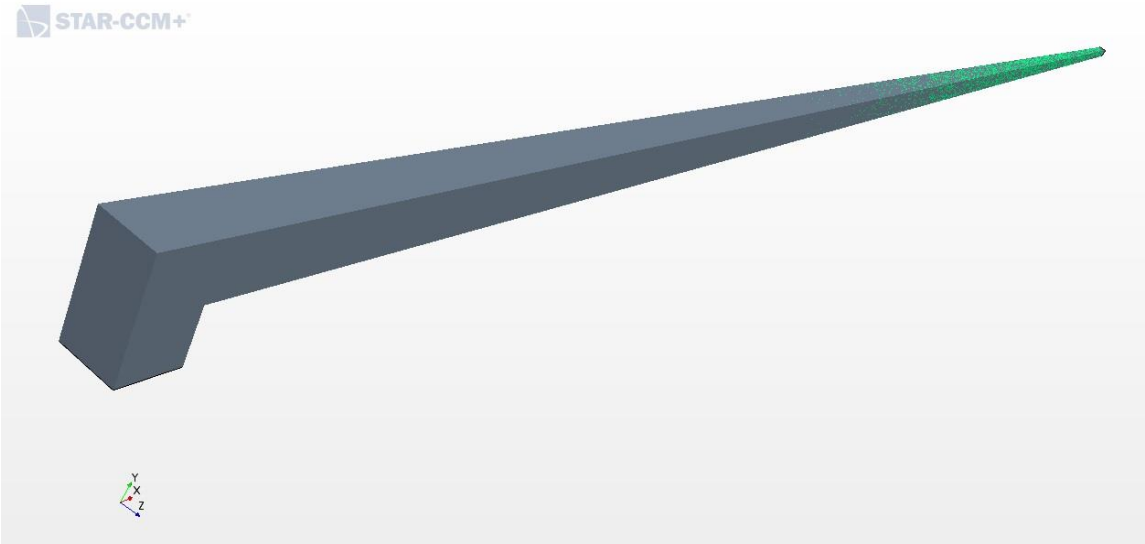

Figure 81. Computational domain of elbow-duct system with uniform inlet velocity.

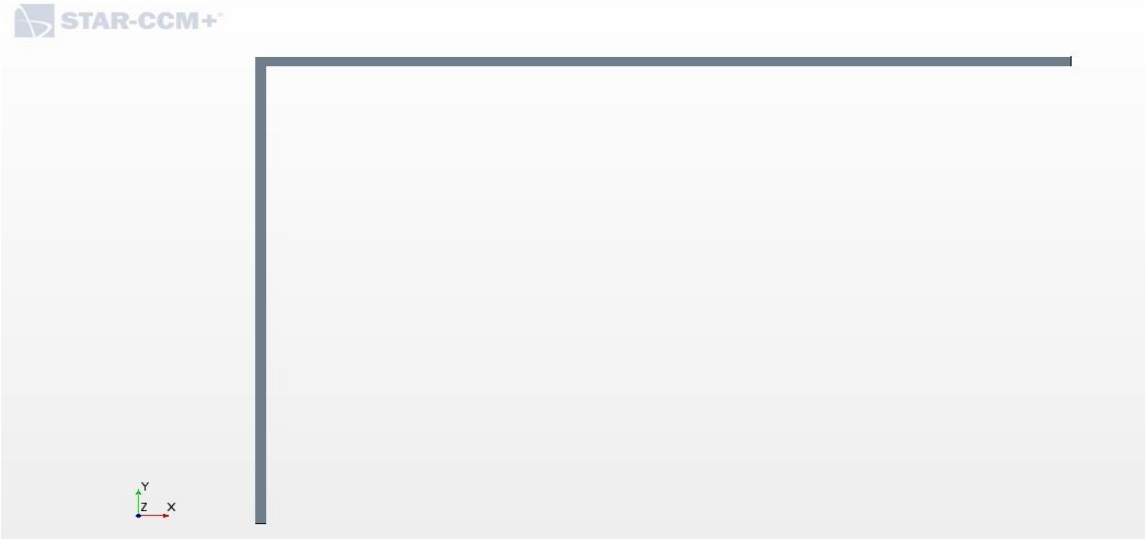

Figure 82. Computational domain of elbow-duct system with fully developed inlet velocity.

7.3.1 Mesh Generation

As we did with the straight duct simulations, the CFD modelling started by generating mesh, or grid, to represents the elbow-duct geometry. In order to do so, the below mesh models were chosen in STAR CCM+ to most accurately simulate the turbulent fluid flow inside the elbow-duct system.

- Surface Remesher.
- Polyhedral Mesher.
- Embedded Thin Mesher.
- Prism Layer Mesher.

By following the user guide in STAR CCM+ for internal flow applications, the geometry mesh base size is selected as 5 cm with a surface growth rate of 1.7. Also, two layers of the thin mesh model, and nine layers of prism mesh are applied to the elbow-duct mesh system. For the prism layer mesh model, the prism layer absolute thickness and the near wall thickness values are selected for each duct size in order to accurately capture the near wall velocity profiles and viscous sublayer of the turbulent flow. For the 0.2 m elbow-duct system, the absolute prism layer thickness value selected is 8.903 mm, while the near wall prism layer thickness selected is 0.053 mm. The resulted total number of cells in the volume mesh found to be 3,310,284 cells in the elbow-duct system with uniform velocity inlet.

For the 0.4 m elbow-duct system hydraulic diameter, the absolute prism layer thickness values selected is 13.35 mm, while the near wall prism layer thickness selected is 0.079 mm. The resulted total number of cells in the volume mesh found to be 3,981,000 cells in the elbow-duct system with uniform velocity inlet, and 6,767,700 cells in the elbow-duct system with fully developed velocity inlet. For the largest size of 0.6 m elbow-duct system, the selected absolute prism layer thickness value is 17.80 mm, while the near wall prism layer thickness selected is 0.106 mm. The resulted

total number of cells in the volume mesh found to be 7,574,059 cells in the elbow-duct system with fully developed velocity inlet. All of these parameters are tabulated in Tables 42 and 43 and the generated volume mesh are shown in Figures 83 and 84.

Table 42 Summary of all mesh models parameters values used in the elbow-duct simulations

Mesh Parameters	**Input Value**
Base Size	0.05 m
Number of Prism Layers	9
Surface Growth Rate	1.7
Thin Mesh Layers	2
Relative Maximum Size	25
Relative Minimum Size	100

Table 43 Detailed prism layer mesh specifications and overall cells number for all of the elbow-duct systems sizes

Duct Diameter (m)	**Prism Layer Absolute Thickness (mm)**	**Thickness of Near Wall Prism Layers (mm)**	**Overall Number of Cells**	
			Uniform Inlet Velocity	**Fully Developed Inlet Velocity**
D_h**=0.2**	8.903	0.053	3,310,284	*
D_h**==0.4**	13.35	0.079	3,981,000	6,767,700
D_h**==0.6**	17.80	0.106	7,574,059	*

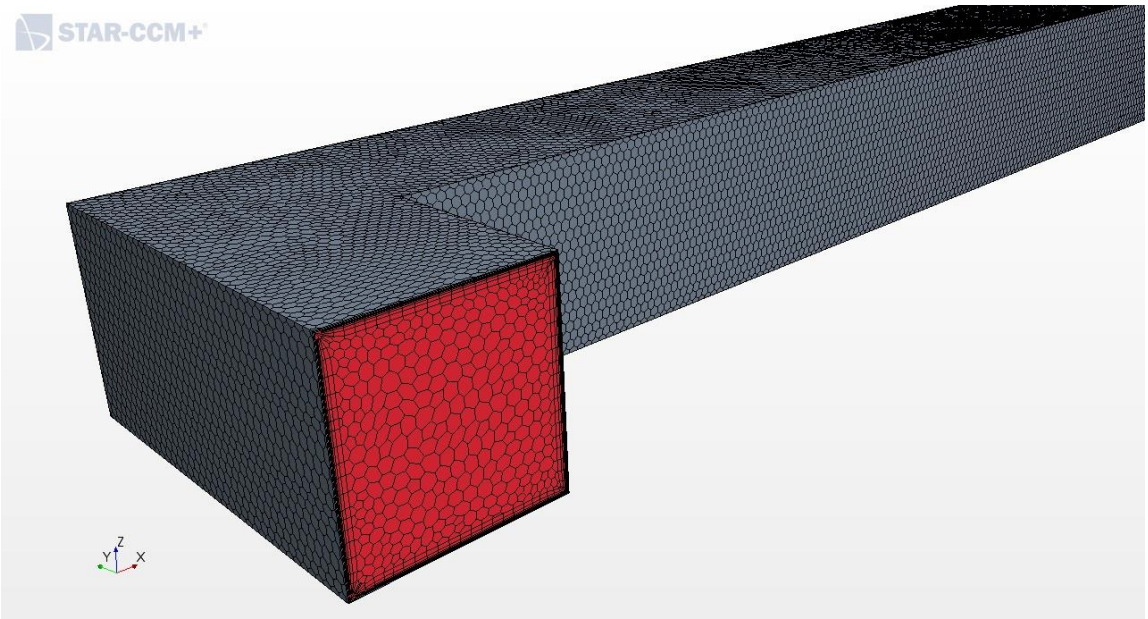

Figure 83. Generated volume mesh for the 0.4 m elbow-duct system with uniform inlet velocity.

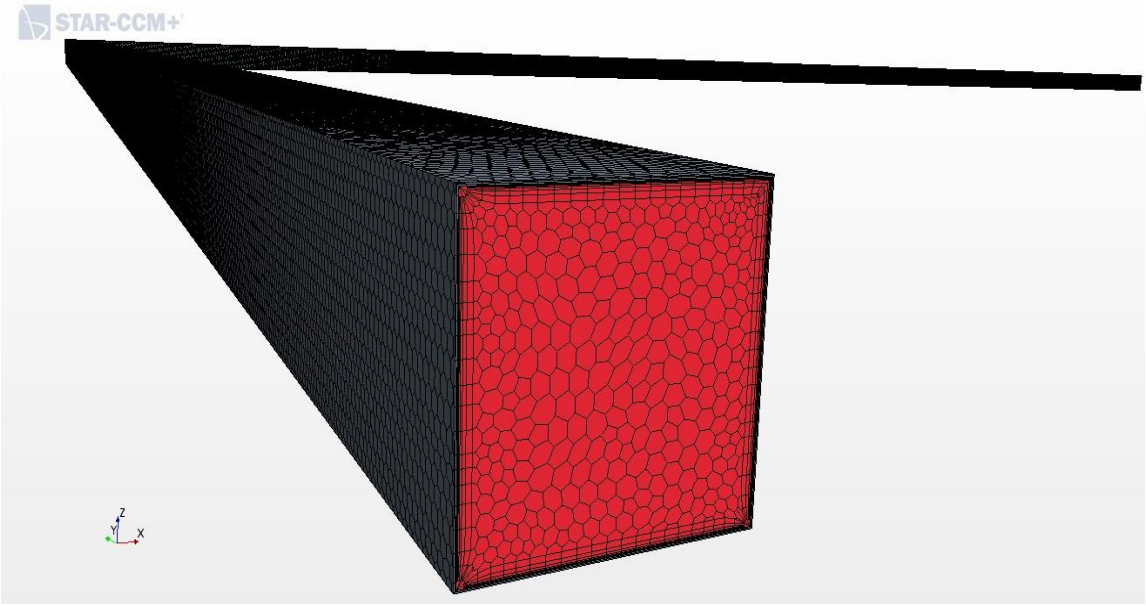

Figure 84. Generated volume mesh for the 0.4 m elbow-duct system with fully developed inlet velocity.

7.3.2 Fluid Physical Properties

Once the mesh or grid was established for both of the elbow-duct system configurations, the next step was to choose the appropriate physical models to accurately simulate the fluid flow. By following the STAR CCM+ user guide, fluid physical models recommended to use for the internal turbulent flow simulation are listed below.

- Constant Density Air.
- Three Dimensional Steady Flow.
- Turbulent Flow.
- $k-\epsilon$ Turbulence Model.
- Exact Wall Distance.
- Reynolds-Averaged Navier-Stokes
- Realizable $k-\epsilon$ Two-Layer.
- Segregated Flow Model.
- Turbulence Suppression
- Cell Quality Remediation
- Two-Layer All y+ Treatment
- Transition Boundary Distance.

7.3.3 Boundary Conditions

The next step was to identify and specify the appropriate boundary conditions of the flow at the duct inlet, $\frac{y}{D}$ of 0, and exit, $\frac{x}{D}$ of 120, with the exit being an arbitrary chosen value that assured achieving the fully developed flow in all cases. For both elbow-duct systems, the flow is assumed to enter with uniform flow velocities of $3\ \mathrm{m/s}$, $6\ \mathrm{m/s}$, and $9\ \mathrm{m/s}$, and the horizontal duct is considered long enough to assume atmospheric pressure at the duct outlet, which corresponds to zero gauge pressure.

Similar to the straight ducts analysis presented before, the turbulence parameters are quantified by the turbulent intensity of the flow and the turbulence length scale. At the

inlet, by assuming a moderate turbulent flow application, it is reasonable to assume 5% inlet turbulent intensity at the duct inlet. At the exit in the fully developed region, the turbulent intensity is estimated by using the Equation (3.12) below.

$$I_{FD} = 0.16 * Re^{-\frac{1}{8}} \tag{3.12}$$

For the turbulence length scale, which is a quantity related to the size of large eddies that contain the turbulent energy, Equation (4.1) below may be used to as an approximation in fully developed region of the flow.

$$l_{FD} = 0.07 * D_h \tag{4.1}$$

In addition to the inlet and outlet boundary conditions, a stationary wall boundary condition, namely a no-slip assumption, is applied at the wall of the square duct, such that the velocity increases from zero at the wall to a maximum velocity in middle of the duct. On the other side of the square duct, a symmetry boundary condition is applied to accelerate the computation process. Moreover, for this model, a wall function method is used for near wall treatment in order to accurately simulate the flow inside the round duct. Figure 85 and Tables 44 through 47 below show the types of different boundary conditions for both of the elbow-duct systems, including the two elbows inlet velocity cases, namely a uniform flow inlet and fully developed flow inlet.

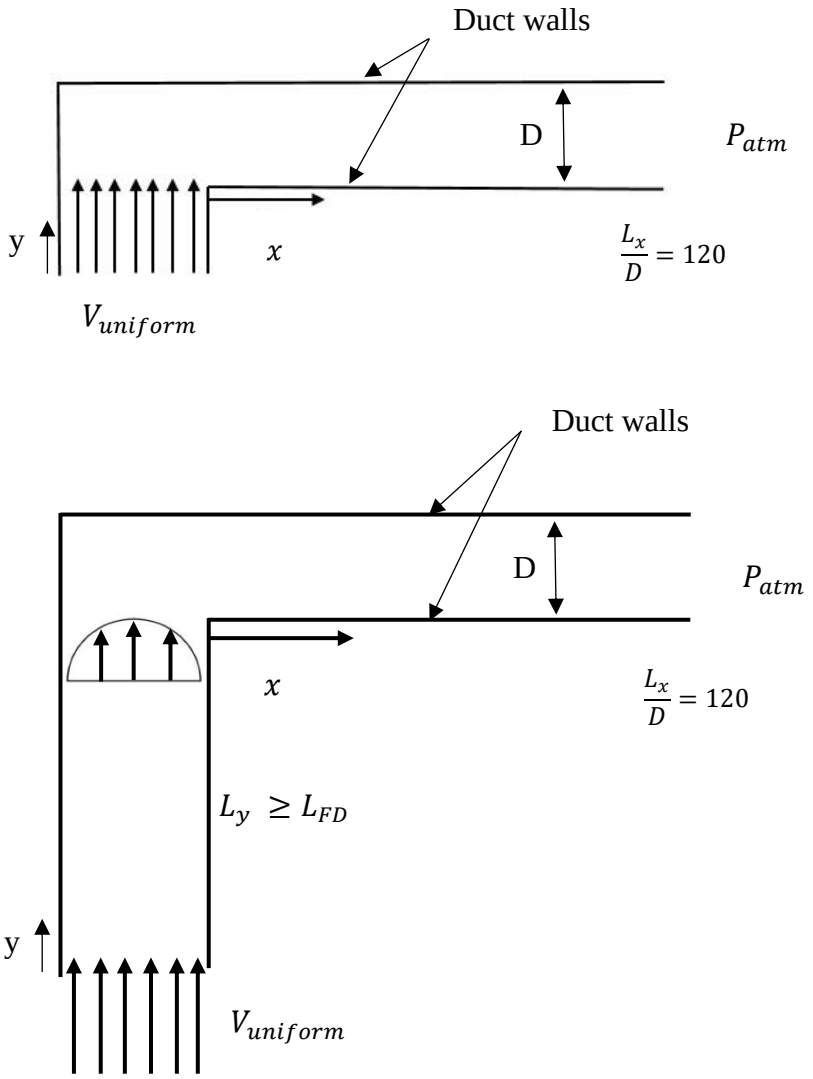

Figure 85. Boundary conditions types for both of the elbow-duct systems.

Table 44 Summary of boundary conditions for all elbow- duct systems sizes

Uniform Inlet Velocity (m/s)	3, 6, 9
Outlet gage Pressure (Pa)	Zero

Table 45 Summary of turbulence parameters boundary conditions for elbow-duct of $d_h = 0.2$ m

Turbulence Parameters		**V=6m/s**
$\boldsymbol{TI_{in}}$	Uniform Inlet Velocity	5%
	Fully Developed Inlet Velocity	5%
$\boldsymbol{l_{in}}$		0.02 m
$\boldsymbol{TI_{FDF}}$		3.8%
$\boldsymbol{l_{FDF}}$		0.014 m

Table 46 Summary of turbulence parameters boundary conditions for elbow-duct of $d_h = 0.4$ m

Turbulence Parameters		**V=3m/s**	**V=6m/s**	**V=9m/s**
$\boldsymbol{TI_{in}}$	Uniform Inlet Velocity	5%		
	Fully Developed Inlet Velocity	5%		
$\boldsymbol{l_{in}}$		0.031 m		
$\boldsymbol{TI_{FDF}}$		3.8%	3.5%	3.1%
$\boldsymbol{l_{FDF}}$		0.028 m		

Table 47 Summary of turbulence parameters boundary conditions for elbow-duct of $d_h = 0.6$ m

Turbulence Parameters		**V=6m/s**
$\boldsymbol{TI_{in}}$	Uniform Inlet Velocity	5%
	Fully Developed Inlet Velocity	5%
$\boldsymbol{l_{in}}$		0.05 m
$\boldsymbol{TI_{FDF}}$		3.1%
$\boldsymbol{l_{FDF}}$		0.042 m

7.4 Results and Discussion

After the simulations were set up for the elbow-duct system with a uniform inlet velocity and a fully developed inlet velocity, STAR-CCM+ was used to determine velocity and pressure profile for different flow velocities. Then, velocity gradient profiles dv/dx and pressure gradient profiles dp/dx downstream of the elbow were developed for each Reynolds number value, which is a necessary step to locate where fully developed flow occurs.

Similar to the earlier straight ducts analysis, the criteria used to define where the fully developed flow is reached inside the ducts is set based on assuming that the flow will be fully developed where the (dv/dx) value is around 99% of the fully developed region (dv/dx),which is $(dv/dx)_{FD}\ of\ 0$. Similarly, by using the pressure gradient profiles, the flow is assumed to be fully developed where(dp/dx) reaches 99% of the (dp/dx) in the fully developed region, assuming that $(dp/dx)_{FD}$ is constant.

7.4.1 Elbow-Duct System with Uniform Velocity Inlet

Three elbow-duct models with a hydraulic diameter of 0.4 m were modeled and simulated with uniform velocities entering the elbow of $3\ \mathrm{m/s}$,$6\ \mathrm{m/s}$, and $9\ \mathrm{m/s}$. By analyzing the velocity profiles downstream of the elbow in each case, and by following the fully developed flow criteria stated previously, the dimensionless developing length $\left(\frac{L}{D}\right)_{FD}$ was found to be 63 with an inlet velocity of $3\ \mathrm{m/s}$, 71 with an inlet velocity of $6\ \mathrm{m/s}$, and 78 with an inlet velocity of $9\ \mathrm{m/s}$.

Similarly, and in order to investigate the duct size effect on the developing length of the flow, two square elbow-ducts systems with diameters of 0.2 m and 0.6 m and uniform inlet velocity of $6\ \mathrm{m/s}$ were modeled. The dimensionless developing lengths $\left(\frac{L}{D}\right)_{FD}$ for hydraulic diameters of 0.2 m and 0.6 m were found to be 62.4 and 80.2, respectively.

Similar to the straight ducts models presented earlier, the results show that the dimensionless developing lengths $\left(\frac{L}{D}\right)_{FD}$ increase with the increasing Reynolds number of the flow, while it remain almost constant with different flow velocity and duct sizes, because they share an identical Reynolds number. All of these results are tabulated in Table 48 and plotted in Figures 86 through 88.

Table 48 Summary of dimensionless developing length $(L/D)_{FD}$ with corresponding Reynolds numbers in uniform velocity inlet elbow- duct system based on velocity profiles

V-based Profile	**v=3m/s**		**v=6m/s**		**v=9m/s**	
D_h **(m)**	**Re**	**$(L/D)_{FD}$**	**Re**	**$(L/D)_{FD}$**	**Re**	**$(L/D)_{FD}$**
0.2	38,480	*	76,960	62.4	115,430	*
0.4	76,960	63	153,910	71	230,870	78
0.6	115,430	*	230,870	80.2	346,300	*

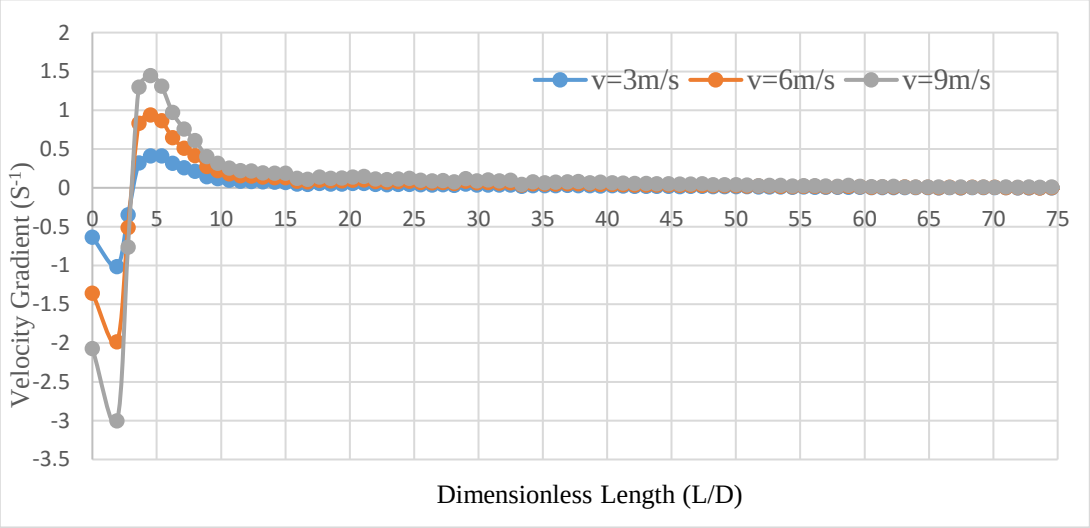

Figure 86. Velocity gradient profiles in square duct with $d_h = 0.4$ m downstream an elbow.

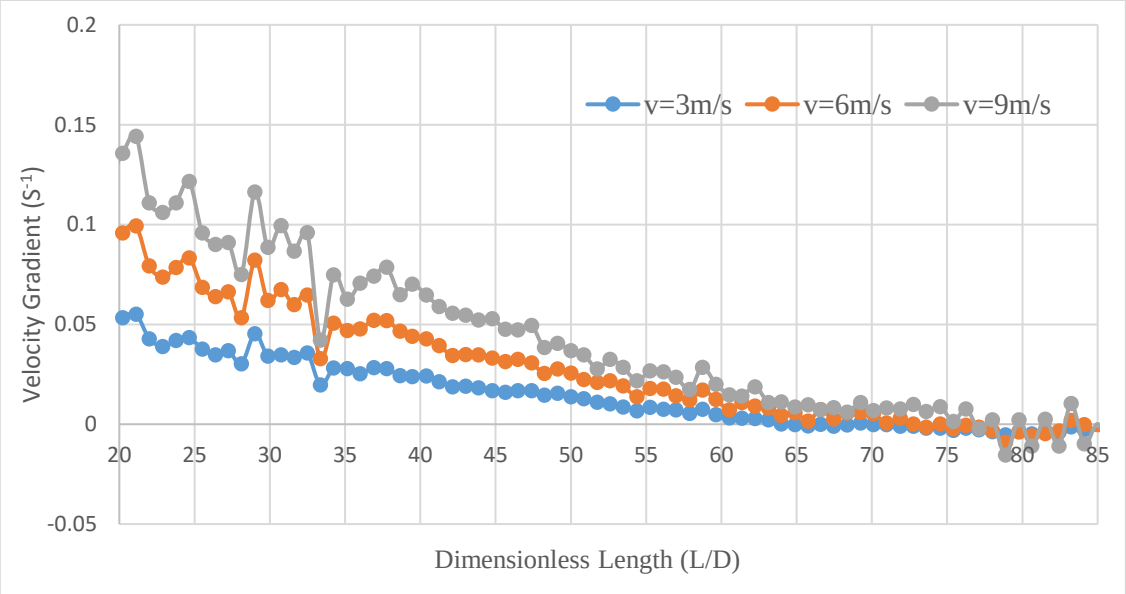

Figure 87. Enlarged velocity gradient profiles in square duct with $d_h = 0.4$ m downstream of an elbow.

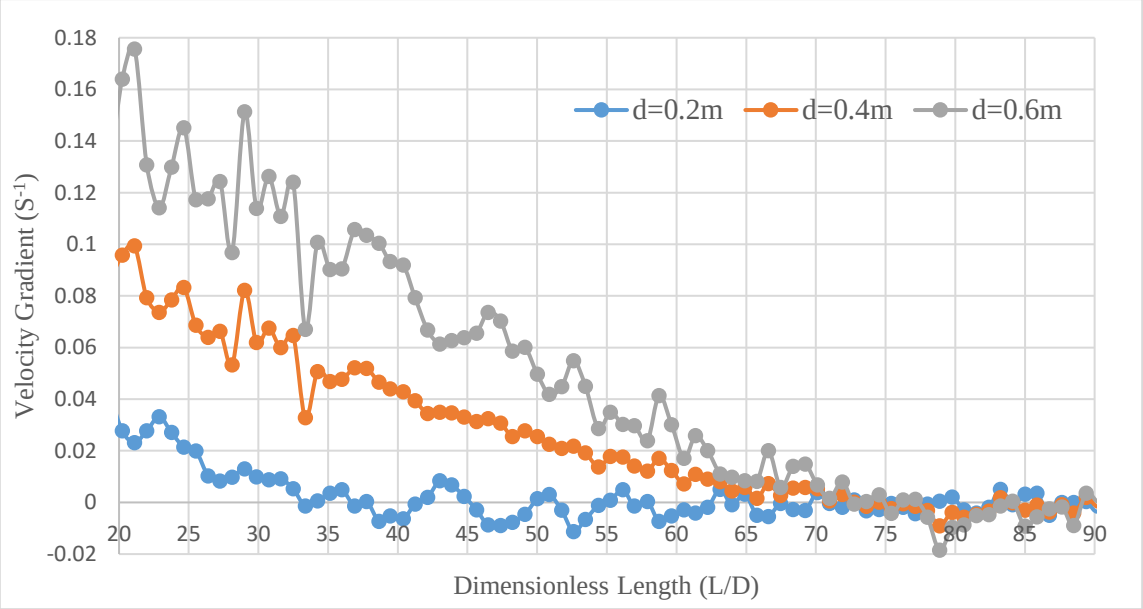

Figure 88. Enlarged velocity gradient profiles in a square duct downstream of an elbow with uniform inlet velocity of $6\ \mathrm{m/s}$.

The above $\left(\frac{L}{D}\right)_{FD}$ results are plotted against the Reynolds number for each case in Figure 89, and by using a curve fitting procedure, a velocity-based CFD correlation for the fully-developed flow location is developed for room temperature air flowing inside an elbow-duct system with the uniform velocity inlet.

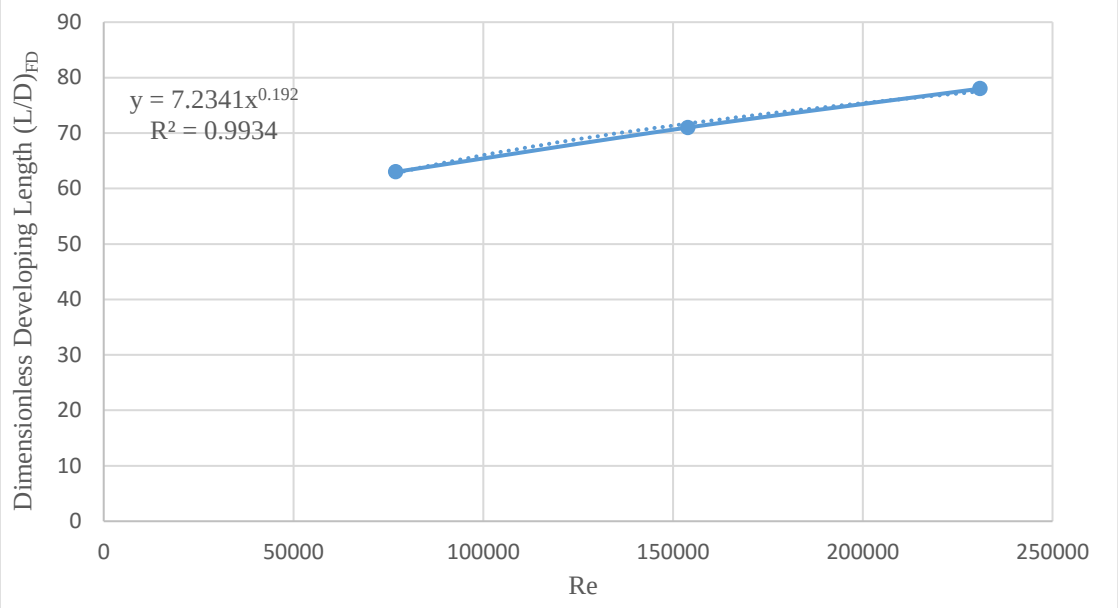

Figure 89. Curve fitting profile (velocity-based correlation) for uniform inlet velocity in a square duct downstream of an elbow.

The resulting correlation based on the curve fitting can be expressed as

$$(\frac{L}{D})_{FD_V} = 7.2341 * Re^{0.192} \tag{7.1}$$

Similar analysis was carried out by using the pressure profiles to investigate the developing length and then compared to the previous velocity based results. In the square duct of $0.4m$ hydraulic diameter, the flow developing length was found to be 54 with a uniform inlet velocity of $3\ \mathrm{m/s}$, 65 with a uniform velocity of $6\ \mathrm{m/s}$, and 75 with a uniform velocity of $9\ \mathrm{m/s}$.

Moreover, 0.2 m and 0.6 m square ducts were simulated with a uniform flow velocity of $6\ \mathrm{m/s}$ to investigate how the pressure-based dimensionless developing length would behave with changing the duct size. For the 0.2 m duct, the dimensionless entrance length was 53.5 while the developing length was found to be 76 in the largest duct with 0.6 m diameter.

Similar to the velocity analysis results, the pressure-based dimensionless developing lengths $\left(\frac{L}{D}\right)_{FD}$ increase with the increasing Reynolds number of the flow, while it remain almost constant with different flow velocity and duct sizes that share an identical Reynolds number. Table 49 and Figures 90 through 93 below present these results.

Table 49 Summary of dimensionless developing length $(L/D)_{FD}$ with corresponding Reynolds numbers in uniform velocity inlet elbow- duct system based on pressure profiles

P-based Profile	**v=3m/s**		**v=6m/s**		**v=9m/s**	
D_h **(m)**	**Re**	**$(L/D)_{FD}$**	**Re**	**$(L/D)_{FD}$**	**Re**	**$(L/D)_{FD}$**
0.2	38,480	*	76,960	53.5	115,430	*
0.4	76,960	54	153,910	65	230,870	75
0.6	115,430	*	230,870	76	346,300	*

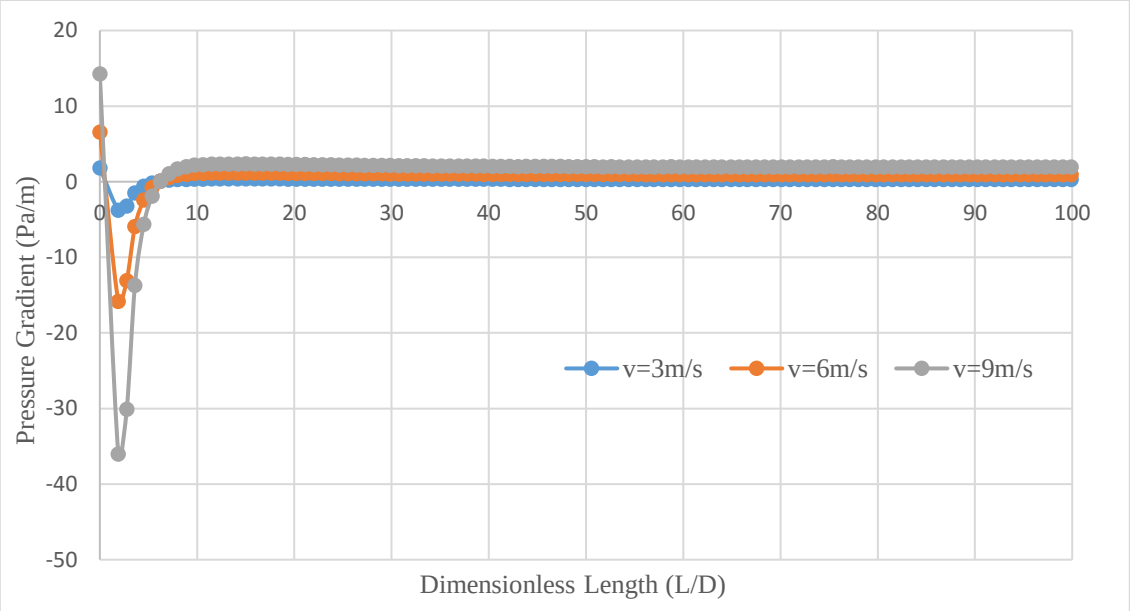

Figure 90. Pressure gradient profiles in a square duct of $d_h = 0.4$ m downstream of an elbow with different uniform inlet velocities.

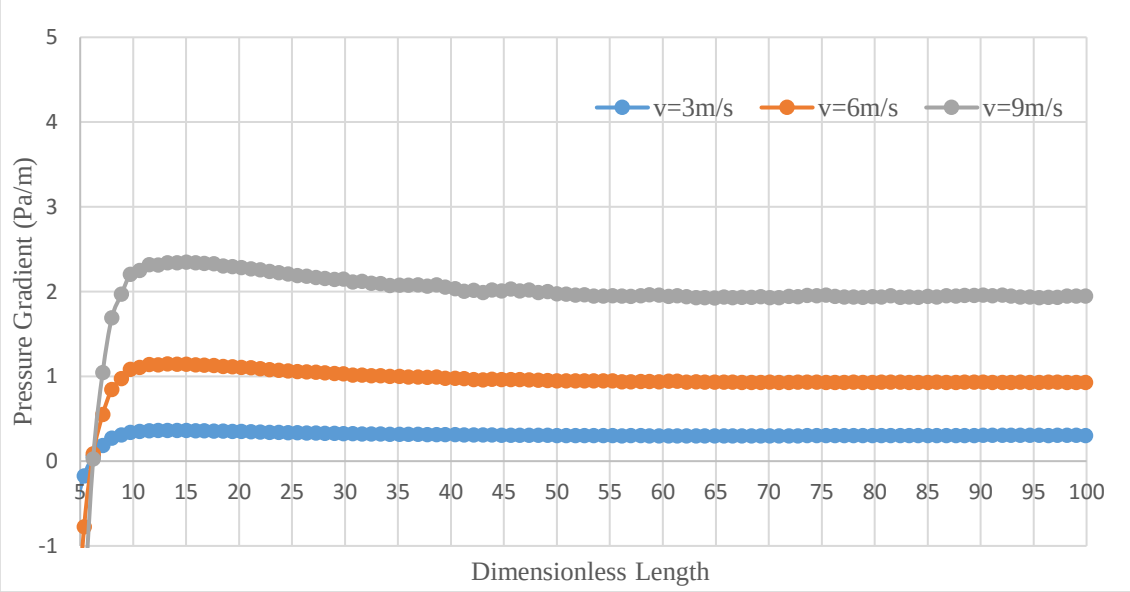

Figure 91. Enlarged pressure gradients profiles in a square duct of $d_h = 0.4$ m downstream of an elbow with different uniform inlet velocities.

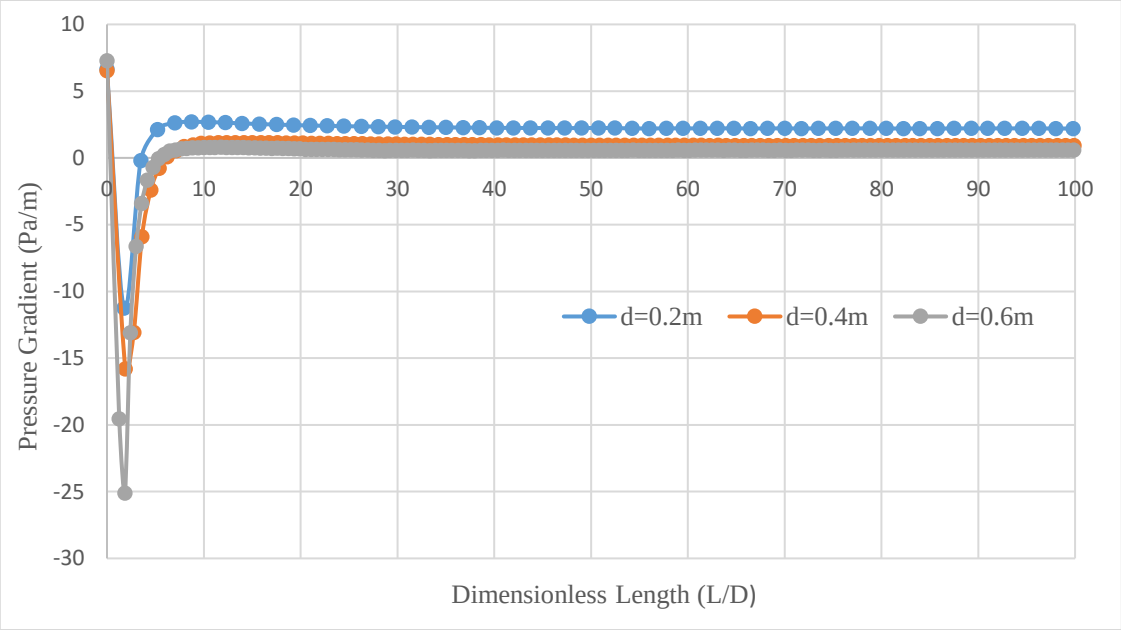

Figure 92. Pressure gradients profiles in a square duct downstream of an elbow with uniform inlet velocity of 6 m/s.

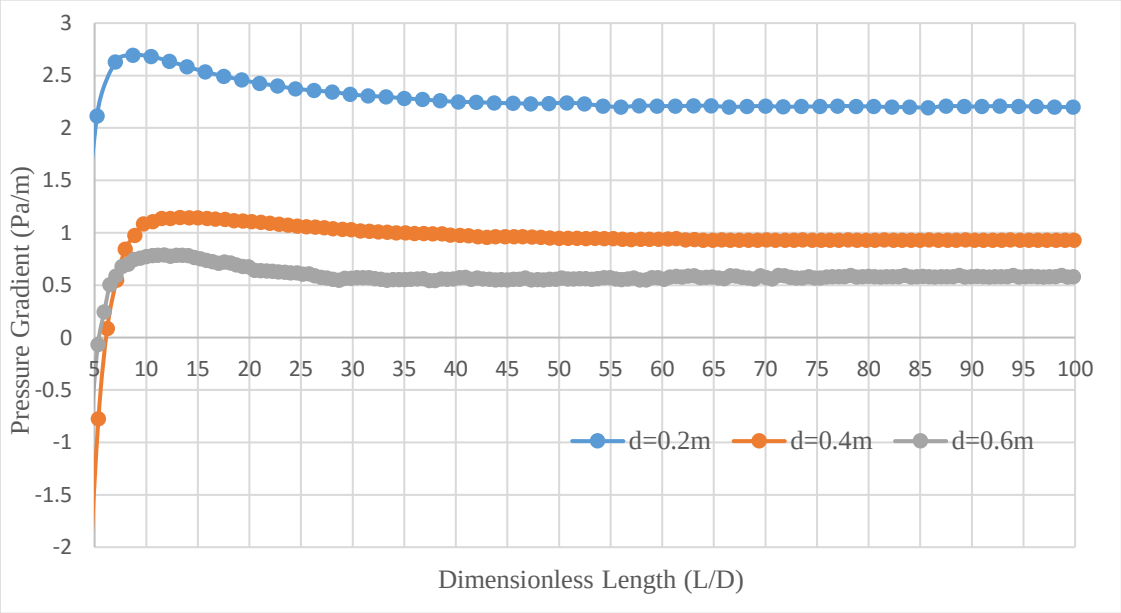

Figure 93. Pressure gradients profiles in a square duct downstream of an elbow with uniform inlet velocity of 6 m/s.

The above $\left(\frac{L}{D}\right)_{FD}$ results were plotted against the Reynolds number for each case in Figure 94, and by using the curve fitting procedure, a pressure-based CFD correlation for the fully developed flow location was developed for room temperature air flowing inside a right-angle elbow-duct system with uniform velocity inlet.

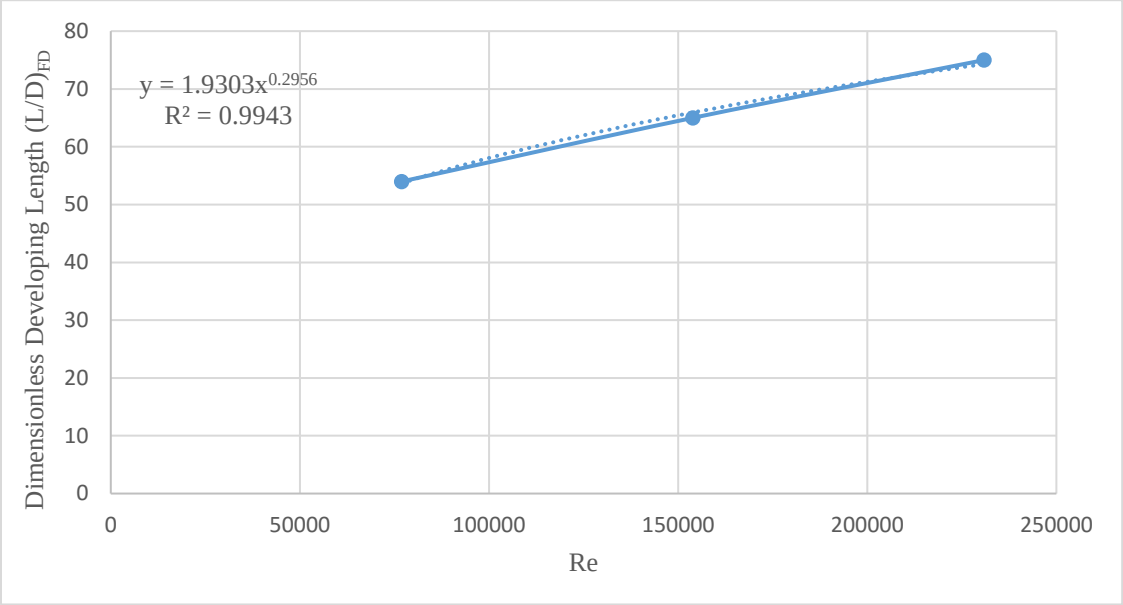

Figure 94. Curve fitting profile (velocity-based correlation) for uniform inlet velocity in an elbow-duct system.

The resulting correlation based on the curve fittings can be expressed as

$$(\frac{L}{D})_{FD_P} = 1.9303 * Re^{0.2956} \quad (7.2)$$

7.4.2 Elbow-Duct System with Fully Developed Velocity Inlet

So far, uniform flow inlet has been considered for our system of interest, either in the straight duct cases presented earlier or the elbow-duct system , which is the subject of this section. In addition to having a uniform flow at the duct inlet, the special case of a fully developed velocity inlet to the elbow-duct system was simulated to investigate how changing the inlet velocity flow condition would affect the flow behavior and developing length of the flow downstream of the elbow.

By using the fully developed flow criteria stated earlier, the dimensionless developing length downstream of the elbow was found to be $55, 64$ and 72 for fully developed flow velocities with centerline velocity of $3.55\ \mathrm{m/s}$, $6.72\ \mathrm{m/s}$, and $9.86\ \mathrm{m/s}$, respectively. Similar to the elbow-duct system, the results revealed that the developing length is a Reynolds number dependent variable such that the larger the Reynolds number, the longer the developing length of the flow. These results are presented in Table 50 and plotted in Figures 95 and 96 below.

Table 50 Summary of dimensionless developing length $(L/D)_{FD}$ with corresponding Reynolds numbers in fully developed velocity inlet to the elbow- duct system based on velocity profiles

V-based Profile	**V_{CL}= 3.55 m/s**		**V_{CL}= 6.72 m/s**		**V_{CL} = 9.86 m/s**	
D_h (m)	**Re**	**$(L/D)_{FD}$**	**Re**	**$(L/D)_{FD}$**	**Re**	**$(L/D)_{FD}$**
0.4	76,960	55	153,910	64	230,870	72

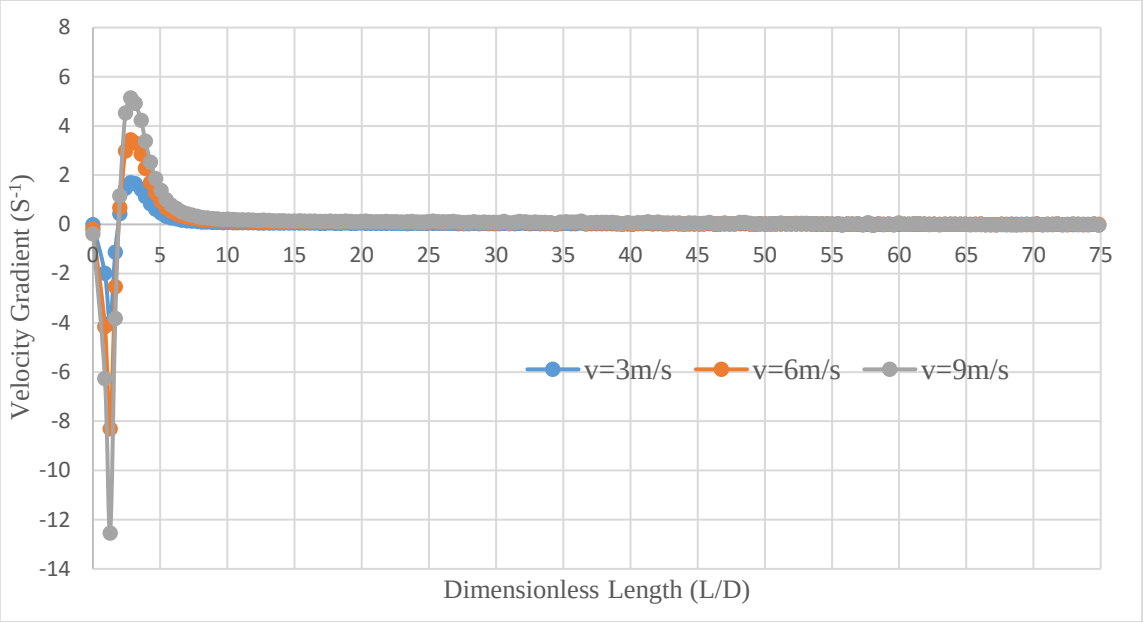

Figure 95. Velocity gradient profiles in a square duct with $d_h = 0.4$ m downstream an elbow with fully developed inlet velocity.

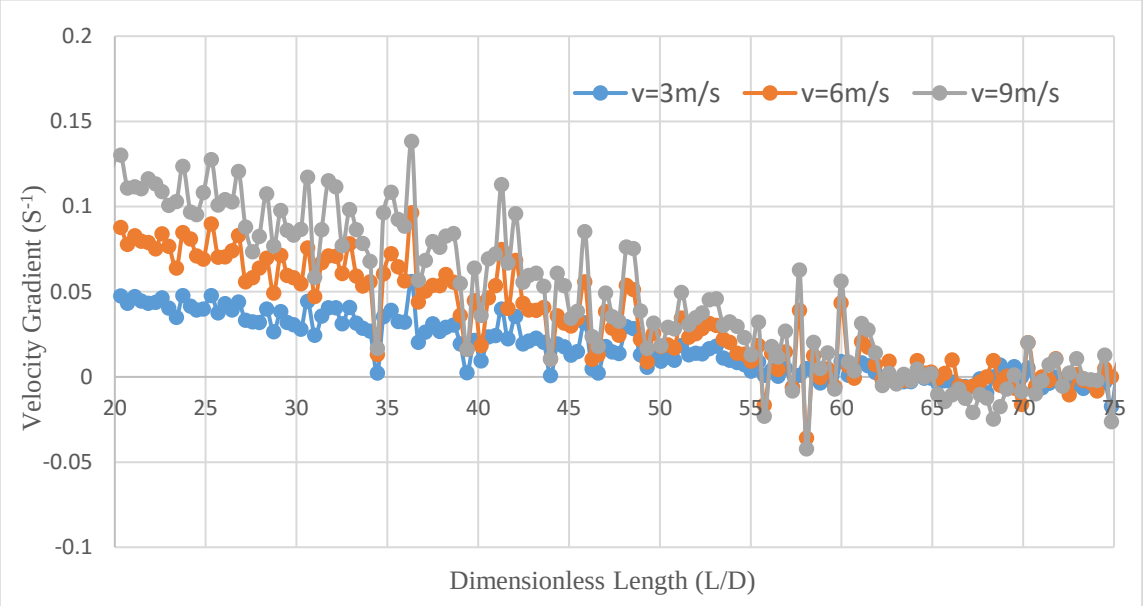

Figure 96. Velocity gradient profiles in a square duct with $d_h = 0.4$ m downstream an elbow with fully developed inlet velocity.

The above $\left(\frac{L}{D}\right)_{FD}$ results are plotted against the Reynolds number for each case in Figure 97, and by using a curve fitting procedure, a velocity-based CFD correlation for the fully developed flow location is developed for room temperature air flowing inside a right angle elbow-duct system with fully developed velocity inlet.

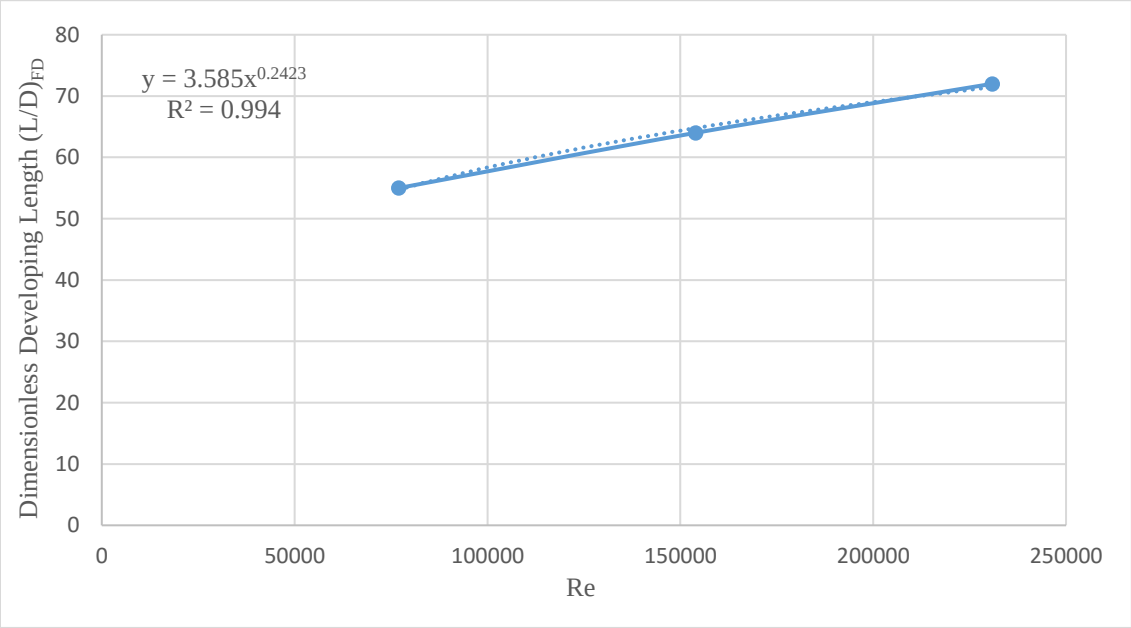

Figure 97. Curve fitting profile (velocity-based correlation) for fully developed inlet velocity in an elbow- duct system.

The resulting correlation based on the curve fittings can be expressed as

$$(\frac{L}{D})_{FD_V} = 3.585 * Re^{0.2423} \quad (7.3)$$

Similar analysis was carried out based the pressure profiles in square ducts downstream of an elbow with fully-developed elbow inlet velocity to investigate the developing length and then compared to the previous velocity based results. In the square duct of

0.4 m hydraulic diameter, the dimensionless developing length found to be 47 with a fully developed velocity of 3.55 m/s, 58 with a fully developed velocity of 6.72 $\mathrm{m/s}$, and 68 with a fully developed flow velocity of 9.86 $\mathrm{m/s}$, as tabulated in Table 51 and plotted in Figures 98 and 99.

Table 51 Summary of dimensionless developing length $(L/D)_{FD}$ with corresponding Reynolds numbers in fully developed velocity inlet to the elbow- duct system based on pressure profiles

P-based Profile	**V_{CL}= 3.55 m/s**		**V_{CL}= 6.72 m/s**		**V_{CL} = 9.86 m/s**	
D_h (m)	**Re**	**$(L/D)_{FD}$**	**Re**	**$(L/D)_{FD}$**	**Re**	**$(L/D)_{FD}$**
0.4	76,960	47	153,910	58	230,870	68

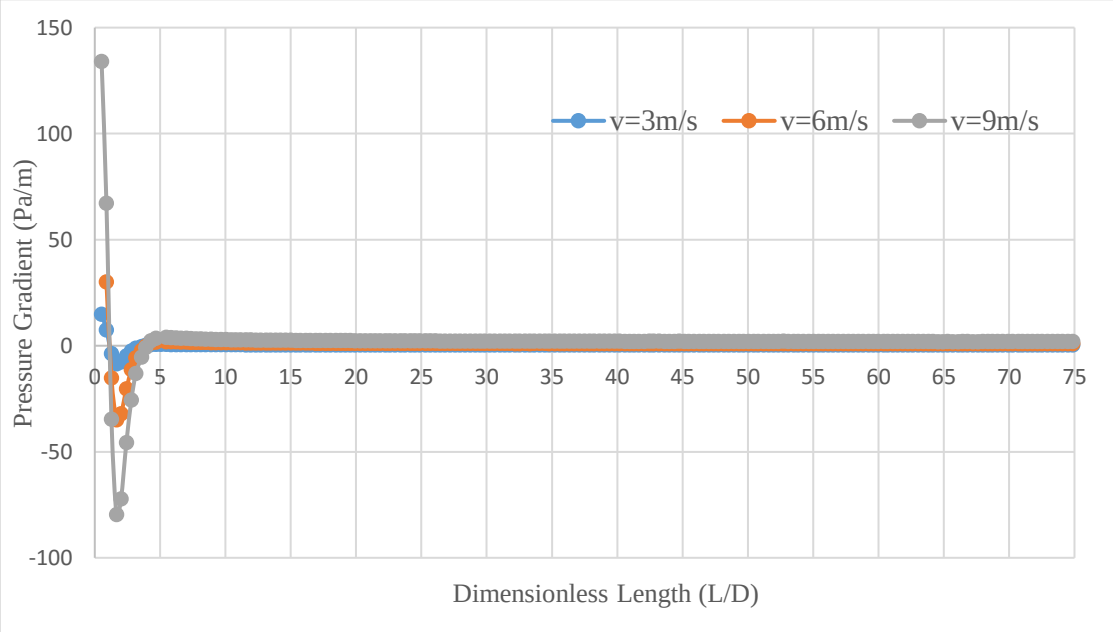

Figure 98. Pressure gradient profiles in a square duct of d_h= 0.4 m downstream of an elbow with fully developed inlet velocity.

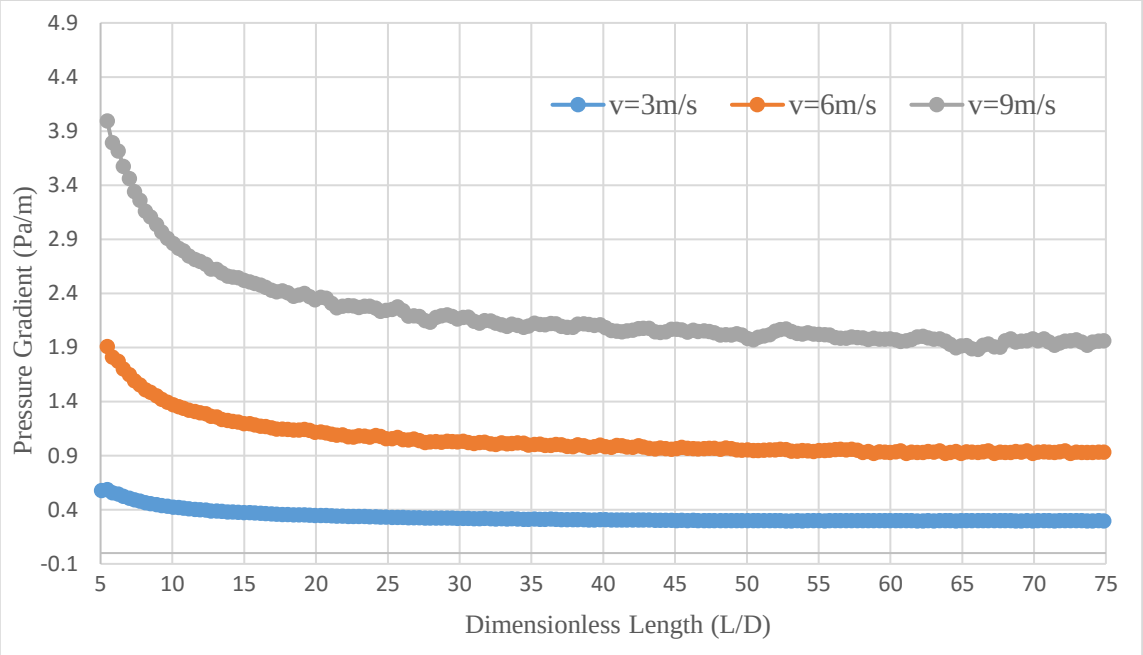

Figure 99. Enlarged pressure gradient profiles in a square duct of $d_h = 0.4$ m downstream of an elbow with fully developed inlet velocity.

The above $\left(\frac{L}{D}\right)_{FD}$ results are plotted against the Reynolds number for each case in Figure 100, and by using a curve fitting procedure, a pressure-based CFD correlation for the fully developed flow location is developed for room temperature air flowing inside a right angle elbow-duct system with fully developed inlet velocity.

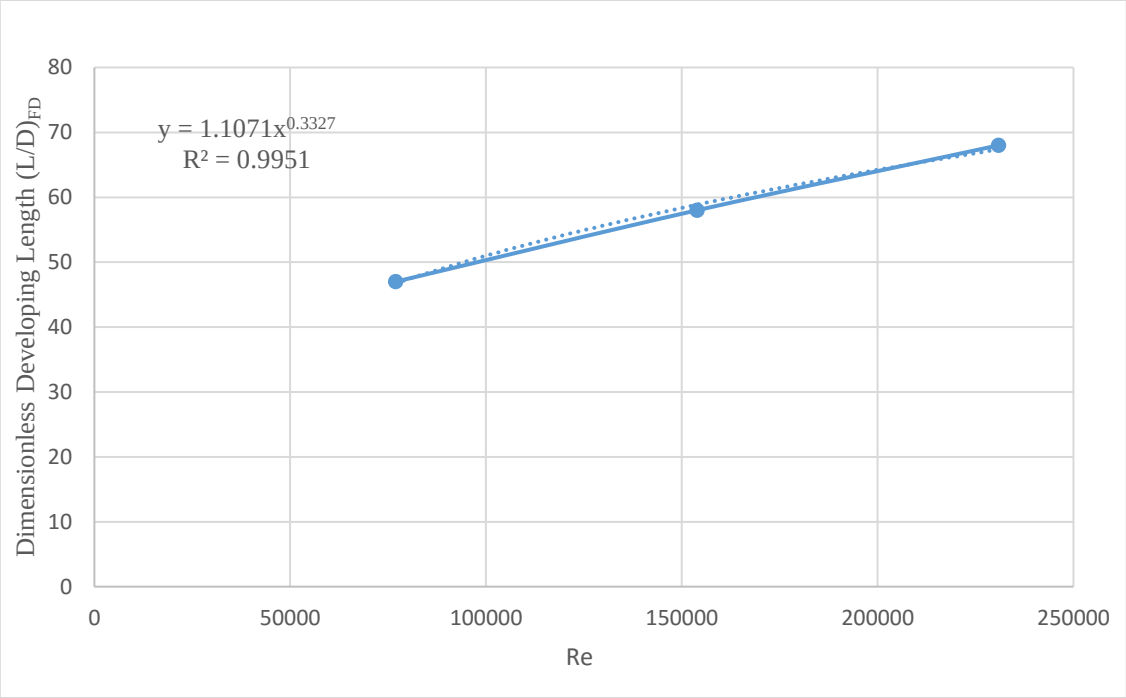

Figure 100. Curve fitting profile (pressure-based correlation) for fully developed inlet velocity in an elbow- duct system.

The resulting correlation based on the curve fitting can be expressed as

$$(\frac{L}{D})_{FD_P} = 1.1071 * Re^{0.3327} \quad (7.4)$$

7.5 Comparison of the Uniform Flow in a Square Duct and Square Elbow Duct System

In Section V, the developing flow analysis and CFD correlations of the entrance length for the case of uniform flow inside a square duct were analyzed. In this section, the same analysis was carried out but with a right-angle elbow installed upstream of the square duct. One interesting question that we may ask ourselves is how exactly having the elbow in the ducting system has effected the developing length of the flow, or how can

we quantity the effect of the elbow on the developing length of the flow. Referring to equation (5.1), the dimensionless developing length for room temperature air inside a square duct with uniform flow inlet was expressed as

$$(\frac{L}{D})_{FD_{V,square}} = (\frac{L}{D})_{No\ Elbow} = 2.9828 * \ Re^{0.221} \tag{5.1}$$

Also, for uniform flow of room temperature air inside an elbow-duct system, equation (7.1) was derived earlier to calculate the dimensionless developing length

$$(\frac{L}{D})_{FDF_{V,Elbow}} = 7.2341 * \ Re^{0.192} \tag{7.1}$$

By dividing equations (5.1) and (7.1), we have

$$\frac{(\frac{L}{D})_{Elbow}}{(\frac{L}{D})_{No\ Elbow}} = 2.43 * \ Re^{-0.029} \tag{7.5}$$

By averaging all the Reynolds number values that have been considered in the analysis, we have

$$\frac{(\frac{L}{D})_{Elbow}}{(\frac{L}{D})_{No\ Elbow}} \approx 1.75 \tag{7.6}$$

Which means that having a right-angle elbow in the square duct with uniform flow increases the developing length value by a factor of 1.75.

7.6 Comparison of Velocity Profiles of Uniform Flow Inlet and Fully Developed Flow Inlet in the Elbow Duct System

As we have seen throughout this section, the entrance length or the developing length of the flow in the elbow-duct system depends on the inlet velocity condition whether its uniform or fully developed velocity. Moreover, as shown in the results before, the flow developing length in the duct downstream the elbow with fully developed flow inlet is relatively shorter than the developing length with uniform flow inlet. As a way of trying to understand such behavior, for uniform velocity inlet of 6 m/s, the velocity profiles are plotted for both of the two cases along the horizontal square duct downstream the elbow in order to understand the flow behavior in the developing region and fully developed region of the duct. Figures 101 through 108 below show the develop of velocity profile in each case.

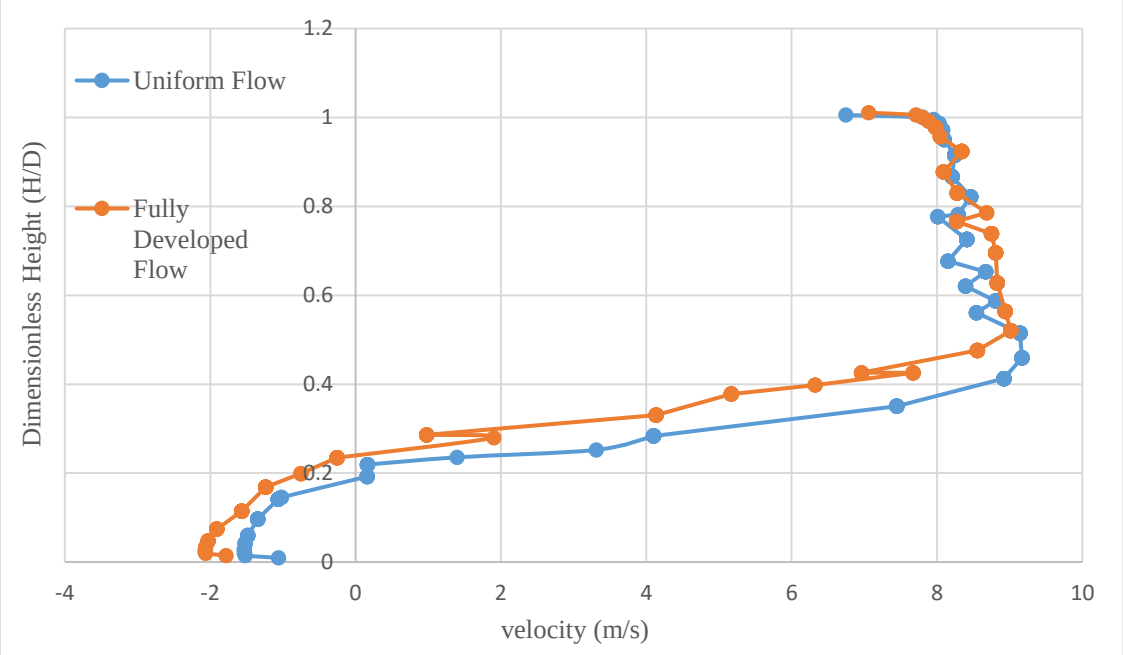

Figure 101. Comparison of velocity downstream of the elbow at (L/D) = 0.25 with uniform flow inlet and fully developed flow inlet.

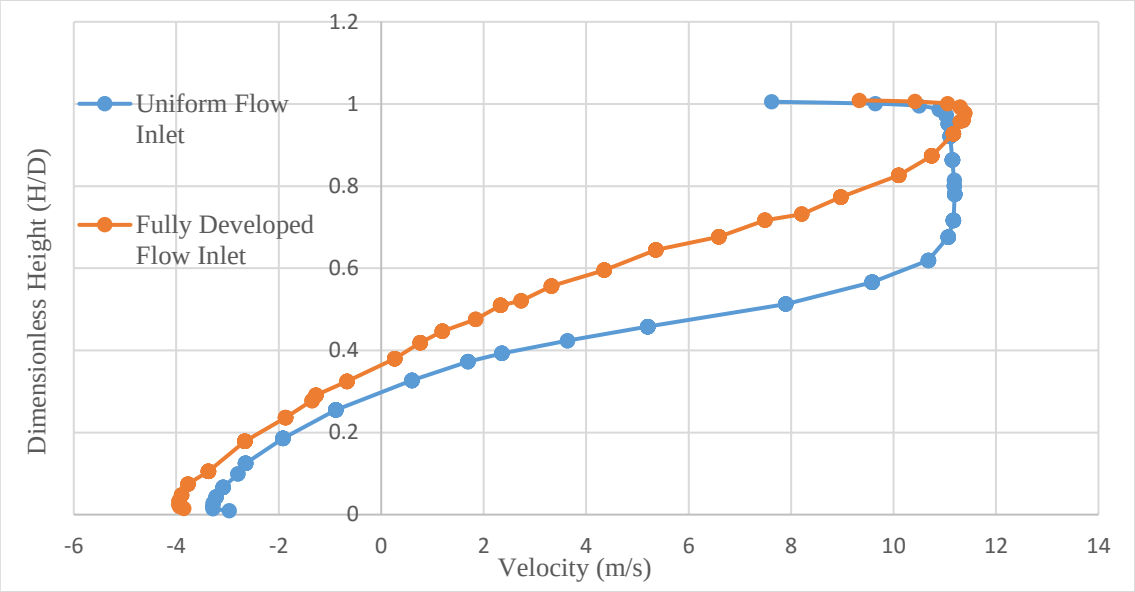

Figure 102. Comparison of velocity downstream of the elbow at (L/D) = 1.25 with uniform flow inlet and fully developed flow inlet.

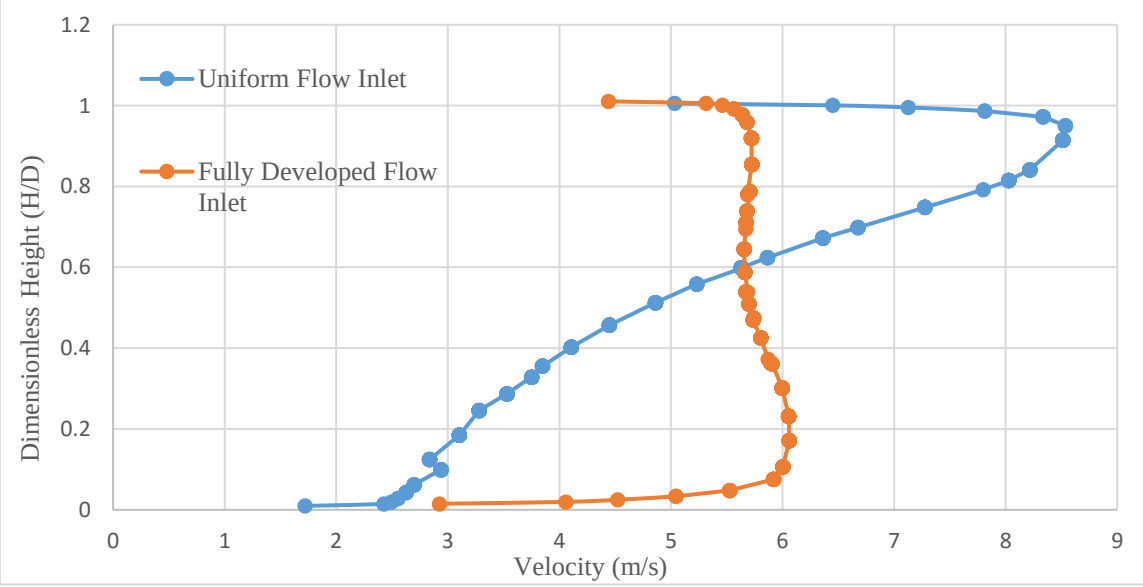

Figure 103. Comparison of velocity profile of the elbow at (L/D) = 5 with uniform flow inlet and fully developed flow inlet.

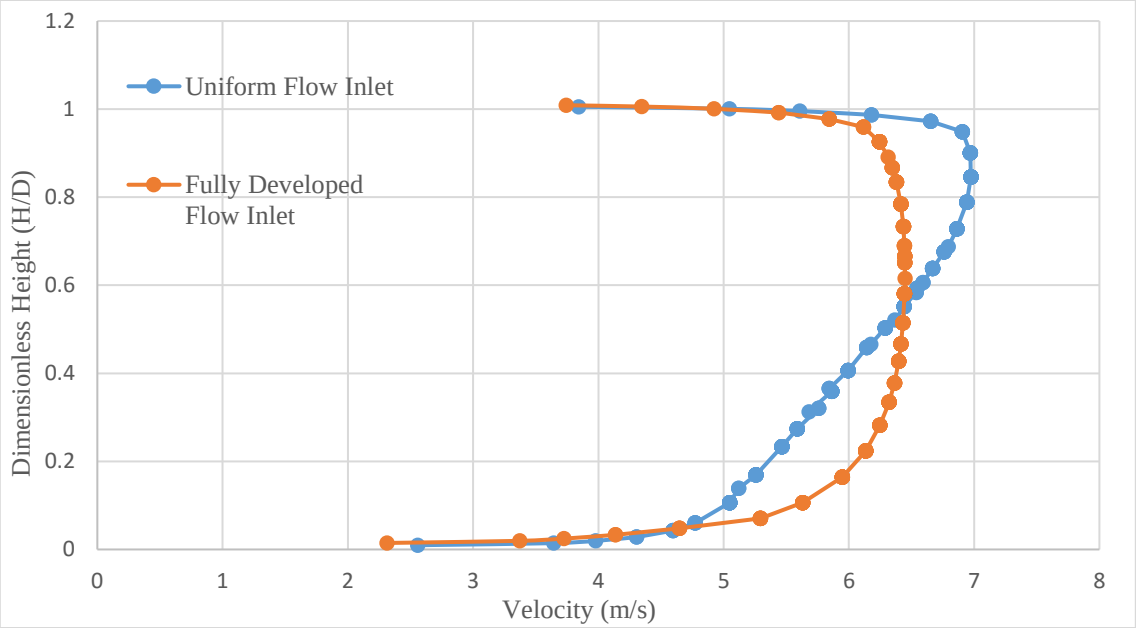

Figure 104. Comparison of velocity downstream of the elbow at (L/D) = 12.5 with uniform flow inlet and fully developed flow inlet.

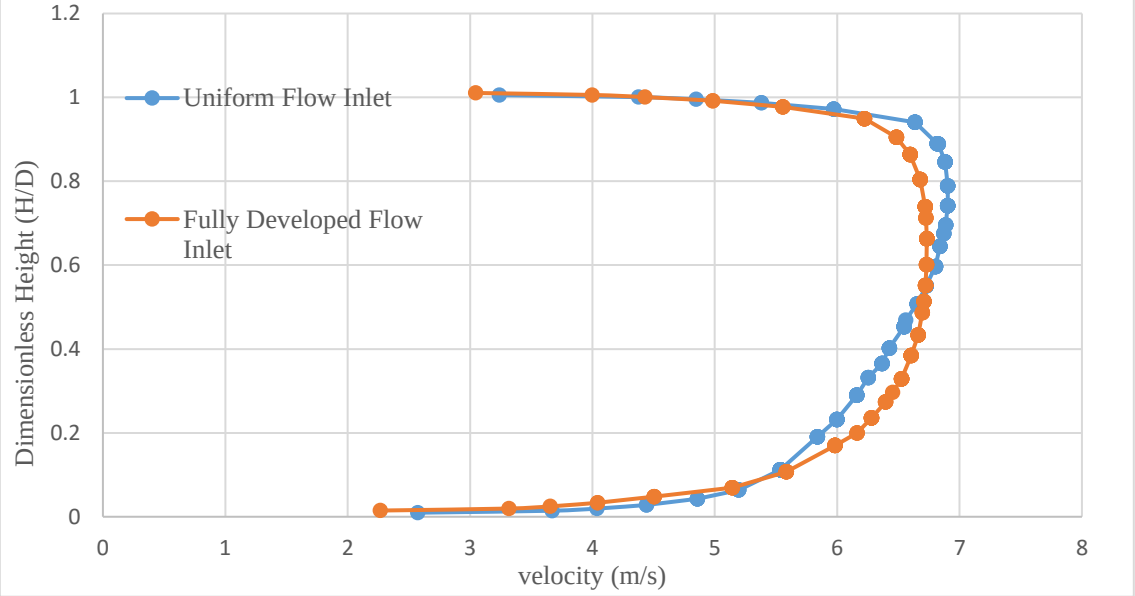

Figure 105. Comparison of velocity downstream of the elbow at (L/D) = 20 with uniform flow inlet and fully developed flow inlet.

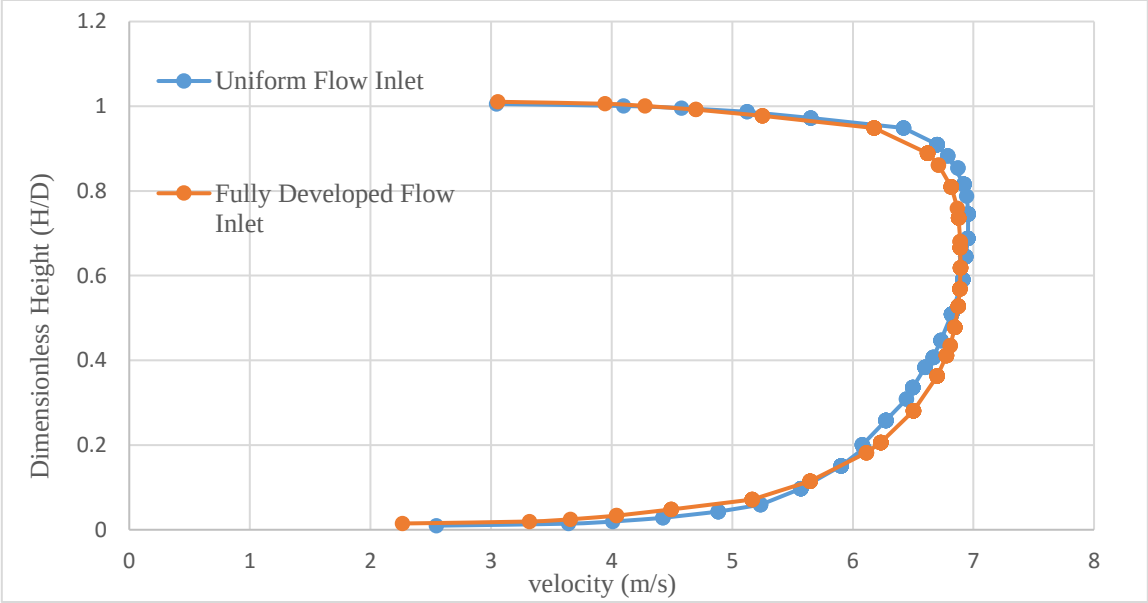

Figure 106. Comparison of velocity downstream of the elbow at (L/D) = 37.5 with uniform flow inlet and fully developed flow inlet.

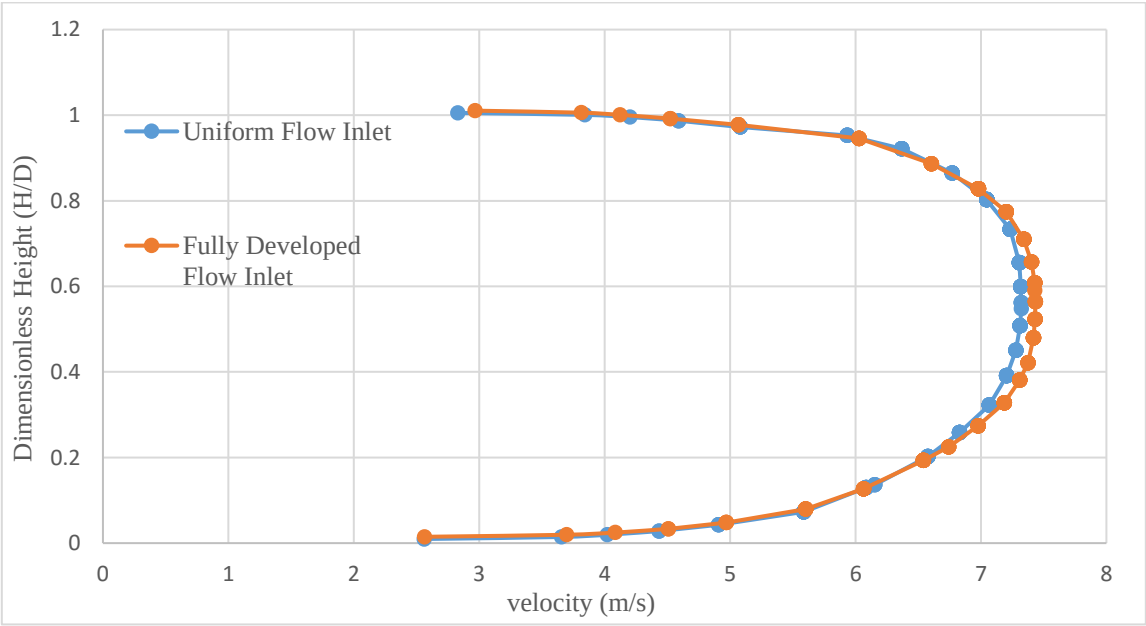

Figure 107. Comparison of velocity downstream of the elbow at (L/D) = 64 with uniform flow inlet and fully developed flow inlet.

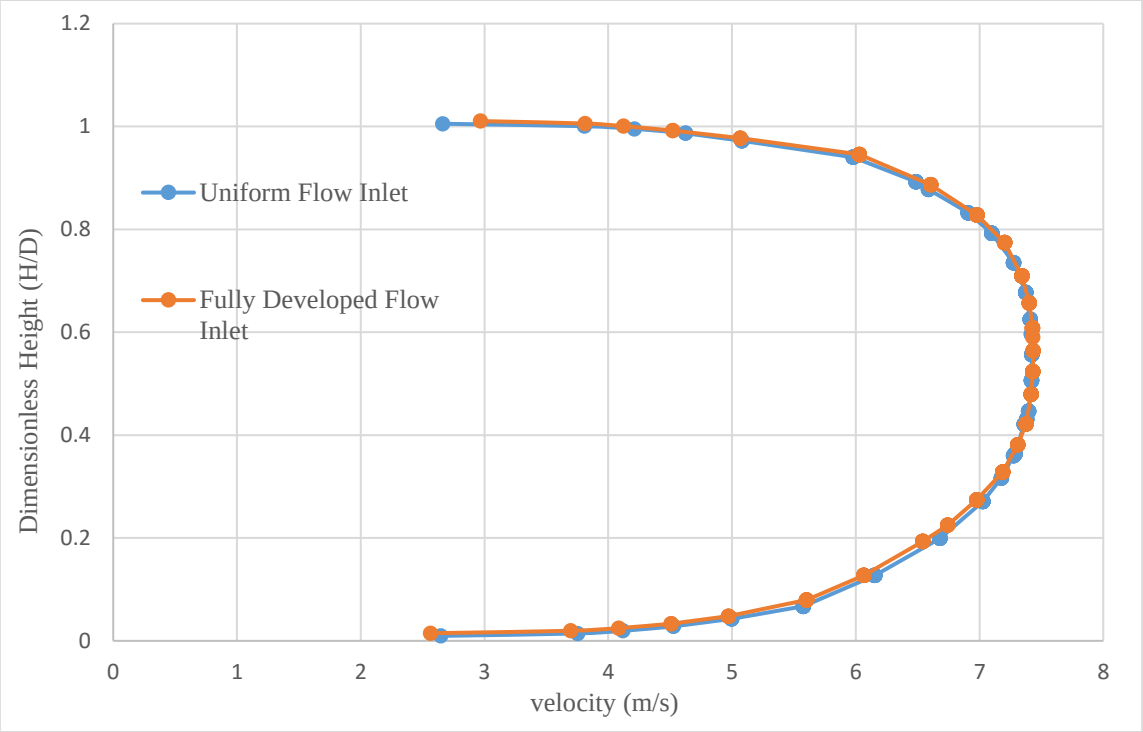

Figure 108. Comparison of velocity downstream of the elbow at (L/D) = 72 with uniform flow inlet and fully developed flow inlet.

As shown in the above figures, the velocity profile develops faster for the case of fully developed velocity inlet, and therefore it reaches the fully developed flow condition earlier than the uniform flow case with a shorter developing length, which agree with the CFD results obtained earlier. However, as shown in Figure 108, somewhere downstream the duct, both of the uniform flow and fully developed flow inlet cases are finally reaching to an identical centerline velocity, which *is* 7.4 m/s for the case of 6 m/s inlet velocity.

7.7 Summary

This section presented a CFD analysis of turbulent flow in a square duct downstream of a right-angle elbow with uniform velocity inlet and fully developed velocity inlet. For the both cases, velocity and pressure profiles were obtained for different flow Reynolds number, and by employing the fully developed flow criterial stated earlier, dimensionless developing length was calculated based on velocity and pressure profiles.

The results revealed for both of the elbow-duct systems, the developing length of the flow increases with increasing inlet velocity and/or increasing duct size. Moreover, in flow cases with identical Reynolds numbers, the developing length of the flow appeared to be the same. As a result, the developing length of the flow is a Reynolds number dependent variable such that larger Reynolds number requires longer developing length to achieve the fully developed flow condition in square ducts downstream of a right-angle elbow.

For a square duct downstream of an elbow with uniform velocity inlet, the dimensionless developing length based on velocity gradient profiles were found to be $63, 71$ and 87 for increasing flow Reynolds number of $(76{,}960), (153{,}910)$, and $(230{,}870)$ respectively. Similarly, based on the pressure gradient profiles, the dimensionless developing length was 54 for Reynolds number of $(76, 960)$, 65 for (153,910), and 75 for (230,870).

In addition, for a square duct downstream of an elbow with fully developed velocity inlet, the dimensionless developing length based on velocity gradient profiles were found to be $55, 64$ and 72 for increasing flow Reynolds number of $(76{,}960), (153{,}910)$, and $(230{,}870)$ respectively. Moreover, based on the pressure gradient profiles, the dimensionless developing length was 47 for Reynolds number of $(76, 960)$, 58 for (153,910), and 68 for (230,870).

Using the above results, velocity-based and pressure-based numerical correlations were developed for each of elbow-duct systems to calculate the required developing length (or

the entrance length) in turbulent elbow-duct flow for any Reynolds number. Also, by comparing the two inlet flow cases, namely uniform inlet velocity and fully developed inlet velocity, the results show that the fully developed inlet developing length to uniform inlet developing length ratio being around 0.9, signifying a shorter entrance length for the fully developed inlet case.

Last but not least, a comparison of uniform velocity inlet in regular square duct and square duct downstream of a right-angle elbow was presented in order to quantify the effect of the elbow in the developing length of the flow. The results revealed that, within our range of Reynolds number, adding the elbow to a simple straight square duct will increase the flow developing length by a factor of 1.75.

VIII. CONCLUSION

8.1 Conclusion

In this research, a CFD analysis of turbulent flow was performed for the case of air flow in straight ducts including both round and rectangular geometries with the latter having aspect ratios of 1.0 ,1.5, and 2.0. An additional analysis was performed with square ducts located downstream of a right-angle elbow. For each case, the duct length required to attain fully developed flow based on velocity and pressure profiles was determined for different flow velocities and duct sizes.

For the round duct flow based on the velocity profiles, the dimensionless developing lengths were found to be $27, 31.3, 34, 36, 39$, and 43.5 for increasing flow Reynolds number of 3.84×10^4 , 7.70×10^4 , 11.5×10^4 , 15.4×10^4 , 23×10^4, and 34.6×10^4, respectively. Similarly, based on the pressure gradient profiles, the dimensionless developing lengths were found to be 21 for Reynolds number of 3.84×10^4 , 26 for 7.70×10^4, 29 for 11.5×10^4, 31 for 15.4×10^4, 36 for 23×10^4, and 38.7 for 34.6×10^4.

For a rectangular duct with an aspect ratio of 1, which is a square duct, the dimensionless developing lengths, based on velocity profiles, were found to be $30.8, 36$,39 ,41.6 ,46, and 50 for flow Reynolds number of 3.84×10^4 , 7.70×10^4 , 11.5×10^4 , 15.4×10^4 , 23×10^4, and 34.6×10^4, respectively . Similarly, based on the pressure gradient profiles, the dimensionless developing lengths were found to be 25.5 for Reynolds number of 3.84×10^4, 31 for 7.70×10^4 , 36.5 for 11.5×10^4, 39 for 15.4×10^4, 45 for 23×10^4, and 48.3 for 34.6×10^4.

Moreover, for a rectangular duct with an aspect ratio of 1.5, the dimensionless developing lengths based on the velocity profiles were found to be $44, 49$ and 53.5 for flow Reynolds numbers of $7.70 \times 10^4, 15.4 \times 10^4$, and 23×10^4, respectively. Also,

based on the pressure gradient profiles, the dimensionless developing lengths were found to be $38, 46$, and 53 for flow Reynolds numbers of $7.70 \times 10^4, 15.4 \times 10^4$, and 23×10^4, respectively.

For a rectangular duct with an aspect ratio of 2, the dimensionless developing length, based on the velocity gradient profiles, were found to be $50, 56.5$ and 62 for increasing flow Reynolds numbers of $7.70 \times 10^4, 15.4 \times 10^4$, and 23×10^4, respectively. Similarly, based on the pressure gradient profiles, the dimensionless developing lengths were found to be $43.5, 52.5$, and 60 for increasing flow Reynolds numbers of $7.70 \times 10^4, 15.4 \times 10^4$, and 23×10^4, respectively.

In addition to the above straight duct flow analysis results, a special case of developing flow in a square duct located downstream of a right angle elbow was analyzed. For this elbow-duct system with a uniform inlet velocity, the dimensionless developing length in the straight duct based on the velocity gradient profiles were found to be 63 , 71 and 87 for increasing flow Reynolds numbers of $7.70 \times 10^4, 15.4 \times 10^4$, and 23×10^4, respectively. Similarly, based on the pressure gradient profiles, the dimensionless developing length was 54 for Reynolds number of 7.70×10^4, 65 for 15.4×10^4, and 75 for 23×10^4 . For the elbow-duct system with a fully-developed inlet velocity entering the elbow, the dimensionless developing lengths, based on the velocity gradient profiles, were found to be $55, 64$ and 72 for increasing flow Reynolds number of $7.70 \times 10^4, 15.4 \times 10^4$, and 23×10^4, respectively. Moreover, based on the pressure gradient profiles, the dimensionless developing length were 47 for Reynolds number of 7.70×10^4, 58 for 15.4×10^4, and 68 for 23×10^4.

Based on all these results, it can be concluded that the velocity-based and the pressure-based developing length of the flow, for any duct geometry, are Reynolds number dependent with the developing length increasing as the Reynolds number increases. Furthermore, a ratio of the pressure-developing length to velocity-developing length for the same duct geometry and inlet flow condition can be calculated. The results show that

this developing length flow ratio is about 0.86 for a round duct and 0.93 on average for rectangular ducts, signifying a shorter entrance length for the velocity analysis compared to the pressure analysis.

An overall comparison of round, square, and rectangular duct flows was performed with the comparison showing that the developing lengths in round ducts were shorter than the corresponding square ducts by around 13% based on velocity profiles and 19% based on pressure profiles. Also, these comparison results show that the developing lengths in round ducts were shorter than the corresponding rectangular ducts with a 1.5 aspect ratio by around 25% based on the velocity profiles and 30% based on the pressure profiles. Similarly, the developing length in the round duct was shorter than the corresponding rectangular duct with an aspect ratio of 2.0 by around 36% based on the velocity profiles and 40% based on the pressure profiles. These results indicate that the developing length of the flow is geometry dependent as well as Reynolds number dependent.

To validate the numerical model results in this research, the numerical pressure drop of each duct flow model was compared to the results of the well-known Darcy–Weisbach correlation. For the case of a moderate turbulent flow with a Reynolds number of 15.4×10^4,the difference between the Darcy's correlation and numerical model results was 2.2% for a round duct, 3.3% for the square duct, 4.7% for the rectangular duct with an aspect ratio of 1.5, and 6.2% for the rectangular duct with an aspect ratio of 2. Also, comparing the CFD entrance length with a well-known experimental entrance length correlation for a round duct shows a difference of around 10%.

IX. FUTURE WORK

9.1 Future Work

Numerical correlations were derived for entrance region lengths of turbulent flows inside round, square, and rectangular ducts for ducts sizes and flow rates representative of building air-distribution systems. In the future, a detailed analysis will be done to generalize these results and to investigate all of the factors that affect these developing lengths for turbulent flows and the resulting correlation.

For the round duct flow case, a wider Reynolds number range will be analyzed to cover lower and higher turbulent flow applications in order to obtain more comprehensive developing length correlations for internal turbulent flow.

For the rectangular duct flow analysis, more aspect ratios that are commonly used in industry will be covered to further investigate the geometry effects on the developing length of turbulent flows. Moreover, with more aspect ratios covered, more accurate generalized developing length correlations can be derived that can in turn be used for any rectangular duct design.

In addition, more elbow-duct system configurations will be investigated to derive a range of developing length correlations that are applicable to elbow-duct configurations used in industry. Also, other types of elbows, such as curved elbows and elbows with turning vanes, will be studied to evaluate the effect of the elbow-type on the developing flow. This analysis will aid engineers to choose the appropriate elbow-type for their ducting designs, especially ducts with lower pressure drops and shorter flow developing lengths. Last but not least, different fluids such as water, oil, refrigerant, liquid/gas hydrogen or ammonia could be included in the analysis to investigate the effect of the fluid type on the developing length of the flow, and also to derive a correction factor for different fluid types.

REFERENCES

1. Barbin, A. R., & Jones, J. B. (1963). Turbulent flow in the inlet region of a smooth pipe. *Journal of Basic Engineering, 85*(1), 29. doi:10.1115/1.3656521.
2. Bejan, A. (1984). *Convection heat transfer*. New York: Wiley**.**
3. Bhatti, M. S. & Shah, R. K. (1987). Turbulent and transition flow convective heat transfer. *Handbook of single-phase convective heat transfer*. New York: Wiley.
4. Bhandari & Singh (2012). Analysis of fully developed turbulent flow in a pipe using computational fluid dynamics. *IJERT Journal, 1(5),*2278-0181.
5. Çengel, Y. A., & Cimbala, J. M. (2014). *Fluid mechanics: fundamentals and applications*. New York: McGraw Hill.
6. Colebrooke, C.F. (1939). Turbulent flow in pipes with particular reference to the transition region between the smooth and rough pipe laws. *Journal of the ICE*, 11(4), 133–156. doi:10.1680/ijoti.1939.13150.
7. Doherty, J., Ngan, P., Monty, J., & Chong, M. (2007). *The development of turbulent pipe flow*. Parkville: The University of Melbourne.
8. Didwania, M., Singh, L., Malik, A., & Sisodiya, M. S. (2014). Analysis of turbulent flow over a 90° bend of duct using in centralized A. C. plant by CFD code. *IOSR Journal of Mechanical and Civil Engineering, 11*(4), 41-48. doi:10.9790/1684-11414148.
9. Joshi, Bisht, and Gupta (2014). Analysis of fully developed turbulent flow in a axi-symmetric pipe using ANSYS FLUENT software. *IJERT Journal, 3(3),*2278-0181.
10. Kai, W., & Ping, W. (2013). *CFD numerical simulation analysis of small and medium caliber 90 ° circular bend*. Paper presented at ICCSEE, Paris, France: Atlantis Press.
11. Koh, Y. (1992). Turbulent flow near a rough wall. *Journal of Fluids Engineering, 114*(4), 537.

12. Laufer, J. (1953). *The structure of turbulence in fully developed pipe flow*. Washington, D.C.: National Advisory Committee for Aeronautics.
13. Han, J. (2011). *Analytical heat transfer*. Boca Raton, FL: CRC.
14. Hunt, J & Morrison, J. (2000). Eddy structure in turbulent boundary layers. *Eur. J. Mech. B-Fluids* 19, 673–694.
15. Markatos, N. (1986). The mathematical modelling of turbulent flows. *Applied Mathematical Modelling Journal,10*(3), 190-220.doi:10.1016/0307-904x(86)90045-4
16. Munson, B. R., Okiishi, T. H., & Huebsch, W. W. (2009). *Fundamentals of fluid mechanics*. Hoboken, NJ: J. Wiley & Sons.
17. Perry, A. E., & Abell, C. J. (1978). Scaling laws for pipe-flow turbulence. *Journal of Fluid Mechanics,67*(02), 257. doi:10.1017/s0022112075000298.
18. Sahu, M, Khatua, K, Patra, K & Naik, T. (2009, February 4-6). Developed laminar flow in pipe using computational fluid dynamics. Paper presented at the 7th International R & D Conference on Development and Management of Water and Energy Resource, Bhubaneswar, India.
19. Schlichting, H., & Gersten, K. (2000). *Boundary-layer theory*. Berlin: Springer.
20. Taylor, N.A. (1984) Modeling of air flows through the sample pipe of a smoke detecting system, United Kingdom Atomic Energy Authority.
21. Versteeg, H. K., & Malalasekera, W. (2007). *An introduction to computational fluid dynamics: The finite volume method*. Harlow, England: Pearson Education.
22. Wilcox, D. C. (2008). Formulation of the k-w turbulence model revisited. *AIAA Journal, 46*(11), 2823-2838. doi:10.2514/1.36541.
23. White, F. M. (1994). *Fluid mechanics*. New York, NY: McGraw-Hill.